

Annecken Nøland

Autonomous Underwater Vehicle (AUV) based study of zooplankton communities, using a silhouette camera and artificial intelligence

Master's thesis in Ocean Resources

Supervisor: Geir Johnsen

Co-supervisor: Nicole Aberle-Malzahn

May 2022

Annecken Nøland

Autonomous Underwater Vehicle (AUV) based study of zooplankton communities, using a silhouette camera and artificial intelligence

Master's thesis in Ocean Resources
Supervisor: Geir Johnsen
Co-supervisor: Nicole Aberle-Malzahn
May 2022

Norwegian University of Science and Technology
Faculty of Natural Sciences
Department of Biology



Kunnskap for en bedre verden

Abstract

Autonomous Underwater Vehicles (AUVs), which can be customized with environmental sensors, have proven useful for plankton ecology studies by providing continuous spatial and temporal observations over the mesoscale. Another novel tool is the SilCam imaging system, which captures images of objects suspended in the water column in situ and classifies the findings. When mounted on an AUV, in situ plankton images and key environmental variables (KEVs) can be captured simultaneously, allowing for an increased understanding of the marine ecosystem.

This study aimed to assess how this novel method, combining an AUV and a SilCam system, performed in a study of zooplankton community composition and KEVs, for providing insights on spatiotemporal variations and plankton dynamics. The usability of the SilCam method was also assessed separately, addressing the performance of two artificial intelligence (AI) algorithms in plankton classification. The findings suggested that the SilCam method best serves as an addition to net samples, as it for now does not allow for the high taxonomic resolution enabled by net samples, due to the low optical resolution of the SilCam. The low optical resolution, combined with a limited training data set, also contributed to a limited plankton classification accuracy obtained by the AI algorithms. The AUV acquired an extensive data set of chlorophyll *a* (as a proxy for phytoplankton biomass), seawater temperature, salinity, and dissolved oxygen. Still, the sensors had different properties, such as response time, sampling intervals, and calibration, resulting in challenges with combining and comparing the data.

Data from the AUV sensors, SilCam system, and ground-truthing were combined to assess the state of the phytoplankton spring bloom conditions in Mausund and Hopavågen in coastal Trøndelag, Norway, as also was one of the aims of the study. Through this coupling of information, it was concluded that a phytoplankton pre-bloom and an ongoing bloom occurred on the first and second visit to Mausund, respectively, and that there was a post-bloom in Hopavågen. Overall, this study elucidated the areas of improvement related to sampling of plankton data using an AUV mounted with a SilCam imaging system, but also the method's potential to be a very valuable tool in future plankton studies, and thereby the monitoring of climate change in the ocean.

Sammendrag

Autonome undervannsfarkoster (AUV), som kan tilpasses med en montert sensorpakke, har vist seg å være nyttige for økologistudier av plankton ved å gi kontinuerlige romlige og tidsmessige observasjoner over mesoskalaen. En annen ny metode er SilCam-bildesystemet, som tar bilder av objekter fordelt i vannsøylen in situ og deretter klassifiserer funnene. Når SilCam-systemet er montert på en AUV, kan in situ planktonbilder og nøkkelmiljøvariabler (KEV) samles inn samtidig, hvilket kan bidra til en økt forståelse av de marine økosystemet.

Denne studien hadde som mål å vurdere hvordan denne nye metoden, som kombinerer en AUV og et SilCam, presterte i en studie av dyreplanktonsamfunnets sammensetning og tilhørende nøkkelmiljøvariabler, for å gi innsikt i variasjoner i tid og rom og planktondynamikk. Nyttigheten til SilCam-metoden ble også vurdert separat, og tok for seg ytelsen til to algoritmer som brukte kunstig intelligens (AI) i planktonklassifisering. Funnene tydet på at SilCam-metoden best fungerer som et tillegg til nettprøver, ettersom den foreløpig ikke tillater den høye taksonomiske oppløsningen som er mulig gjort av nettprøver, på grunn av den lave optiske oppløsningen til SilCam. Den lave optiske oppløsningen, kombinert med et begrenset treningsdatasett, bidro også til en begrenset klassifiseringsnøyaktighet oppnådd av AI-algortimene. AUV-en anskaffet et omfattende datasett av klorofyll a (som et mål for planktonalgebiomasse), havtemperatur, saltholdighet og oppløst oksygen. Likevel hadde sensorene forskjellige egenskaper, som responstid, prøvetakingsintervaller og kalibrering, noe som resulterte i utfordringer med å kombinere og sammenligne dataene.

Data fra AUV-sensorene, SilCam-systemet, vannprøver og verifisering med nettprøver ble kombinert for å vurdere tilstanden til våroppblomstring av planktonalger på Mausund og i Hopavågen i kystnære Trøndelag, Norge, som også var et av målene med studien. Gjennom denne kombinasjonen av informasjon ble det konkludert med at de to besøkene til Mausund ble gjort henholdsvis før og i løpet av en planktonalgeoppblomstring, og at Hopavågen ble besøkt etter en planktonalgeoppblomstring. Samlet sett belyste denne studien forbedringsområdene knyttet til denne metoden, men også dens potensiale til å være et svært verdifullt verktøy i fremtidige planktonstudier og dermed overvåking av klimaendringer i havet.

Acknowledgments

The work of this study was conducted between January 2021 and May 2022 at the Norwegian University of Science and Technology (NTNU). The preparation and lab work were performed at Trondhjem Biological Station (TBS), while most of the writing was done at NTNU SeaLab, both at the Department of Biology. The fieldwork was performed in the coastal part of Trøndelag, Norway, i.e. Mausund (Frøya) and Hopavågen (Agdenes) in April and May 2021, respectively. The work was funded by the NTNU Centre for Autonomous Marine Operations and Systems (NTNU AMOS, Research Council of Norway (RCN) project #223254) and was a part of the Interdisciplinary Algal Bloom Observation Field Experiment. This study is in special collaboration with the Autonomous Imaging and Learning Ai RObot identifying plankton taxa in situ (AILARON) project (RCN project number 262741). I want to thank the teams for a great experience and collaboration, and for sharing your valuable and extensive knowledge.

I want to give a special thanks to my main supervisor Geir Johnsen. You have a unique way of sharing your knowledge through enthusiasm and passion, that I truly inspire. Not to mention that it is impossible to leave a conversation with you without you making a joke. Thank you, for teaching me about the importance of interdisciplinary work and new technology for ecological studies, for giving me this opportunity, and for always encouraging me. Hopefully, I can continue to learn from you also in the future.

Thank you Nicole Aberle-Malzahn, my co-supervisor, for sharing your extensive knowledge about zooplankton and plankton sampling, for helping during sampling, and for important input on my thesis. I want to give a huge thanks to Annette Stahl, Aya Saad, and Andreas Våge (the AILARON team), for your much-needed technological expertise related to the Light Autonomous Underwater Vehicle (LAUV) and processing of the Silhouette Camera (SilCam) data. Your skills and hard work are inspirational, and I appreciate the opportunity to learn from you. I want to thank Siv Anina Etter for helping with the nutrient analyses, Sanna Majaneva, and Torkild Bakken for helping with taxonomic identification, and Rune Bjørgum for being a cheerleader that is always there to help. Thank you to Mausund Field Station for your hospitality and especially Odd Arne Arnesen for your excellent boat driving skills during data sampling.

My fellow students at Ocean Resources: thank you for your much-appreciated company over the last two years, and a special thanks to my master group, Maren Thu, Mikkel Bjerkvoll, Marte Opsahl Søreng, Camilla Marnor, and Malin Bø Nevstad, for valuable discussions and insights, including a lot of fun during fieldwork. Maren Thu, you deserve a special thanks for sticking with me throughout this whole process and I greatly appreciate the friendship we have made. You have been a pleasure to work with and I admire your good mood and collaboration skills.

I want to thank my family and friends for supporting me. Last, but not least, I want to thank my father, Sam Arne Nøland, who was a marine biologist and taught me from an early age how to be curious about the ocean and appreciate the value of science. He was all that I aspire to be, and it is with great gratitude that I dedicate my master thesis to him.

Annecken Nøland

Trondheim, May 2022

Table of contents

Abstract.....	i
Sammendrag.....	ii
Acknowledgments	iii
1 Introduction	1
1.1 Why plankton?	1
1.2 Traditional and new sampling methods.....	2
1.3 Environmental data.....	4
1.4 Plankton analyses with silhouette camera (SilCam)	5
1.5 The AILARON project and plankton classification.....	5
1.6 Overview and aim of study	6
2 Materials and methods.....	7
2.1 Study area	7
2.1.1 <i>Mausund</i>	7
2.1.2 <i>Hopavågen</i>	9
2.2 Weather conditions.....	10
2.3 Materials.....	11
2.3.1 <i>The Light autonomous underwater vehicle (LAUV)</i>	11
2.3.2 <i>The SilCam system</i>	13
2.3.3 <i>Artificial intelligence (AI) algorithms</i>	13
2.4 Fieldwork.....	14
2.4.1 <i>LAUV with SilCam</i>	14
2.4.2 <i>Ground-truthing with net hauls and seawater samples</i>	15
2.5 Laboratory work	18
2.6 Data analyses.....	19
2.6.1 <i>Net sample zooplankton community analysis</i>	19
2.6.2 <i>SilCam classification and the labeling process</i>	21
2.6.3 <i>Data analysis of Key Environmental Variables (KEVs)</i>	23
3 Results	24
3.1 SilCam montages from PySilCam	24
3.2 SilCam montages of classification results from the YOLO-based model	25
3.3 Detection of zooplankton groups in SilCam images	33

3.4	In vivo analysis of zooplankton community composition in net samples.....	34
3.4.1	<i>Net sample groups</i>	34
3.4.2	<i>Zooplankton community composition in net samples</i>	38
3.5	Key Environmental Variables (KEV) data from the LAUV	41
3.5.1	<i>Seawater temperature</i>	41
3.5.2	<i>Salinity</i>	42
3.5.3	<i>Dissolved Oxygen</i>	43
3.5.4	<i>Chlorophyll a concentration</i>	44
3.6	Nutrient availability	44
3.6.1	<i>Nitrate</i>	45
3.6.2	<i>Phosphate</i>	47
4	Discussion	49
4.1	The SilCam System as a method for plankton studies.....	49
4.1.1	<i>Optical resolution</i>	49
4.1.2	<i>Detection and identification of taxonomic groups</i>	50
4.1.3	<i>Overlapping and incomplete organisms</i>	51
4.1.4	<i>AI algorithms in copepod classification</i>	51
4.1.5	<i>Effectiveness of the SilCam method</i>	53
4.1.6	<i>Challenges experienced with the SilCam method</i>	54
4.2	State of the spring bloom 2021.....	56
4.2.1	<i>First visit to Mausund (Day M1 and M2)</i>	56
4.2.2	<i>Second visit to Mausund (Day M3 and M4)</i>	57
4.2.3	<i>Hopavågen (Day H1 and H2)</i>	57
4.3	<i>Assessment of the combination of LAUV and SilCam</i>	58
4.4	<i>Overall challenges</i>	60
5	Conclusion	61
	Future perspectives	61
	References	63
	APPENDIX A: Seawater samples for nutrient analysis.....	xi
	APPENDIX B: Taxonomic groups of zooplankton	xii
	APPENDIX C: Additional classified SilCam images from the YOLO-based model	xv

Figures

Figure 1	LAUV Roald carried at Mausund Field Station	3
Figure 2	Map of the two sampling locations, Mausund and Hopavågen.....	8
Figure 3	Mausund Field Station and islands in the Mausund Bank.....	9
Figure 4	Hopavågen, Agdenes.....	10
Figure 5	LAUV with sensor suite, including SilCam.....	12
Figure 6	Schematic illustration of the SilCam.....	13
Figure 7	Block diagram of the classification process.....	14
Figure 8	LAUV launching and visualization of the yoyo transect.....	15
Figure 9	Images from plankton net sampling and seawater sampling.....	16
Figure 10	Seawater filtration and related equipment.....	18
Figure 11	Net sample analysis in stereomicroscope with a camera system.....	19
Figure 12	Pictorial guide to relevant taxonomic zooplankton groups.....	20
Figure 13	Labeling of SilCam images in Roboflow.....	22
Figure 14	PySilCam montages of SilCam images.....	24
Figure 15	Montage of classification of copepods using the YOLO-based model, before processing.....	26
Figure 16	Selection of copepods classified with the YOLO-based model.....	32
Figure 17	Selection of objects misclassified by the YOLO-based model.....	33
Figure 18	Net sample images of Copepoda.....	35
Figure 19	Net sample images of other crustaceans.....	35
Figure 20	Net sample images of Bryozoa larva.....	36
Figure 21	Net sample images of Radiolaria.....	36
Figure 22	Net sample images of Polychaeta larva.....	36
Figure 23	Net sample images of Cnidaria.....	36
Figure 24	Net sample images of Echinodermata.....	37
Figure 25	Net sample images of Mollusca.....	37
Figure 26	Net sample images of eggs.....	37
Figure 27	Net sample images of phytoplankton.....	37
Figure 28	Temperature measurements from the LAUV.....	41
Figure 29	Salinity measurements from the LAUV.....	42
Figure 30	Dissolved oxygen measurements from the LAUV.....	43
Figure 31	Chlorophyll <i>a</i> measurements from the LAUV.....	44
Figure 32	Nitrate measurements from seawater samples.....	45
Figure 33	Boxplot of nitrate measurements from seawater samples.....	46
Figure 34	Phosphate measurements from seawater samples.....	47
Figure 35	Boxplot of phosphate measurements from seawater samples.....	48
Figure 36	Pictorial key to taxonomic groups of zooplankton.....	xii
Figure 37	Pictorial key to non-crustacean zooplankton and larvae.....	xiii
Figure 38	Pictorial key to crustacean zooplankton.....	xiv

Tables

Table 1	Time, locations, and weather data.....	11
Table 2	Overview of sensors of the LAUV.....	12
Table 3	Overview of net sampling.....	17
Table 4	Copepod montages from day M1 using the YOLO-based model.....	27-29
Table 5	Copepod montages from day M2 using the YOLO-based model.....	30-32
Table 6	Zooplankton group detectability in the SilCam images.....	34
Table 7	Zooplankton community composition in the net samples.....	39
Table 8	Associated groups in the net samples.....	40
Table 9	Overview of seawater samples at Mausund.....	xi
Table 10	Overview of seawater samples in Hopavågen.....	xi
Table 11	Montages of SilCam images classified as "Other" from day M1.....	xv-xvii
Table 12	Montages of SilCam images classified as "Other" from day M3.....	xviii-xx

Abbreviations

AI	Artificial Intelligence
AILARON	Autonomous Imaging and Learning Ai RObot identifying plaNkton taxa in situ
AMOS	Centre for Autonomous Marine Operations and Systems
AUR-Lab	Applied Underwater Robotics Laboratory
AUV	Autonomous Underwater Vehicle
DOM	Dissolved organic material
Chl <i>a</i>	Chlorophyll <i>a</i>
CSV	Comma-separated values
CTD	Conductivity, Temperature, Depth
DCNN	Deep Convolutional Neural Network
DUNE	Unified Navigational Environment
DVL	Doppler Velocity Log
DVM	Diel Vertical Migration
HELCOM	The Baltic Marine Environment Protection Commission
H1	Hopavågen day 1
H2	Hopavågen day 2
IFCB	Imaging flow-cytobot
IMC	Inter-module communication
ISIIS	In Situ Ichthyoplankton Imaging System
KEV	Key Environmental Variables
LAUV	Light Autonomous Underwater Vehicle
LED	Light-emitting diode
LISST	Laser In Situ Scattering and Transmissometer
ML	Machine learning
M1	Mausund day 1
M2	Mausund day 2
M3	Mausund day 3
M4	Mausund day 4
NAC	The North Atlantic Current
NCC	The Norwegian Coastal Current
NO ₃ ⁻	Nitrate
NTNU	Norwegian University of Science and Technology
OSPAR	The Convention for the Protection of the Marine Environment of the North-East Atlantic
O ₂	Oxygen
PO ₄ ³⁻	Phosphate
PySilCam	SilCam python package
ROV	Remotely Operated Vehicle
SilCam	Silhouette Camera
TSM	Total suspended material
UAV	Unmanned Autonomous Vehicle
USV	Unmanned Surface Vehicle
YOLOv5	You Only Look Once version 5

1 Introduction

1.1 Why plankton?

Plankton can function as an indicator for change in the marine ecosystem, as a range of studies have highlighted (e.g. Druon et al., 2019; Estes Jr. et al., 2022; Hays et al., 2005). They comprises small, drifting microalgae (phytoplankton) and animals (zooplankton) that based on general description are unable to move against the ocean currents (Kaiser et al., 2011). Some zooplankton have both a planktonic and a benthic life stage (meroplankton), while others are planktonic throughout their entire life cycle (holoplankton, Brander et al., 2016; Kaiser et al., 2011). Both phytoplankton and zooplankton have essential roles in the marine ecosystem, as they dominate in terms of abundance and biomass (Bar-On & Milo, 2019) and transfer energy to higher trophic levels in the marine food web (Barange et al., 2010). Due to their short lifespan, plankton organisms can rapidly respond to changes in the marine environment, and as they are free-floating, their distribution can change dramatically with changes in ocean current systems and abiotic conditions (e.g. temperature, light). They are also not yet intensively commercially exploited, such as commercial fish species, which allows future predictions of long-term changes of plankton standing stocks in relation to changes in biotic and abiotic conditions. Additionally, as a natural community, their response can amplify even subtle environmental perturbations (Taylor et al. 2002). In this way, plankton organisms can serve as biological indicators of water quality and ecosystem health (Estes Jr. et al., 2022). The regional conventions OSPAR and HELCOM are already utilizing plankton information for this purpose (HELCOM, 2009, 2010, 2014; OSPAR, 2003, 2008).

The size of plankton varies greatly, ranging from micrometer (μm) to several meters (Hays et al., 2005). Zooplankton in the size range 0.2-2 mm are called mesozooplankton, and together with microzooplankton (20-200 μm), they make up an important trophic component at lower levels of the marine food web (Hays et al., 2005). They consume phytoplankton and other microplankton, and then in turn serve as a food source for predators higher up in the food web (Barange et al., 2010; Hablützel et al., 2021; Hays et al., 2005). This is how they mainly contribute to energy transfer up the food web. Among the zooplankton, a group of small crustaceans, called copepods, dominate (Barange et al., 2010; Kiørboe, 2010). When abundant, these copepods serve as food for fish and birds (Fragoso et al., 2019a), but they also have another important role in the ecosystem. Through the production of relative fast-sinking faecal pellets, shedding of exoskeletons, diel vertical migration (DVM), and seasonal migrations, they contribute to the carbon capture and sink-out process via the biological carbon pump. DVM is a light-mediated behaviour that enables the zooplankton to benefit from the higher food availability at the ocean surface while avoiding visual predators (Barange et al., 2010; Berge et al., 2020; Gliwicz, 1986; Hays, 2003). By seeking refuge at depth during the day, the carbon consumed in the surface layer at night is defecated and respired at depth (Barange et al., 2010; Brun et al., 2019).

In 2015, Ernesto found that climate change is expected to affect the copepod community substantially (Villarino et al., 2015). A poleward shift in distribution, shifts in phenology

resulting in an earlier seasonal peak, as well as changes in biodiversity, are expected for the copepods in the North Atlantic (Barange et al., 2010; Villarino et al., 2015), and all these changes may propagate higher up in the food web. It is thus crucial to take efforts to predict the impacts of climate change on planktivorous fish and predators further up in the food web and to understand how zooplankton communities are affected by climate change (Ljungström et al., 2020). In August 2021, the Intergovernmental Panel on Climate Change (IPCC) report called for a Code red and stated that climate change is rapid, intensifying, and widespread (Masson-Delmotte et al., 2021). Every region on Earth is already affected by it, and the ocean is no exception. Climate change affects the distribution, occurrence, and abundance of species in the marine environment, as well as the ecosystem function (Barange et al., 2010; Overland et al., 2010; Philippart et al., 2011). As the oceans cover 71% of the Earth's surface and contribute to oxygen production, climate regulation, and contain enormous biodiversity and essential resources (Kaiser et al., 2011; Visbeck, 2018), understanding how climate change affects the ocean is a key issue.

1.2 Traditional and new sampling methods

Plankton abundance and diversity are patchily distributed across the ocean (Kaiser et al., 2011). To increase the understanding of the planktonic community structure, and their spatial and temporal variability, systematic and persistent observations of the upper water column are essential (Saad et al., 2020). Traditional methods, such as seawater samples, net samples, and manual inspection, are useful techniques and have enabled valuable knowledge of plankton composition and dynamics to be obtained (Wiebe & Benfield, 2003). However, traditional techniques are often time-consuming, expensive, and have limited time and space coverage (Saad et al., 2020). Data collection has often been restricted to ship- or station-based measurements and static sensors placed on buoys providing time-series measurements at a given point (Fossum et al., 2018). These methods lack the spatial and temporal coverage and the consistency that is needed to understand the changes that are occurring (Estes Jr. et al., 2022), leading to a low spatiotemporal resolution (Saad et al., 2020) and undersampling (Fossum et al., 2018).

Recently, new tools for ocean sampling and observation have been developed (Barange et al., 2010; Davies & Nepstad, 2017). These include mobile robotic platforms and sensors that facilitate a better ocean data acquisition with a high spatiotemporal resolution. The platforms have become more affordable and robust in recent years and have proven useful for scientific exploration (Fossum et al., 2018). Sensors mounted on satellites, aircrafts and marine robots expand the scope of traditional sampling (Estes et al., 2021), and advances in artificial intelligence (AI) and machine learning (ML) allow for more autonomy (Saad et al., 2020). Additionally, computational science has enabled high-resolution imaging, image analysis, and interpretation in real-time (Saad et al., 2020).

Among the new marine robots, autonomous underwater vehicles (AUVs, Bellingham & Rajan, 2007; Sørensen et al., 2020), have proven especially useful for plankton ecology studies, as they can provide continuous spatial and temporal observations over the mesoscale (Johnsen et al., 2018; Moline et al., 2005; Saad et al., 2020). With its torpedo shape (Fig. 1), high

scientific payload capacity, and 8-24 hour in-water duration (Sørensen et al., 2020), AUVs are efficient platforms for collection of oceanographic data in situ, while being affordable and robust (Fossum et al., 2018). They have a set of orientation sensors and can be customized with different sensors measuring environmental variables as well. They are available in different sizes, for example, the Light AUV (LAUV, Fig. 1, Berge et al., 2020; Fragoso et al., 2019a; Sousa, 2012; Sørensen et al., 2020). Dependent on the power supply, the range of an AUV can vary between 1-100 km and it can cover an area of 0,1-10 km² (Sørensen et al., 2020). It has the unique ability to map the ocean in 3D (longitude, latitude, and depth) and operates either supervised or autonomously. The autonomous nature of the AUV, as well as it being untethered, makes it suitable for operations in unstructured environments with limited accessibility, like under the ice (Berge et al., 2020).

As different platforms, suited with a variety of sensors, capture different information at different scales in time and space, a combination of approaches and a coupling of the information can increase our understanding at multiple levels. It also enables adjustment of model parameters, analysis of performance, cross-verification, and assimilation of data (Fossum et al., 2018). Remote sensing satellite data, near real-time data from buoys or Unmanned Surface Vehicles (USVs), or aerial surveys from Unmanned Aerial Vehicles (UAVs; e.g. drones), are some examples (Sørensen et al., 2020).



Figure 1: LAUV (Light Autonomous Underwater Vehicle) Roald carried by Maren Thu and Andreas Våge at Mausund Field Station prior to deployment. Photo: Annecken Nøland.

Ship-based surveys combined with traditional sampling approaches are suited for in situ ground-truthing of robotic data (e.g. Fossum et al., 2018). Creating such an observational pyramid is a prerequisite for a holistic understanding of the marine environment over large temporal and spatial scales (Sørensen et al., 2020).

1.3 Environmental data

The ocean is responding to natural variations in biotic and abiotic parameters. To understand how these variations are affected by climate change and how it affects the plankton community structure, sampling of physical and biological data is needed (Barange et al., 2010). Key environmental variables (KEVs), such as light, salinity and temperature gives valuable information about the physical ocean processes (Johnsen et al., 2020) and can affect biological processes directly or indirectly. For example, temperature impacts zooplankton distributions directly, as well as their growth (Richardson, 2008).

Biological variables, such as chlorophyll *a* (Chl *a*, a proxy for phytoplankton biomass), zooplankton density, fish abundance, and plankton diversity provide important insights into how the biological environment is responding (Berge et al., 2020; Fossum et al., 2018; Fragoso et al., 2019a; Johnsen et al., 2020). A high concentration of Chl *a* relative to the average concentration indicates a phytoplankton bloom, and in temperate regions, a bloom often occurs in the spring because of calming weather conditions, stratification of the water column, high nutrient availability and longer photoperiods. The high abundance of phytoplankton serves as food for the zooplankton (Assmy & Smetacek, 2009), and a higher abundance of zooplankton results in greater nutrient recycling (Richon & Tagliabue, 2021) and a stronger grazing pressure. This can again affect the phytoplankton community in many ways (Attayde & Hansson, 1999). In this way, the phytoplankton and zooplankton communities are linked and affect each other through top-down and bottom-up controls (Assmy & Smetacek, 2009).

Biogeochemical variables, such as nutrients (Richon & Tagliabue, 2021), oxygen (Estes Jr. et al., 2022), total suspended material (TSM), and dissolved organic material (DOM) also have a strong impact on the ecosystem (Ramírez-Pérez et al., 2017). Especially carbon (C), inorganic nitrogen (N), silicate (Si), and phosphorus (P) are important for plankton, as these nutrients play essential roles in terms of phytoplankton and zooplankton physiology and food quality (Morel et al., 2014). Zooplankton obtain these nutrients by grazing on phytoplankton, and in this way, zooplankton is affected by nutrient availability in the surface ocean (Richon & Tagliabue, 2021). Hence, measurements of KEVs and estimates of biological components and community compositions are important to understand the ocean processes and dynamics, as they can be indicators of productivity, distribution, diversity, and ecosystem health in the ocean (Estes Jr. et al., 2022). Additionally, anthropogenic stressors, like chemical, sound, and light pollution can have additional impacts on the plankton community and the ocean health (Barange et al., 2010; Beaugrand, 2014).

1.4 Plankton analyses with silhouette camera (SilCam)

When seeking to obtain information on plankton abundance and biodiversity, plankton net sampling is the traditional, and well-established method (Wiebe & Benfield, 2003). A new era of advanced bio-optical techniques has emerged in recent years. It has brought along methods such as satellite imaging of phytoplankton blooms and ship-towed equipment that enables high-speed imaging of plankton, such as the Video Plankton Recorder (VPR, Hablützel et al., 2021).

In the period from 2015 to 2017 (Davies & Nepstad, 2017), the silhouette camera (SilCam) for in situ imaging of plankton, was developed by SINTEF. This camera system can be mounted on platforms such as ROVs (Remotely Operated Vehicles, Brandvik et al., 2021), AUVs (Saad et al., 2020), or profiling frames (Davies & Nepstad, 2017). It was originally meant to measure gas bubbles and oil droplets, but today it is used to monitor a variety of objects, among them phytoplankton, holo- and meroplankton (Fossum et al., 2018; Fossum et al., 2019; Fragoso et al., 2019a). Fragoso et al. (2019a) showed that SilCam images can reveal faecal pellets, diatom chains, and marine snow, and Saad et al. (2020) presented images of copepods, bubbles, and fish eggs. The images resemble microscope images, albeit with lower magnification (Fragoso et al., 2019a).

The SilCam imaging system serves as an effective and promising technique for in situ particle recording that, unlike plankton net sampling, is non-destructive (Davies & Nepstad, 2017; Fragoso et al., 2019a; Fragoso et al., 2019b; Sosik & Olson, 2007). It provides information on particle size distribution and concentration (Fragoso et al., 2019a) and can give valuable information about plankton diversity, biomass, and 3D distribution in real-time (Saad et al., 2020). Additionally, when mounted on an AUV together with a variety of sensors, plankton data and other environmental data can be captured simultaneously.

1.5 The AILARON project and plankton classification

The integrated effort of the RCN-funded AILARON (Autonomous Imaging and Learning Ai ROBot identifying plankton taxa in situ, The Research Council of Norway Project #262741) project has shown how a SilCam mounted on an AUV can not only capture images of plankton but also classify targeted plankton in situ (Saad et al., 2020). The goal of the AILARON project is to characterize targeted plankton in situ (Saad et al., 2020) by combining a LAUV with a SilCam and using robotic vision and ML to detect and classify microorganisms in the photic zone (Borgersen et al., 2022; Haug et al., 2021a, 2021b; Salvesen et al., 2022; Teigen et al., 2021), creating a probability density map, and thereby autonomously targeting areas in the survey volume with species of interest (Oftedahl & Sørensen, 2022). More testing and assessment of the method are necessary to reach this goal, which this study will contribute to.

Adaptive sampling is the process where the AUV autonomously follows a target of interest by continuously analysing the captured data online and thereby updating its trajectory

accordingly (Sørensen et al., 2020; Saad et al., 2020). In this adaptive strategy, the images from the SilCam are transferred to an online algorithm onboard the AUV, for plankton classification. This onboard processing is based on ML methods (Saad et al., 2020), where the algorithm is trained to detect certain plankton groups in the images. This allows for monitoring of plankton distribution and community composition, and potentially species-specific biodiversity assessments at high spatiotemporal resolution (Saad et al., 2020).

Besides the adaptive sampling strategy, the AUV can also be programmed to follow a predefined trajectory, or it can be controlled remotely during the mission. It can then be programmed to follow different types of transects, such as a “yoyo” transect (up and down the water column) or an elevator transect (spiralling up and down the water column). It can also do a horizontal transect at a given depth, visit predefined geolocalization points or follow gradients (Fossum et al., 2018; Fossum et al., 2019; Sørensen et al., 2020).

1.6 Overview and aim of study

Through identification, mapping, and monitoring, appropriate knowledge about plankton communities can be obtained. This is crucial to understanding the varying marine ecosystem, especially in the context of global change research, which is constantly pushed further into the field of big data science through the automatic collection of large data sets (Hablützel et al., 2021). This ability to obtain an increased amount of data in both time and space has great importance for ecosystem surveillance, nature management, and monitoring of global change effects (Saad et al., 2020). An understanding of the biological responses also enables the prediction of the global change effects and hopefully mitigation of adverse effects (Hablützel et al., 2021). To be able to do this, utilization of new technologies is a prerequisite to providing information at the time and space scales needed. This study is a part of the bigger Interdisciplinary Algal Bloom Observation Field Experiment at Mausund Field Station 2021, using platforms at different levels in the observational pyramid (ground-truthing, AUV, USV, drone, small plane, and satellite). More specifically, this study is a part of the AILARON project, which is connected to AMOS (Centre for Autonomous Marine Operations and Systems, The Research Council of Norway Project #223254).

This study aims to test the usability of a new method combining an AUV and a SilCam to assess zooplankton community composition in combination with KEVs, providing insights on spatiotemporal variations and plankton dynamics. It also aims to assess the usability of the SilCam system for plankton studies, as well as the performance of two chosen AI algorithms in plankton classification. Zooplankton net samples were obtained to provide data about the actual plankton community composition (ground-truthing), to align this with the SilCam findings of the detectability of different zooplankton groups. The gathering of KEVs by an AUV with a fitted sensor suite was also assessed. This data was combined with nutrient concentration data of nitrate (NO_3^-) and phosphate (PO_4^{3-}) obtained from seawater samples. Altogether, the information from the AUV sensors, the SilCam system and the ground-truthing was combined to give a holistic understanding of the plankton dynamics and community composition at Mausund and in Hopavågen during the spring of 2021.

2 Materials and methods

2.1 Study area

In this section, the two areas of interest, Mausund and Hopavågen, are described (Fig. 2). Both were visited during the spring 2021 and sampling was conducted at Mausund in April (13th and 14th, 20th and 21st) and in Hopavågen in May (4th and 5th). The two locations were chosen based on their accessibility, the productivity of the ecosystems, and their different degrees of exposure.

2.1.1 Mausund

The first study area was located in the Mausund bank (63.8° – 64.2°N, 8.2° – 9.0° E), which is an exposed area located in Froan Archipelago (Fig. 2, Fragoso et al., 2019a; Fragoso et al., 2021). The area lies within Frøya municipality in Trøndelag county, mid-Norway (Fragoso et al., 2019a). The Froan archipelago is a shallow bank that consists of over 3000 islands (Fig. 3). Because of its irregular bathymetry, primary production is facilitated through internal waves, wind, and tidal mixing which in turn stimulates secondary production by zooplankton. This also facilitates biological diversity, which is why the Froan archipelago is considered a biological hotspot (Saetre, 2007). It is a valuable area for the fishing and seafood industry (Fragoso et al., 2019a) through the catch of large scallop (*Pecten maximus*), edible crab (*Cancer pagurus*), Atlantic cod (*Gadus morhua*), and saithe (*Pollachius virens*). The Froan region also serves as a breeding ground for several organisms high up in the food web, such as the grey seal (*Halichoerus grypus*) (Jenssen et al., 2010) and the great cormorant (*Phalacrocorax carbo*) (Lorentsen et al., 2010). Knowledge about the plankton dynamics and distribution in this area is nevertheless limited (Fragoso et al., 2019a).

The Norwegian Coastal Current (NCC) flows through the Froan Archipelago and the Mausund Bank. It consists of brackish water from the Baltic Sea and transports surface water northwards along the coast of Norway, mixing with freshwater runoff from the Norwegian fjords on its way (Skagseth et al., 2011). The North Atlantic Current (NAC) also flows through the Mausund Bank, through side branches reaching the shelf and flowing underneath the NCC surface water. This brings nutrient-rich, saline, and warm water to the Mausund Bank, that can reach the surface through coastal upwelling or internal waves (Barange et al., 2010; Fragoso et al., 2019a).

Mausund was chosen based on its high productivity, biodiversity, and economic value due to commercial fisheries, as well as its dynamic KEV conditions. The 1 km² square with sample points (Fig. 2) was intentionally placed in a relatively exposed area, where it did not interfere with the ferry or boat traffic. The size of the area allowed for use of multiple platforms with different ranges. Additionally, it was not far away from the Mausund Field Station, which made the travel time and expenses low. This allowed for multiple visits to the area of interest in one day.

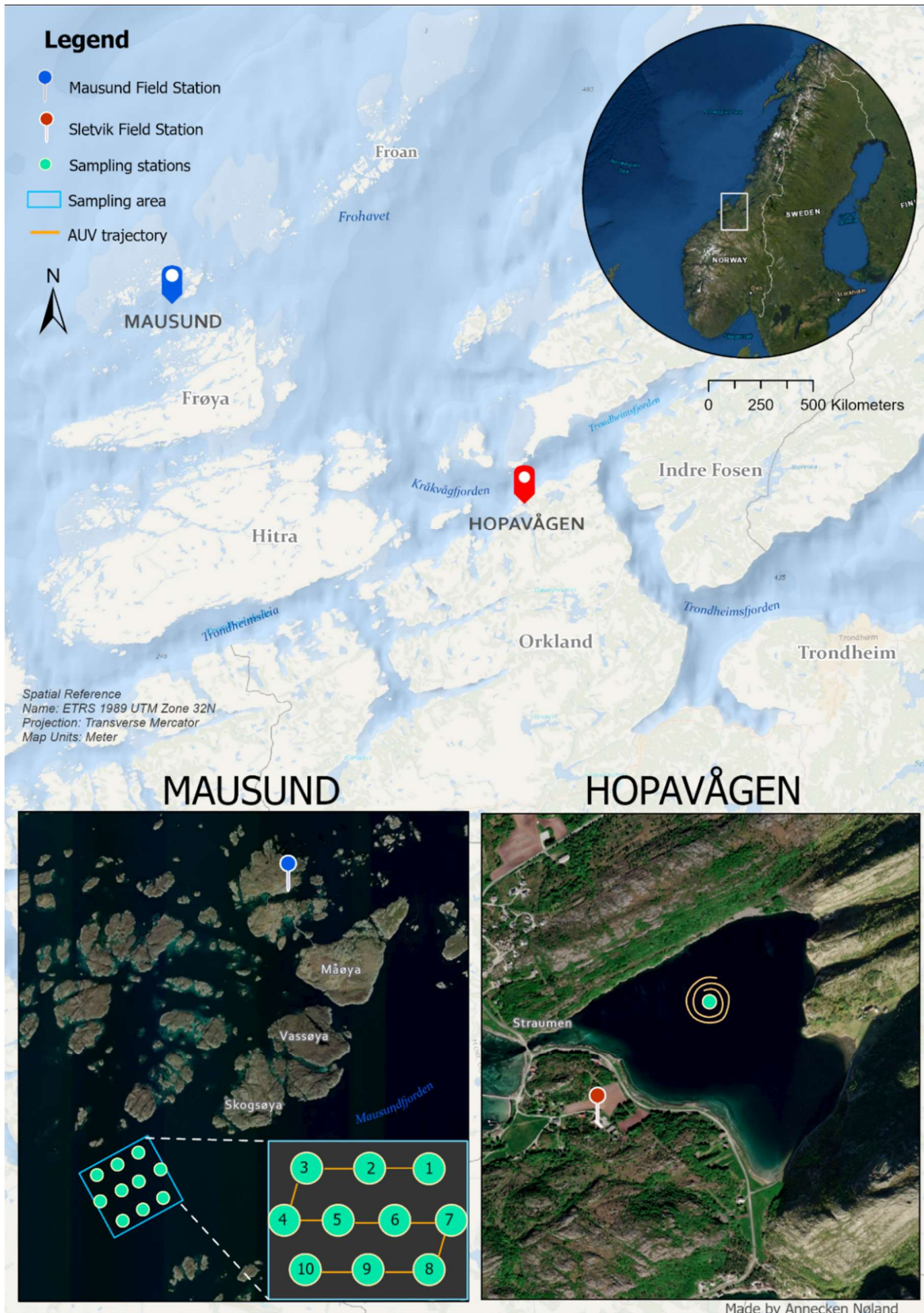


Figure 2: The two sampling locations, Mausund and Hopavågen, including field stations, sampling stations and LAUV trajectory. The sampling station in Hopavågen is station 11. The map is made using ArcGis Pro.



Figure 3: Mausund field station and several small islands located in the Mausund Bank. Photo: Pål Kvaløy.

2.1.2 Hopavågen

The second area of interest was the Hopavågen lagoon, located in Agdenes, Trøndelag (Fig. 2, 63°35'37.8"N 9°32'44.5"E). The lagoon resembles a landlocked bay with a narrow channel that transports seawater in and out of the bay with the tidal currents (Fig. 4). It is sheltered and covers an area of approximately 370.000 m² (van Marion, 1996) with a maximum depth of 32 m (Moriceau et al., 2018) and 1/3 of the basin has a depth exceeding 25 m (van Marion, 1996). Hopavågen is connected to Kråkvågfjorden through a shallow sill called Straumen. At low tide, the depth of the "sill" at the outlet (under the bridge) is 1.0 m and at maximum high tide, it is 1.7 m. Due to the shallow nature of the sill, it partly or completely prevents the renewal of deep water in the basin (van Marion, 1996). Previous studies of zooplankton in Hopavågen suggested that Straumen has a "sorting-effect", based on the discovery that the diversity of plankton taxa in surface layers is lower in the bay than outside the bay. This indicates that most of the zooplankton in Hopavågen originates from outside the bay (van Marion, 1996). Straumen also allows for the daily resupply of nutrients (Sommer et al., 2004). A few small streams bring freshwater into the bay, but relative to the daily inflow from Straumen (14%), their contribution is insignificant (van Marion, 1996).

Stagnant deep water characterizes the hydrography in Hopavågen, separating the upper water column from the deep, and van Marion (1996) found that stratification of the upper layers, having a relatively low salinity and high temperature, takes place in May. This limited mixing of the deep-water can result in oxygen depletion near the bottom, resulting in the production of hydrogen sulphide (H_2S) (van Marion, 1996). Unlike the Mausund Bank, Hopavågen only consists of seawater from the NCC, not the NAC.









Figure 4: Drone photography of Hopavågen, Agdenes. The boat used for sampling is visible on the left-hand side, and the sill is located further to the left. Photo: Annecken Nøland.

2.2 Weather conditions

In the weeks prior to the first visit to Mausund, there had been a storm in the area, leading to the postponement of the trip. The first sampling of data was conducted on the 13th of April 2021, referred to as day M1 from now on. An overview of the name and dates of the six sampling days, including the location and the weather conditions, is shown in Table 1. During sampling on day M1, highly variable weather occurred, consisting of occasionally sunny and cloudy weather conditions, with moments of strong winds, rain, and snowfall. Day M2 had calm conditions with cloudy cover and some sunny moments. In the weekend between the first and the second visit to Mausund, the weather was warm and sunny, with little wind. The nice weather continued to last until day M3 of sampling, but on day M4 it shifted to more windy weather, rain, and a cloud-covered sky. On days H1 and H2, the weather in Hopavågen was sunny with some clouds, and a relatively strong wind was experienced during sampling on day H2.

Table 1: The six sampling days presented with date, time of sampling, location, cloud cover, mean air temperature (°C), mean wind (m/s) and tide (cm). Weather data was obtained from yr.no.

Name of day	Date (DDMMYY)	Time (UTC/GMT+2h)	Location	Cloud cover	Mean temperature in air (°C)	Mean wind (m/s)	Tide (cm)
M1	13.04.21	09:42-13:13	Mausund		2.7	8.4*	118-215 (rising-top)
M2	14.04.21	08:55-09:17	Mausund		5.1	8.0*	69 (rising)
M3	20.04.21	08:46-10:31	Mausund		7.3	6.8	128-100 (falling)
M4	21.04.21	08:42-09:08	Mausund		4.0	7.5	154 (falling)
H1	04.05.21	12:21-14:51	Hopavågen		6.1	4.5	77-96 (bottom-rising)**
H2	05.05.21	10:11-11:35	Hopavågen		6.8	9.2	173-116 (falling)**

*Only daily average is available, potentially resulting in a conflict between observed and measured wind. The area of sampling is more sheltered than the location of the weather station.

**The tide is measured from Ørland metrological station, Trøndelag. There is a delay between the time of high tide in the main fjord compared to when the water enters Hopavågen (van Marion, 1996).

2.3 Materials

In this section, relevant information about the AUV, SilCam, and the algorithms used for plankton classification is presented.

2.3.1 The Light autonomous underwater vehicle (LAUV)

The platform used to obtain data in situ was a LAUV called Roald (Fig. 5, manufactured by OceanScan – Marine Systems & Technology L.da, AUR-lab; Sousa, 2012). It is 226 cm long, weighs 35 kg and can operate down to 100 m depth while moving with a speed of 0,5-2,0 m/s. With a full payload, it has an endurance of 9 hours, and it has a data storage of 3TB. The onboard software (Unified Navigational Environment, DUNE), the message based communication protocol (inter-module communication, IMC) and the command and control software (Neptus) all make up its control architecture (Pinto et al., 2012). LAUV Roald was mounted with a sensor suite consisting of a CTD (Conductivity, Temperature, and Depth) sensor (AML Oceanographic, n.d.), a DVL (Doppler Velocity Log, Nortek, n.d.), and an oxygen optode (Inc., n.d.). It also had a fluorometer to measure chlorophyll *a* (Chl *a*, Turner Designs, 2007). The sensors are presented in Table 2. A SilCam was also mounted on the LAUV (Fig. 5), for imaging of objects present in the water column.

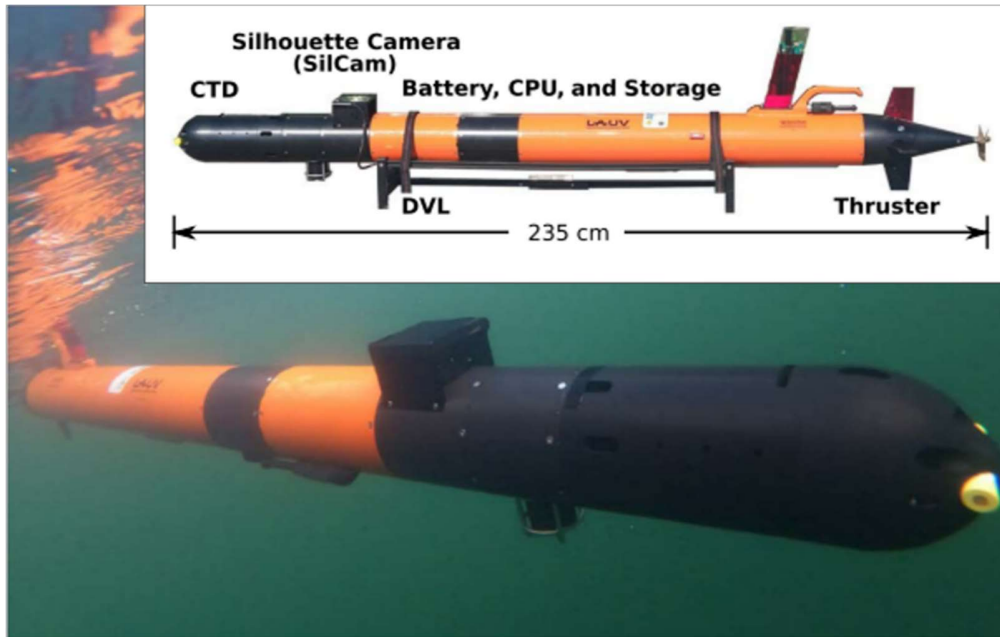


Figure 5: The diagram shows the LAUV mounted with a sensor suite consisting of a CTD, DVL and a SilCam. Its total length is presented, including a picture of the LAUV in situ. The figure is modified from Saad et al. (2020).

Table 2: The sensors on the LAUV relevant for this study, including the name of the producer and model, the parameter they measure and the unit of the parameter.

Sensor	Producer name and model	Parameter measured	Unit
CTD (Conductivity, Temperature, Depth)	AML	Salinity*	Dimensionless
	Oceanographic: X2change sensors	Temperature	°C
		Depth**	m
DVL (Doppler Velocity Log)	Nortek: DVL1000	Water current velocities	Hz
Oxygen optode	Xylem: Aanderaa Oxygen Optode 4831F	[O ₂]	μM
Fluorometer	Turner Designs: Cyclops-7	[Chl <i>a</i>]	μg/L
Silhouette camera	SINTEF: SilCam	Images of plankton and particles	fps

* Measured from conductivity

** Measured from pressure (Bar)

2.3.2 The SilCam system

A SilCam was mounted on the LAUV during the missions, creating quasi-silhouettes of objects in the water column (Davies et al., 2017). The SilCam system consists of three parts: a light source, a water chamber, and a camera unit (Fig. 6). The background illumination consists of a white LED array, and a holographic diffuser helps create a diffuse and clean background. As the water flows through the water chamber, the objects are suspended between the light and the high-resolution colour camera. The camera unit then captures four frames per second (4 fps). Although the objects are suspended at different distances (here: planes) to the camera unit, the telecentric receiving optics create an image where all planes in the image have a constant pixel size and are in focus (Fig. 6, Davies et al., 2017). The SilCam captures a volume of 75.6 cm³ (45 mm × 56 mm × 30 mm) in an image with a circular diameter of >108 mm. The optical resolution used in this project is 27.5 μm (Saad et al., 2020).

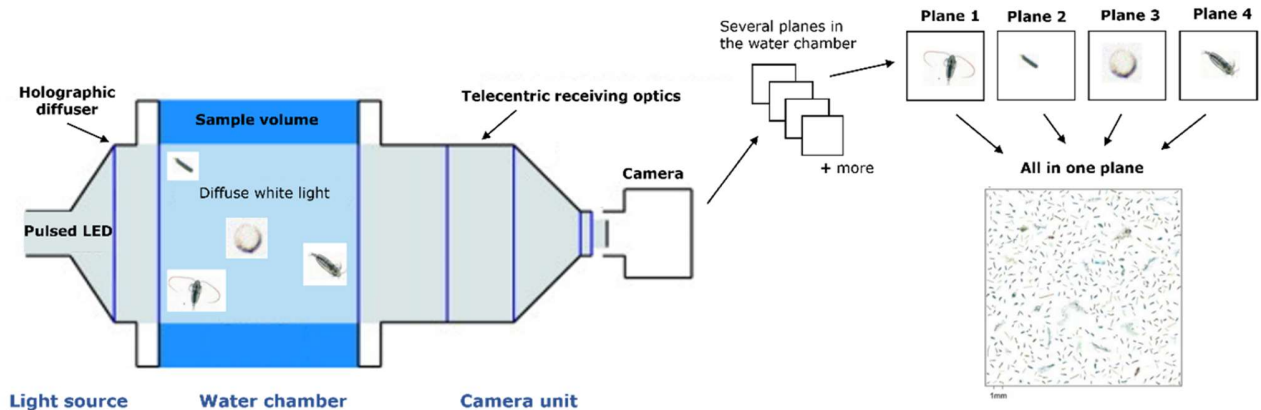


Figure 6: Schematic illustration of the optical configuration of the silhouette camera (SilCam) system, and visualization of how the telecentric receiving optics creates an image of the suspended objects where the pixel size is constant for all planes and all objects are in focus. The figure is modified from Davies & Nepstad (2017), Fragoso et al. (2019a) and Saad et al. (2020).

2.3.3 Artificial intelligence (AI) algorithms

The post-processing of the SilCam images and the classification of the captured objects were initially based on the PySilCam software made by Emlyn John Davies. PySilCam is a Python interface to the SilCam that acquires SilCam images and processes them in real-time or from disk (<https://github.com/emlynjdavies/PySilCam>). The objects (e.g. copepods, faecal pellets, diatom chains) were classified using a subset of ML called Deep Convolutional Neural Network (DCNN, Fragoso et al., 2019a). DCNN identifies patterns in the images. Using a supervised ML method, the deep learning algorithm is trained on a labelled data set created by a human domain expert, to detect objects in the SilCam images and assign these objects into predefined groups (Fig. 7).

The second algorithm used has a new model architecture based on YOLOv5 (You Only Look Once version 5, <https://github.com/ultralytics/yolov5>). YOLO is a novel, fast approach that detects objects in real-time with high accuracy. It trains on full images and directly optimizes detection performance (Redmon et al. 2016). YOLOv5 is the latest version, making it the most advanced object identification algorithm available. PySilCam is based on a shallow network with fewer layers than the new YOLO-based model.

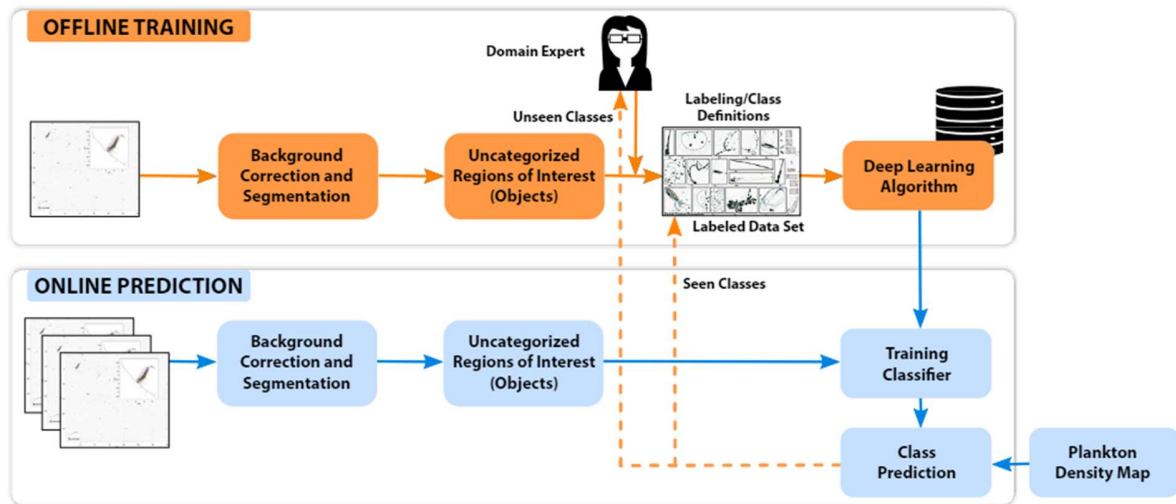


Figure 7. Block diagram of the classification process, obtained from Saad et al. (2020). The model is built offline and through machine learning the model is trained with the help of a domain expert. In the online prediction the onboard in situ processing of detected objects is performed. The offline and online process is visualized in orange and blue, respectively. The dotted arrows represent the predicted objects in situ, where the seen classes represent the groups the algorithm was trained on. The unseen classes represent the groups the algorithm was not trained on. Hence, a domain expert is needed to update the data set.

2.4 Fieldwork

2.4.1 LAUV with SilCam

The mission plan, defining the depth, path, operational area, and type of transect, was pre-programmed in Neptus for all sampling days. At Mausund, the LAUV was programmed to move up and down the water column, in a yoyo transect pattern, from 0 to 40 m depth (Fig. 8). It visited 10 evenly distributed stations in the 1 km² area of interest. In Hopavågen, the LAUV was programmed to encircle a buoy located near the middle of the bay. It did an elevator transect covering the water column from 0 to 20 m depth. Both locations and the LAUV trajectory are presented in Figure 2. The LAUV was deployed and operated by Applied Underwater Robotics Laboratory (AUR-lab) personnel. The SilCam images were uploaded, post-processed on land and then the objects were classified using PySilCam and the new YOLO-based model.



Figure 8: Launching of the LAUV by the AILARON team from motorboat at Mausund, and visualization of the yoyo transect (orange). Photo: Annecken Nøland

2.4.2 Ground-truthing with net hauls and seawater samples

Zooplankton net samples and seawater samples for nutrient analysis were collected at Mausund on days M1 to M4, and in Hopavågen on days H1 and H2, together with Thu (2022). The ground-truthing was done at the same time as the LAUV followed its pre-programmed transect. At Mausund, the 10 stations in the 1 km² area of interest were visited by a motorboat, while in Hopavågen, the single station near the middle of the bay was visited by a rowboat. All sample containers were marked before sampling.

Zooplankton net samples were captured from station 3 (sample M1A and M3A) and station 6 (sample M1A and M3B) at Mausund, and the station in Hopavågen (Fig. 2). They were captured at 30 m at Mausund, using a 200 µm WP2 zooplankton net (Fig. 9, b, 30 cm/s), and at 10-, 15- and 20-meters depth in Hopavågen (Tab. 3) using a smaller 200 µm zooplankton net (Fig. 9, c). The material was collected in marked plastic bottles (250 ml) prefilled with fixatives. Ethanol (97%) was used to preserve the zooplankton net samples, using a concentration of 10%. When returning to the field stations, the samples were kept dark and cold.



Figure 9: Pictures from fieldwork. a) Emptying the NTNU-made seawater sampler. Photo: Maren Thu. b) WP2 plankton net (200 µm) towed from a winch on the motorboat at Mausund. Photo: Annecken Nøland. c) A smaller zooplankton net (200 µm) used from a rowboat in Hopavågen. Photo: Annecken Nøland. d) Seawater sampler in situ. Photo: Geir Johnsen. e) Seawater sample filtrated through a 200 µm sieve into a brown bottle. Photo: Maren Thu.

Table 3: Date and location for the six sampling days, including net sample names, time of sampling and depth. Samples M1A and M3A were taken at station 3. Samples M1B and M3B were taken at station 6. Net samples from Hopavågen were taken from station 11. See Figure 2 for stations, and Table 8 and 9 in Appendix A for seawater samples.

Name of day	Date (DDMMYY)	Location	Net samples			Name of net sample
			Sample	Time (UTC/GMT+2h)	Depth (m)	
M1	13.04.21	Mausund	A	09:08	30**	M1A
			B	11:55	30**	M1B
M2	14.04.21	Mausund	-	-	-	-
M3	20.04.21	Mausund	A	09:15	30	M3A
			B	10:09	30	M3B
M4	21.04.21	Mausund	-	-	-	-
H1	04.05.21	Hopavågen	A	12:37	10	H1A
			B	12:49	15	H1B
			C	12:56	20	H1C
			D	14:31	10	H1D
			E	14:34	15	H1E
			F	14:39	20	H1F
H2	05.05.21	Hopavågen	A	10:41	10	H2A
			B	10:46	15	H2B
			C	10:52	20	H2C
			D	11:22	10	H2D
			E	11:25	15	H2E
			F	11:30	20	H2F

* Because of strong winds, the boat was drifting away from the sample point and the zooplankton net achieved an oblique angle in the water column. To reach 30 m depth, the rope was dragged out to 60 m (marked on the rope), resulting in an increased filtration period.

Seawater samples for nutrient analysis were captured at all stations and multiple depths (0, 5, 15, and 20 m, Appendix A) using a bucket (for surface samples) and a seawater sampler made by NTNU (Fig. 9, a, d). The water was filtrated through a 200 µm sieve while transferred to a brown bottle (Fig. 9, e). When returning to Mausund and Sletvik Field Stations, the seawater samples were filtrated through Whatman GF/F glass-fibre filters (25 mm in diameter, pore size 0.4 µm) using a vacuum pump with gentle pressure (Fig. 10, left), excluding any organic material. Approximately 40 ml of the filtered seawater was then transferred to a test tube (Fig. 10, right) and placed in the freezer. Three replicates (n=3) were taken for each seawater sample, corresponding to a specific station and depth.

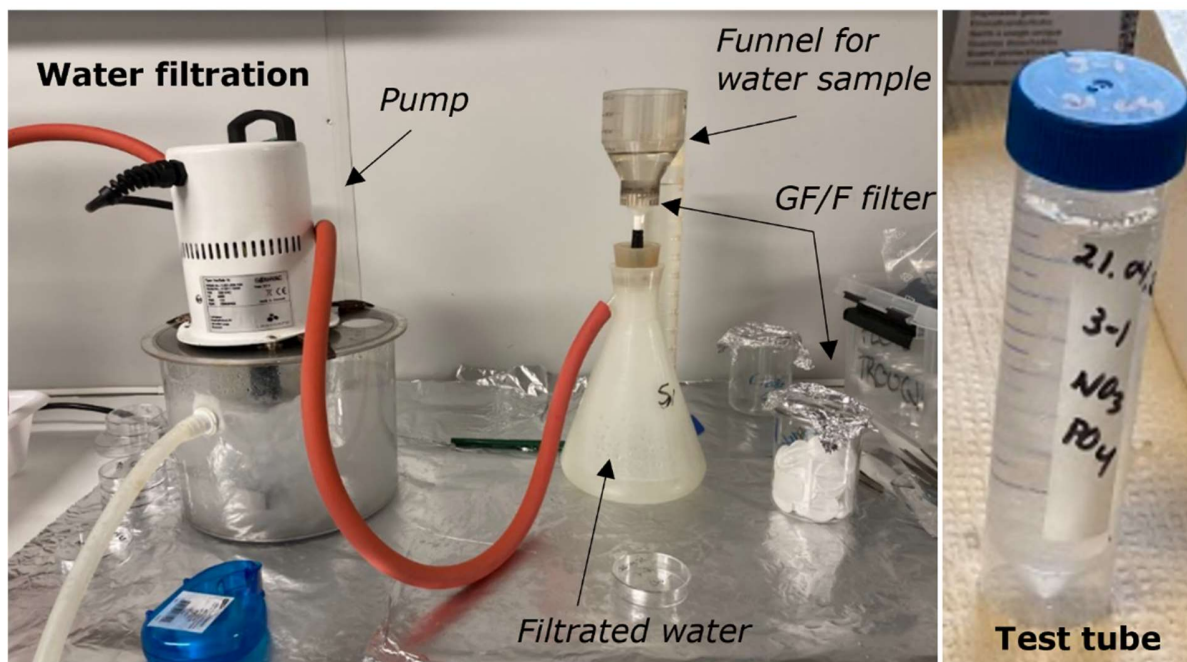


Figure 10: Left: The seawater filtration process showing the funnel (250 ml) for the seawater sample ($n=3$) mounted on a filtering unit containing a plastic grid (filter holder) with a GF/F filter. The filtering unit was placed in a silicon stopper on top of a conical flask containing the filtrated water. The filtration was assisted by the vacuum pump, connected with a rubber hose. Right: A marked test tube used as a container for one ($n=1$) filtrated seawater sample, later analyzed for nutrient concentration. Photo: Annecken Nøland.

2.5 Laboratory work

The fixated net samples were analysed at the zooplankton lab at TBS (Trondhjem Biological Station). Approximately five subsamples were taken from each sample. They were poured through a 200 μm sieve onto a counting tray or Petri's dish, and the sieve was then rinsed with filtered seawater to collect all the material. The material was investigated with a stereomicroscope with an Axiocam ERc 5s camera (ZEISS, n.d.) allowing live images to be sent and observed on a computer (Fig. 11). Pictures of the individuals were obtained to do a qualitative analysis of the zooplankton community composition. Where there was a significant increase in the abundance of a certain plankton group relative to other groups or samples, it was noted.

The seawater samples for nutrient analyses were thawed and transferred to smaller test tubes prior to the analysis of phosphate (PO_4^{3-} , $\mu\text{g/L}$) and inorganic nitrate (NO_3^- , $\mu\text{g/L}$) present in the samples, using the autoanalyzer (Flow Solution IV from O.I.Analytical). The nutrient analysis was conducted according to the Norwegian Standards; NS-EN-ISO6878 for $\text{PO}_4\text{-P}$, and NS4745 for $\text{NO}_3\text{-N}$ (NS4745, 1991; NS-EN ISO 6878, 2004).



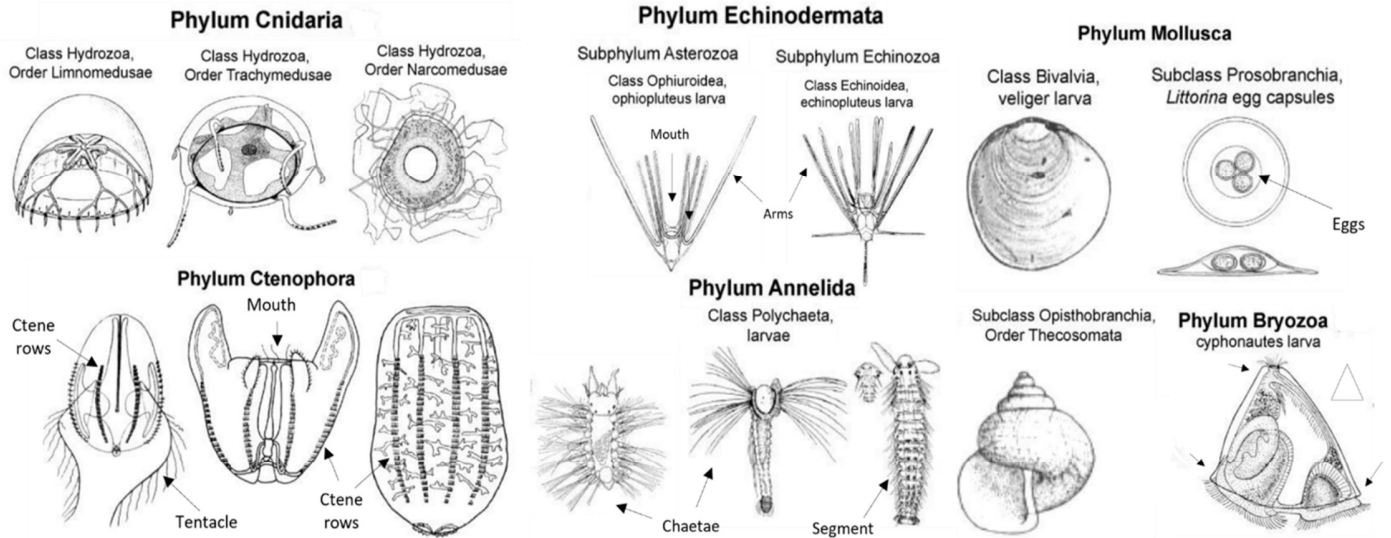
Figure 11: Net sample analysis. Left: Sample M1A and a subsample, including the sieve (200 μm) and seawater used to obtain it. Photo: Annecken Nøland. Right: The stereomicroscope with camera system (AxioCam ERc 5s) attached at the top, enabling images of separate individuals to be obtained (see inset photo). Photo: Annecken Nøland.

2.6 Data analyses

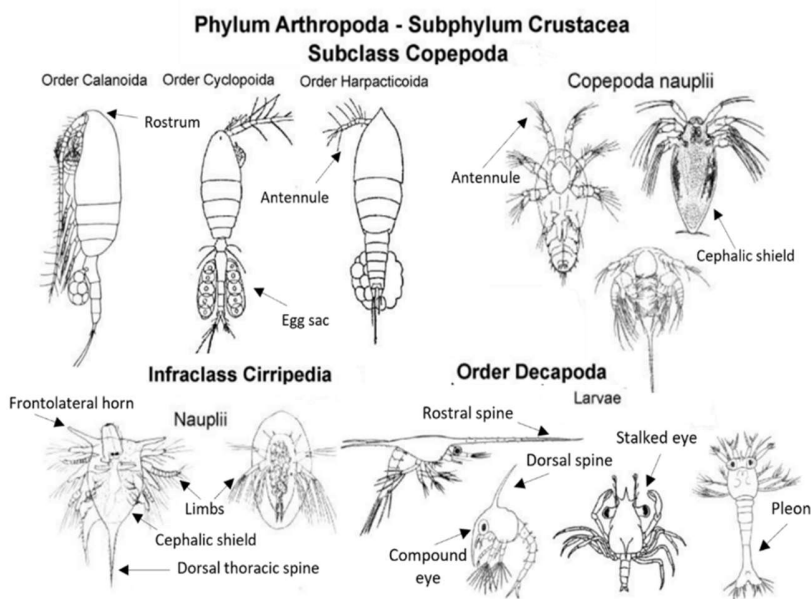
2.6.1 Net sample zooplankton community analysis

The individuals in the pictures were identified according to Coastal Zooplankton (Larink & Westheide, 2011) and WoRMS (World Register of Marine Species (Horton et al., 2022)), with help from more experienced taxonomists at NTNU. They were then placed into folders corresponding to their respective plankton groups. Figure 12 gives an overview of the morphological features of the taxonomic groups most relevant for this study (see Appendix B for more groups). The images that best visualized the characteristic features of each plankton group were collected in folders. These folders were shared with AILARON to function as a labelled data set in future ML of another AI algorithm.

KINGDOM ANIMALIA
NON-CRUSTACEAN ZOOPLANKTON



KINGDOM ANIMALIA
CRUSTACEAN ZOOPLANKTON



KINGDOM PROTOZOA
Phylum Sarcomastigophora
Subphylum Radiolaria

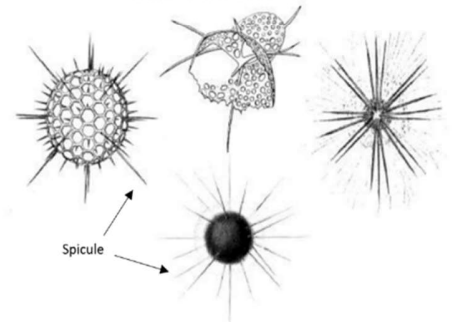


Figure 12: Relevant taxonomic groups of zooplankton. Arrows show morphological characteristics. Figure modified from Conway (2012). For more groups see Appendix B.

2.6.2 SilCam classification and the labelling process

The PySilCam (see 2.3.3) was trained on 7738 images, where 657 of them were copepods, 514 were faecal pellets and 850 were diatom chains. The rest of the images were used for bubbles, oil, oily gas, and the group "other". The reported training accuracy was 95%, but in the analysis, objects with the highest probability of being classified to a given class compared to the other classes were classified, even if the probability did not exceed 95% (because it rarely did).

The new YOLO-based model (see 2.3.3) needed to be trained on a labelled data set, so raw SilCam images from the fieldwork, including some images from fieldwork in Hopavågen in September 2021, were labelled manually. Of the 213 065 images captured, slightly over half of the images were checked by Annette Stahl, whereas only ~5% of them contained biological material of interest. 3619 (~60%) of these images were labelled in the software Roboflow (Dwyer & Nelson, 2019) with help from Maren Thu (Fig.13). Roboflow is a computer vision platform here used for annotation of images for ML. The objects were labelled into groups of e.g. Copepoda, Cnidaria, Echinodermata, faecal pellets, and bubbles. Several objects could not be identified and were therefore separated into groups with similar features, such as objects with round or linear morphology, creating the group "Other". The idea of also labelling these objects was to see which and how many of the objects were unidentified during classification. The algorithm was then trained on the labelled data set and used to classify the objects in the SilCam images into the different groups. Montages showing detected objects identified as copepods, at different depth intervals, were created by Annette Stahl (from the AILARON team). This was also done for the group "Other". It is worth mentioning that this thesis presents the very first version of the entire pipeline of the YOLO-based model.

In the post-processing of the SilCam images using the YOLO-based algorithm, the images were normalized and scaled. Considering scaling, the images are resized so that they all have the same size, thus not necessarily containing their original size. A more detailed description of the post-processing is described below, from background correction (1 to 3), cropping (4) and then normalization (5 and 6):

- 1) A median image, M , is created from five images (I).
- 2) A background-corrected image, C , is computed ($C = |I - M|$), creating an absolute value of the difference in I and M , so that all values are positive. This gives an image with a black background.
- 3) The image is inverted and reflectance, R , is obtained through $R = 255 - C$, for all three colour channels.
- 4) The regions of interest (ROI) containing the detected object is then cropped (the sub-image is extracted).
- 5) The minimum and maximum values of the grey values are computed and linear mapped to the new range with $MIN=0$ to $MAX=255$. This increases the contrast of the image.
- 6) By thresholding (and hole-closing) a mask is computed; a binary image indicating the location of an object in the image. The parts in the mask image where no object is found have a pixel value of 0, while the parts where an object is present have a pixel value of 1.

Knowing in which pixels the object is found, the rest of the image can be neglected, and the object can be visualized without the noisy background. The non-object pixels are all set to 255 (white).

The PySilCam algorithm was assessed based on its identification accuracy and ability to detect different taxonomic groups that were discovered in the net samples. For the YOLO-based model, the labelling process was assessed, as well as the results from the classification of copepods. The same principle as for copepods applies to the other groups labelled in Roboflow. An overall assessment of the functionality of the SilCam system in plankton studies was then done, dealing with the optical resolution of the SilCam and its subsequent taxonomic resolution and its effectiveness.

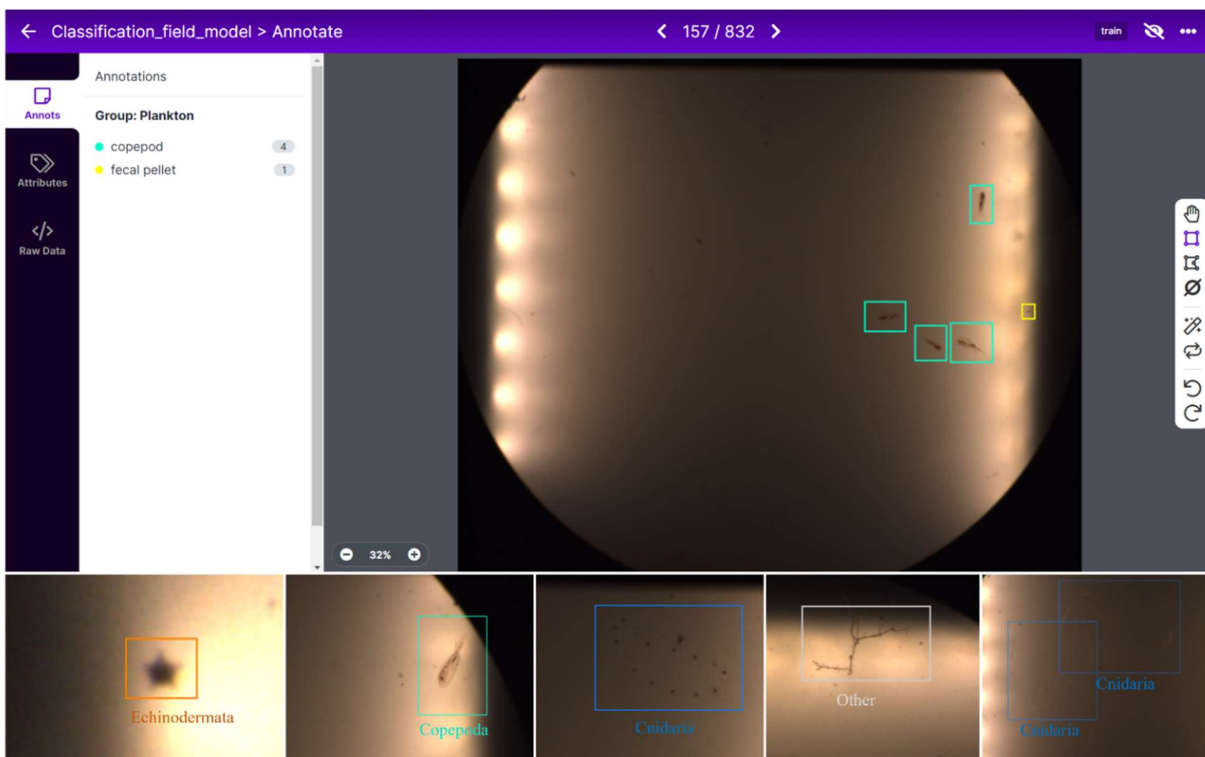


Figure 13: Raw images from the SilCam system imported in Roboflow and manually labelled by drawing a polygon and assigning the objects to different groups. Shown here (from bottom left) is an echinoderm, a copepod, a hydromedusa (grouped as Cnidaria), detritus (grouped as "Other") and two overlapping cnidarians.

2.6.3 Data analysis of Key Environmental Variables (KEVs)

KEV data collected by the sensors on the LAUV (Tab.2) was analysed using RStudio, an integrated development environment for the statistical software R. Merged data of the salinity, temperature (°C), and depth (m) measurements from each mission were obtained as CSV files from the CTD through Neptus. Dissolved oxygen [μM] and chlorophyll *a* ($\mu\text{g/L}$) measurements were obtained in the same way from the oxygen optode and the fluorometer, respectively. The CSV files, including the navigation data, were exported to RStudio and plots were generated mainly using the packages ggplot2, dplyr and cowplot. See Thu (2022) for a principal component analysis (PCA) of the effects of the KEVs on the phytoplankton biomass and community structure.

The nutrient data obtained from seawater samples were analysed using Excel and RStudio. The mean of the three replicates ($n=3$) for each seawater sample was calculated in RStudio using the `group_by()` and the `summarise()` function. The packages ggplot2, dplyr, and RColorBrewer were used to plot the measurements for each day, separating the different days and depth by colour and point shapes. A boxplot of the measurements was also created using the function `geom_boxplot()`, showing the distribution of the data.

3 Results

3.1 SilCam montages from PySilCam

Presented here are montages from day M1 (Fig. 14) created by the PySilCam. The identified objects are those with the highest probability of being classified to a given group. This is a collection of various objects, some relatively easy to identify (marked with a green circle) and

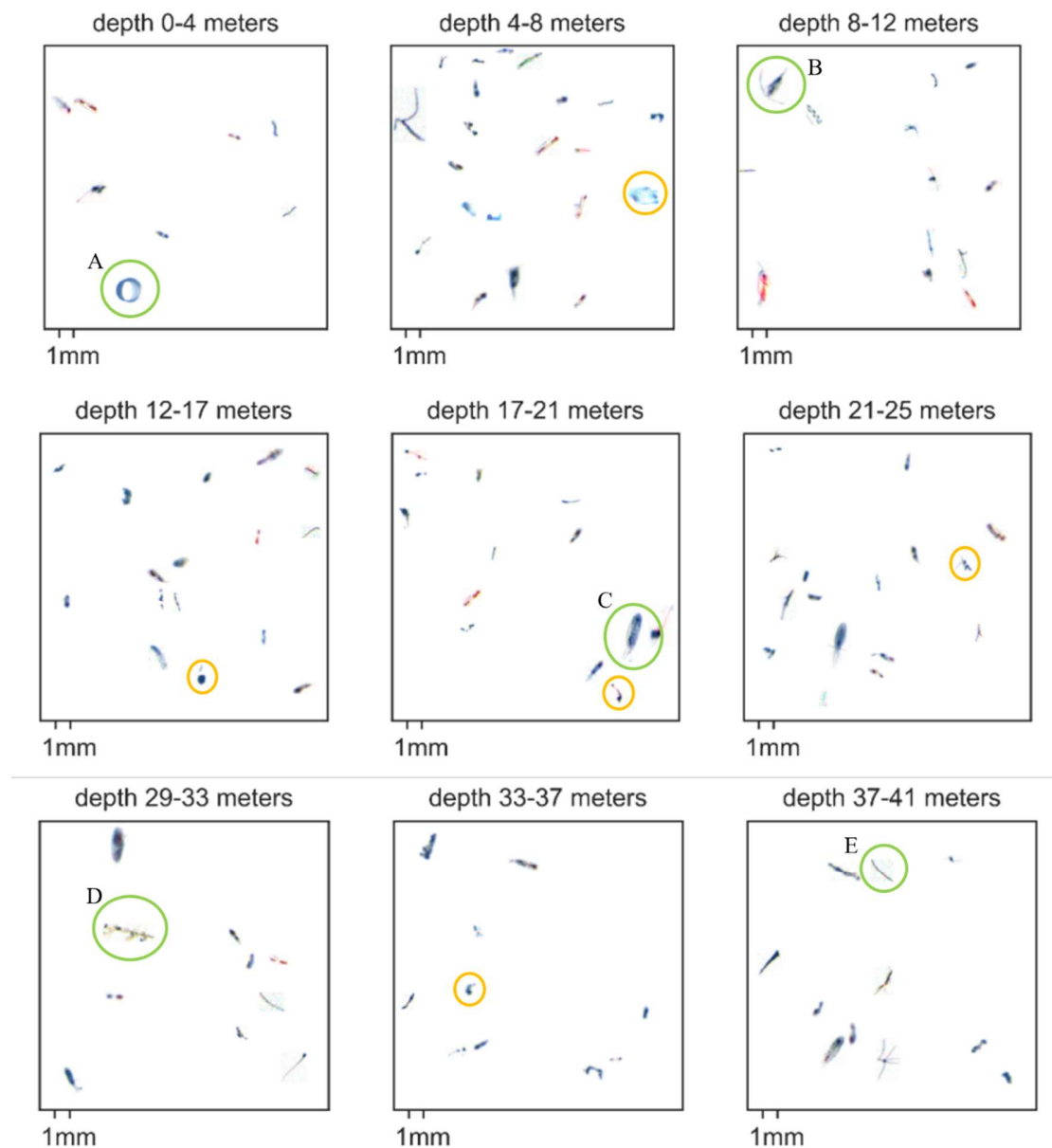


Figure 14: Montages of post-processed SilCam sub-images of detected objects from day M1 from 0 to 41 m depth, obtained with PySilCam. Green circles mark examples of identifiable objects; bubble (A), copepod (B, C), detritus (D), faecal pellet (E). Yellow circles mark examples of unidentifiable objects.

some unidentifiable (marked in yellow). Copepods, bubbles, detritus, and faecal pellets are detectable, but smaller objects with less distinct characteristic features cannot be identified to any of the given classes with certainty.

3.2 SilCam montages of classification results from the YOLO-based model

The objects in the SilCam images classified as copepods by the YOLO-based model were gathered in montages. Figure 15 gives an example of the montages of objects classified as copepods before post-processing of the images, showing the depth interval 20-30 m on day M1. These images are sub-images from the SilCam images, thus retaining the same optical settings, background, and original size relative to each other. They are the basis for the further post-processing. The montages for the different depth intervals from day M1 (Tab. 4) and M3 (Tab. 5) contain the post-processed images where the objects are normalized and scaled (see 2.6.2). Montages of objects classified as belonging to the group "Other" are presented in Appendix C.

The montages of the post-processed images classified as copepods (Tab. 4 and 5) showed mostly copepods. Still, in a lot of the images only the internal parts of the copepods were visible, thereby losing characteristic morphological features. Some of the objects were also too blurry to identify. The montages contained images of detritus, faecal pellets, and bubbles, but no other taxonomic groups were present in the copepod montages, nor in the montages of the group "Other" (Appendix C).

A collage of the best images of copepods found in the SilCam montages from day M1 and M3 is presented in Figure 16, and a collage of other objects misclassified as copepods found in the copepod montages is presented in Figure 17. The latter shows detritus, bubbles, faecal pellets, and unidentifiable objects and indicates which forms and features the classifier fails to separate from the copepods. Not included in the collages are the sub-images where no object is visible, leaving only a blank image, but this is also an important finding.

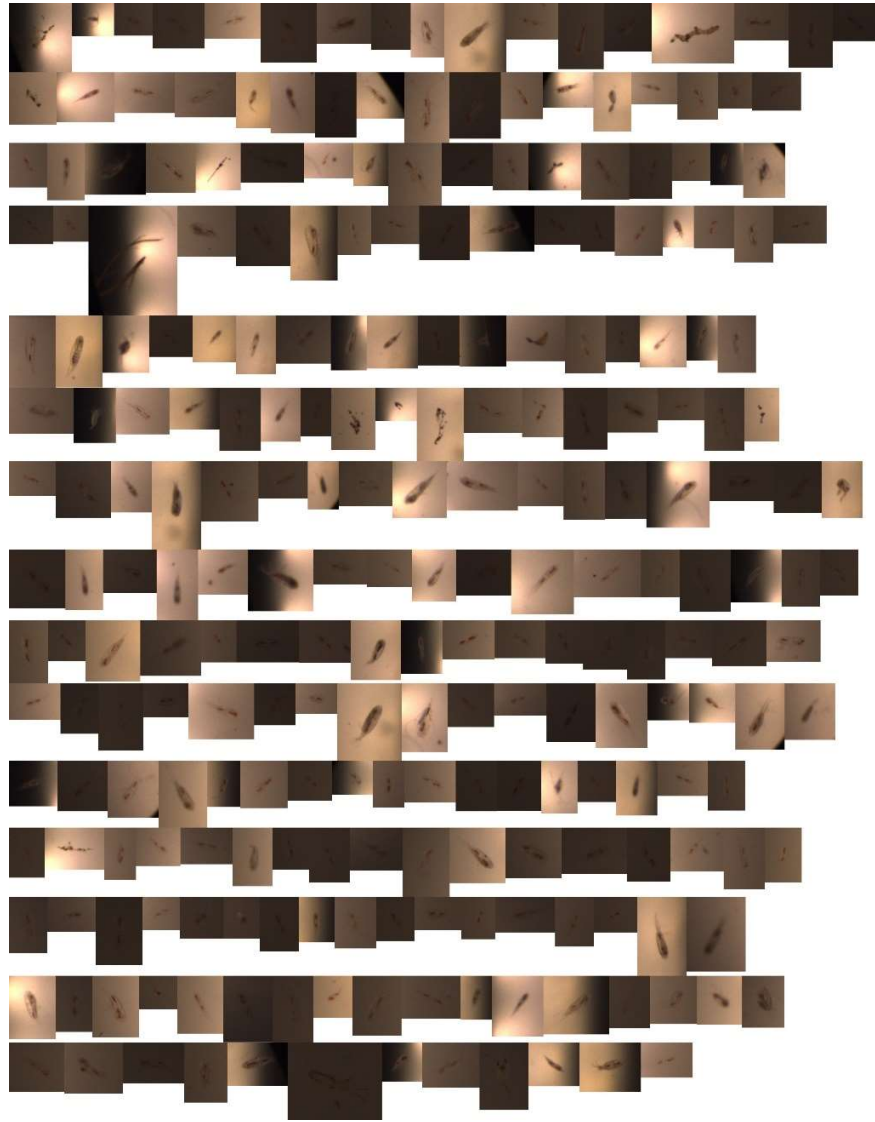




Figure 15: Montage of objects of interest in the SilCam images classified by the YOLO-based model as copepods. The images are from day M1, and from the depth interval 20-30 m. They are not post-processed and are in their original size relative to each other.

Table 4: Montages of objects in the SilCam images from day M1 classified by the YOLO-based as copepods, presented for the depth intervals 0-10, 10-20, 20-30, and 30-40 m. The objects are normalized, and the images are scaled.

COPEPOD MONTAGES	
Normalized objects – scaled	
Depth (m)	DAY M1
0-10	

(Table 4 proceeds on the next page)

<p>10-20</p>	
<p>20-30</p>	

(Table 4 proceeds on the next page)

30-40

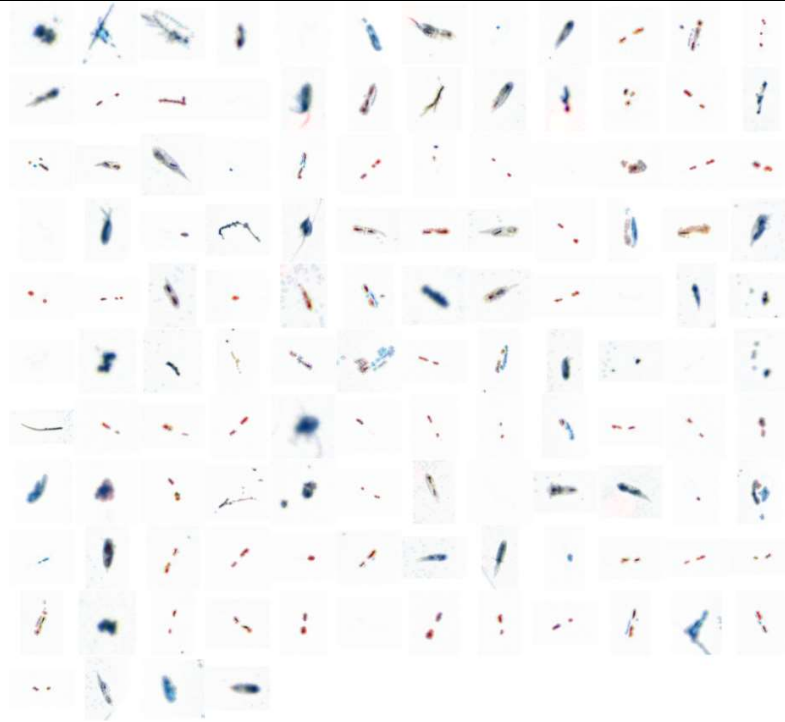
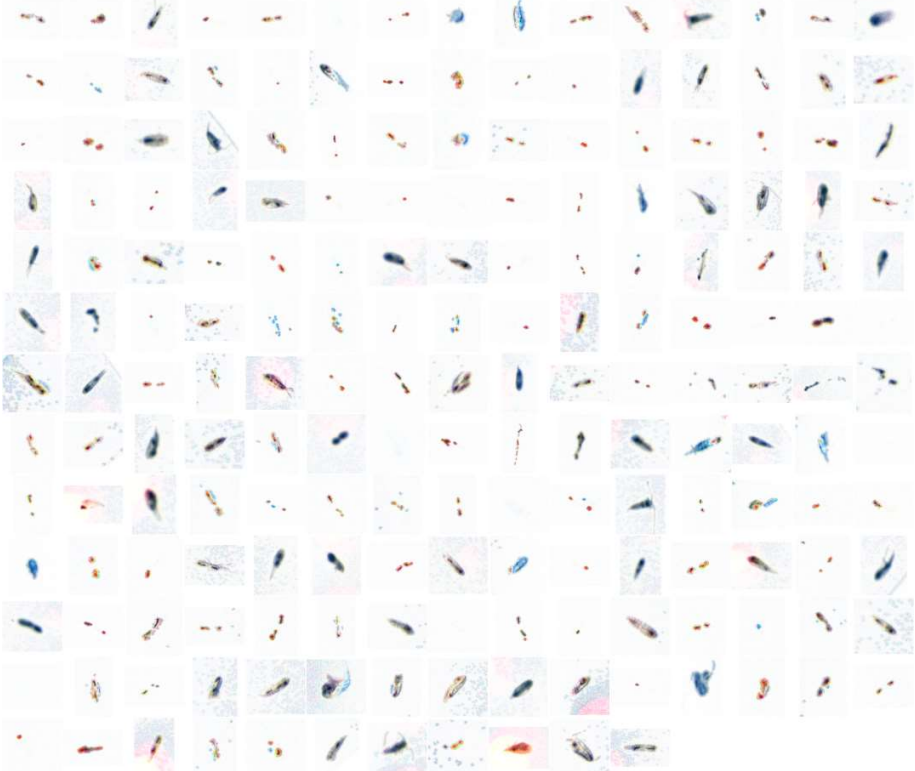



Table 5: Montages of objects in the SilCam images from day M3 classified by the YOLO-based model as copepods, presented for the depth intervals 0-10, 10-20, 20-30, and 30-40 m. The objects are normalized, and the images are scaled.

COPEPOD MONTAGES Normalized objects - scaled	
Depth (m)	DAY M3
0-10	

(Table 5 proceeds on the next page)

<p>10-20</p>	
<p>20-30</p>	

(Table 5 proceeds on the next page)

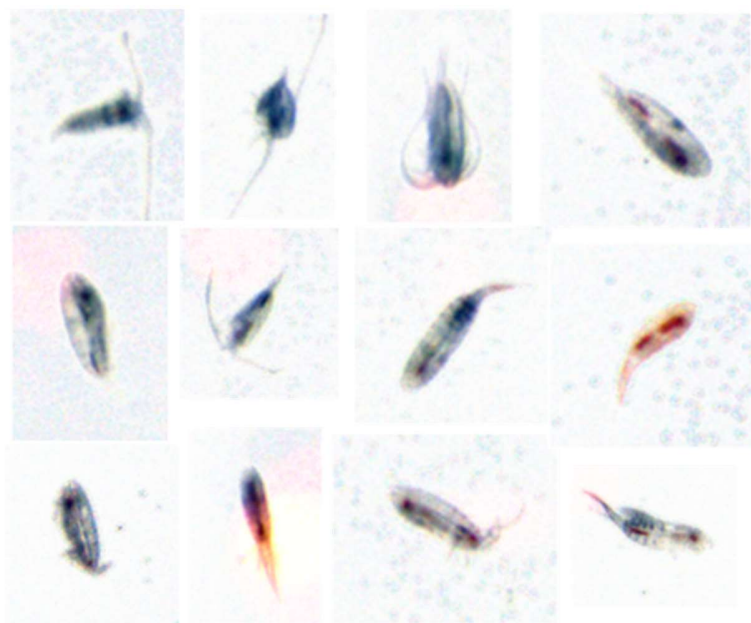


Figure 16: A selection of classified copepods from the SilCam montages using the YOLO-based model classification (Tab. 4 and 5). The copepods are visualized in their in situ orientation to the camera.

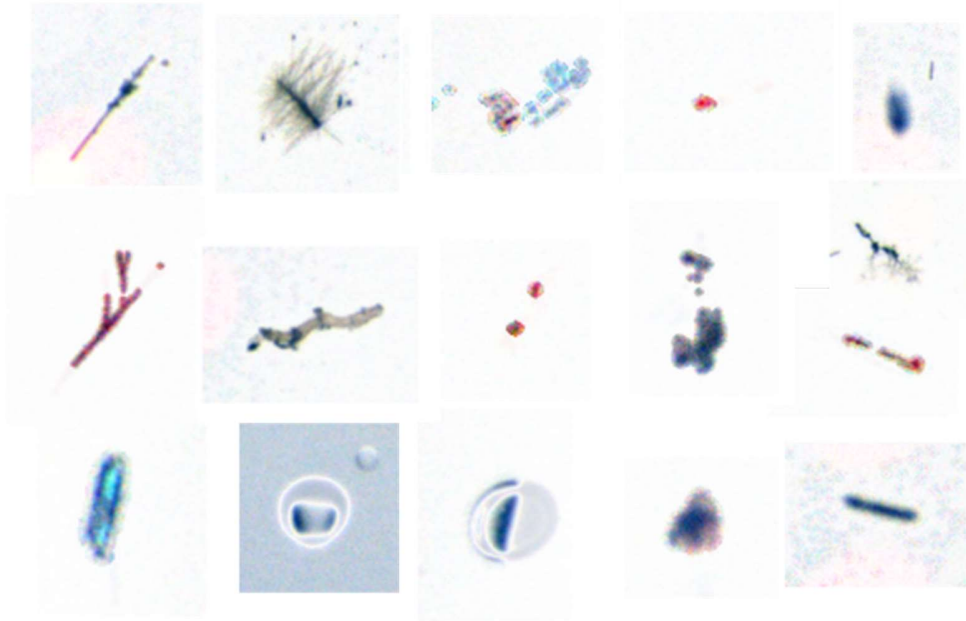


Figure 17: A selection of other objects misclassified as copepods from the SilCam montages created from the YOLO-based model classification (Tab. 4 and 5). The images show detritus, bubbles, faecal pellets, and objects out of focus and with low optical resolution. Some of the images are also overexposed, making only a part of the object visible.

3.3 Detection of zooplankton groups in SilCam images

For assessment of the detection of the chosen plankton groups in the SilCam images, the raw images labelled in Roboflow were used. This was done due to complications with data retrieval of classified SilCam images (see 4.1.6). Table 6 shows the groups detected in the raw SilCam images. Copepods and cnidarians were most detectable, including faecal pellets. Some round objects considered as the phytoplankton diatom *Coscinodiscus* sp. were observed and labelled, as well as one Decapoda, one Polychaeta larvae, and one more developed echinoderm.

Table 6: Detection of zooplankton groups present in the net samples (see section 3.4) in the raw SilCam images during the labeling process, including eggs, phytoplankton, and faecal pellets.

Detection of	SilCam	Detection of	SilCam
Crustacea		Mollusca	
Copepods	Yes	Bivalvia	No
Copepod nauplii	No	Gastropoda	No
Cirripedia	No		
Decapoda	Yes		
Bryozoa larva	No	Radiolaria	No
Echinodermata larva	Yes	Eggs	No*
Cnidaria			
	Yes	Phytoplankton	
		Dinoflagellata	No
		Diatoms	Yes
		<i>Coscinodiscus sp.</i>	Yes
Annelida		Miscellaneous	
Polychaeta larva	Yes*	Faecal pellets	Yes

*Some of the objects could belong to this group, but a higher optical resolution would be needed to confirm this.

3.4 In vivo analysis of zooplankton community composition in net samples

This section presents the taxonomic zooplankton groups detected in the net samples through stereomicroscopy and imaging, including some other selected groups. The groups are presented through stereomicroscope images and then the manual inspection of the community composition in the separate net samples is presented in tables.

3.4.1 Net sample groups

The net samples (Tab. 3 and 7) analysed in vivo contained several zooplankton groups, some of which are presented in Figure 15 to 22. The figures show species lying in different directions related to the lens, as to give a perspective of how the SilCam might capture them floating in the water masses. This is to visualize how the AI algorithm must be trained on several floating individuals to be able to identify a species from several directions and angles. Figure 12 shows characteristic morphological features that are used to identify the plankton groups. The species presented in the collages were identified to the highest taxonomic level possible from the stereomicroscope images. Some selected groups of other marine objects drifting in the water column together with the zooplankton are also included (Fig. 27 and 28). The groups (eggs, phytoplankton, and faecal pellets) were chosen based on their abundance, size (they are visible in the stereomicroscope), and their importance in the zooplankton community.

CRUSTACEA: COPEPODA

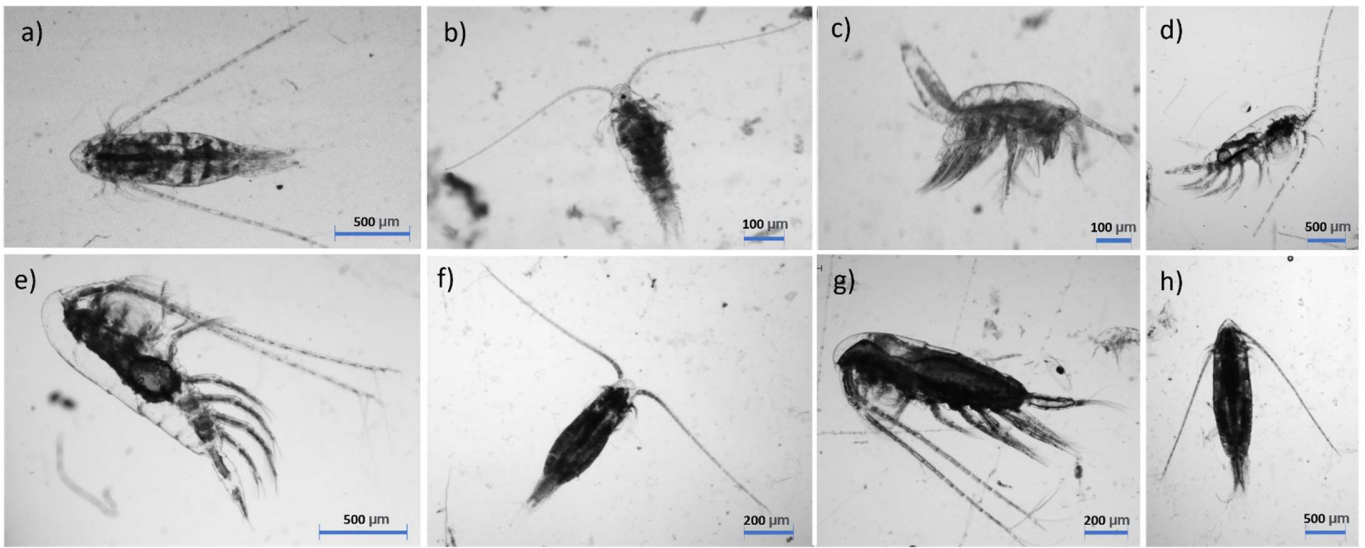


Figure 18: Selected stereomicroscope images of copepods from the net samples, lying in different orientations relative to the lens. From top left: a-h) Calanoid copepods.

CRUSTACEA: OTHER

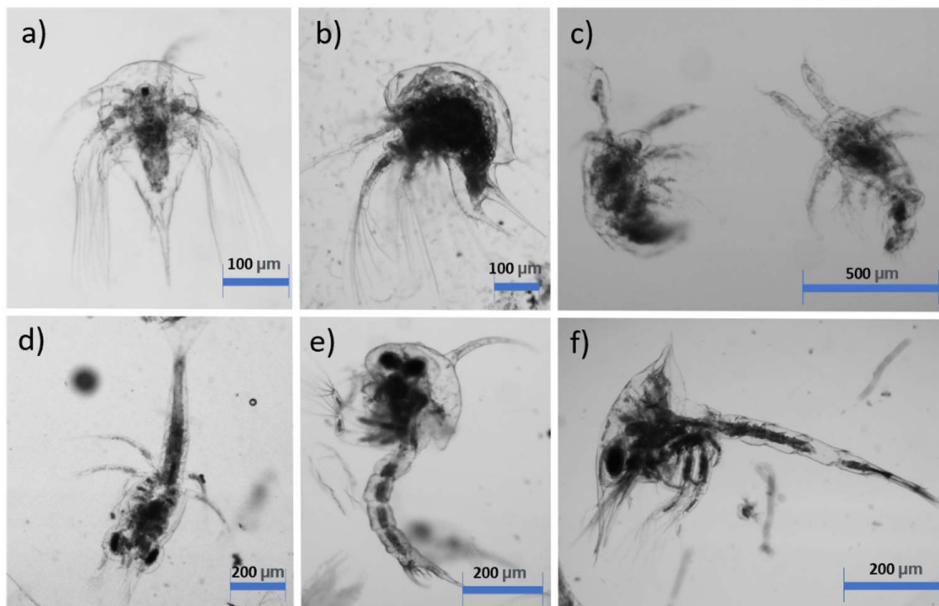


Figure 19: Selected stereomicroscope images of other crustaceans from the zooplankton net samples. a-b) Ventral and lateral view of Cirripedia nauplius (Barnacle larva), *Balanus* sp., c) Copepoda nauplii, d) Decapoda, e) Decapoda, *Carcinus maenas*, f) Decapoda, *Pagurus bernhardus* (hermit crab).

NON-CRUSTACEAN ZOOPLANKTON

BRYOZOA LARVA

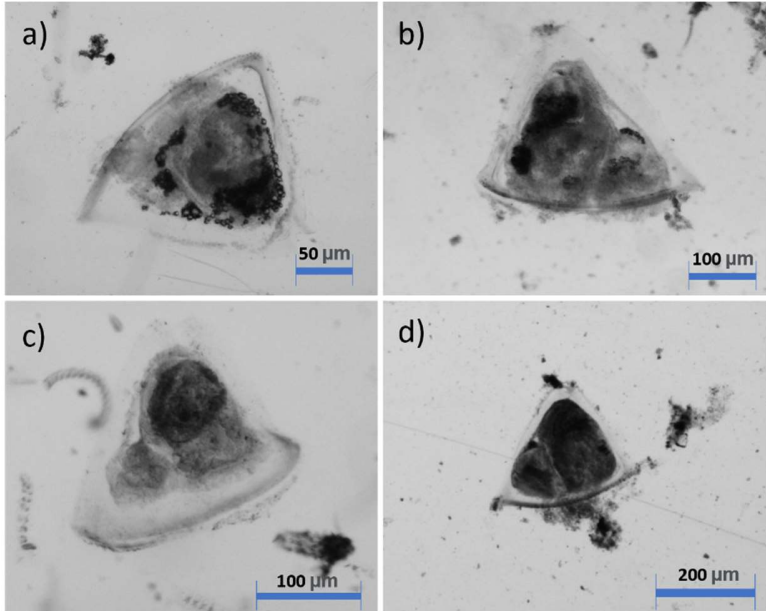


Figure 20: a-d) Bryozoa larva.

RADIOLARIA

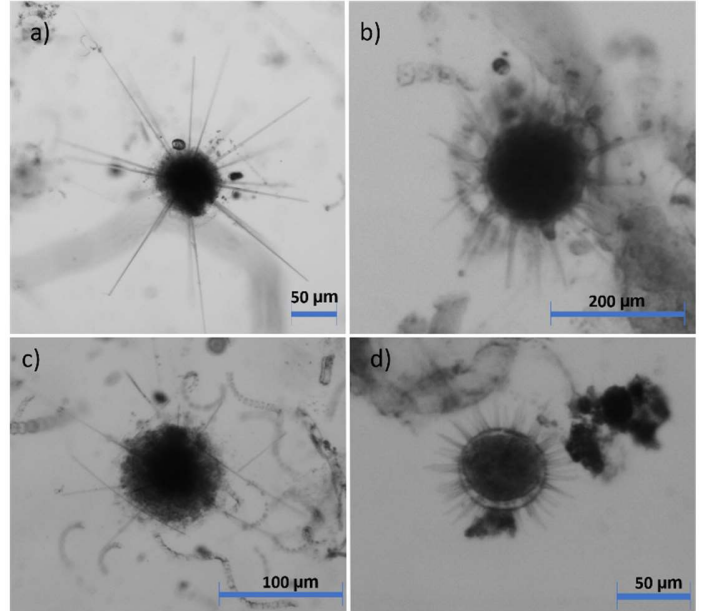


Figure 21: a-d) Radiolaria.

POLYCHAETA LARVA

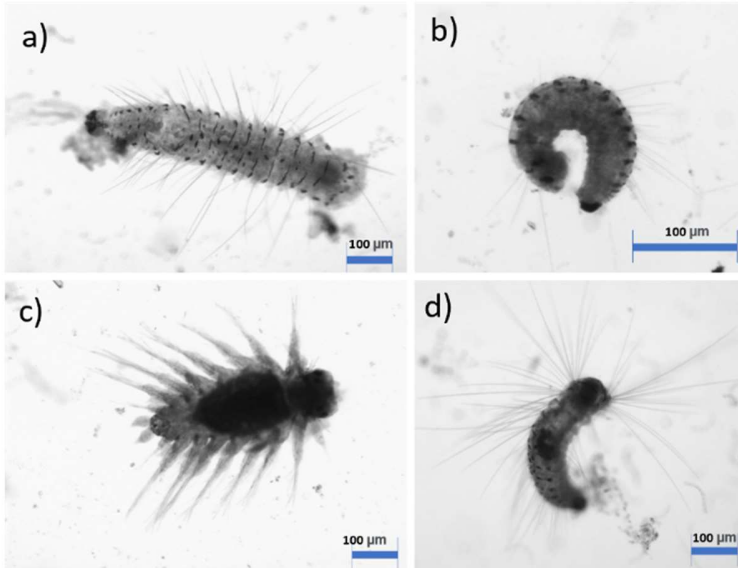


Figure 22: a-b, d) Spionidae larvae, c) Nereididae larvae.

CNIDARIA

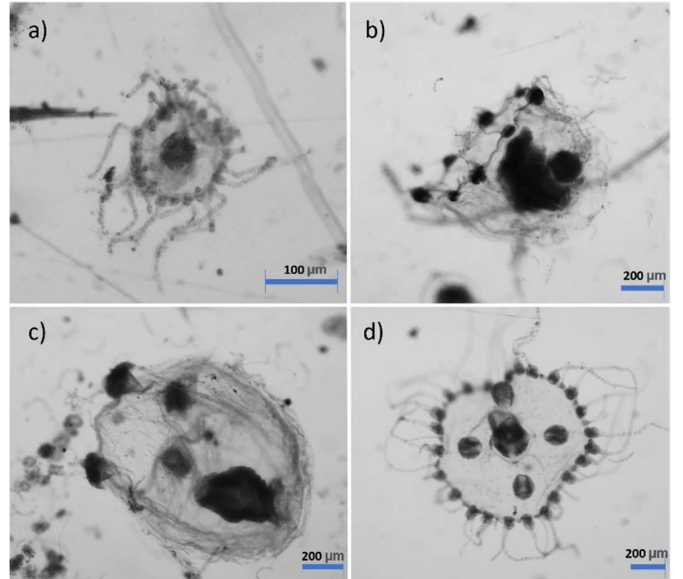


Figure 23: a) Hydrozoa indet, b) *Rathkea octopunctata*, c) Hydromedusae, d) *Obelia* sp.

ECHINODERMATA

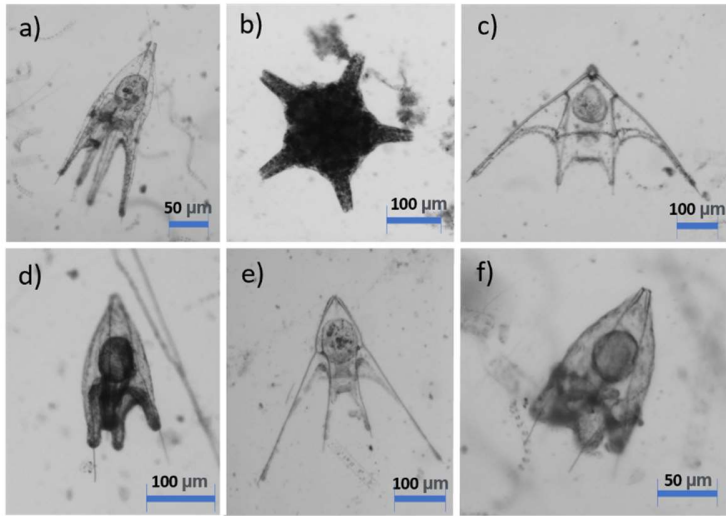


Figure 24: a, e, f) Echinodermata larva, b) Ophiuroidea larva, c) *Ophiothrix* sp. (Common brittle star).

MOLLUSCA

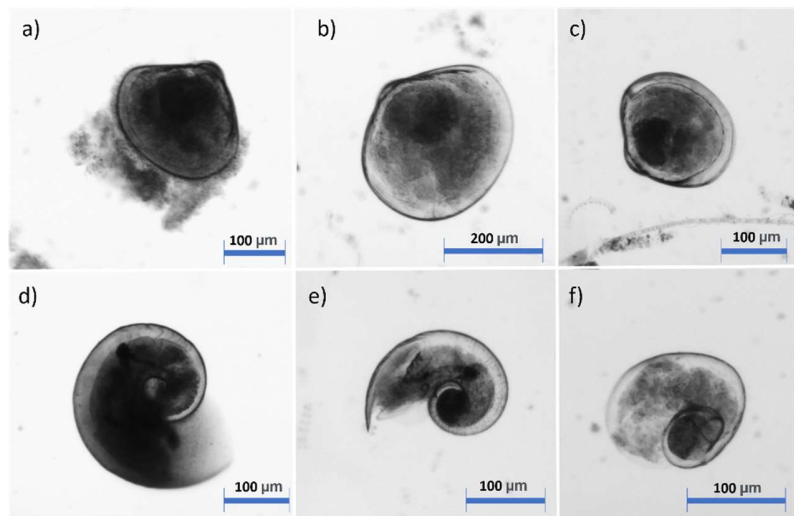


Figure 25: a-c) Bivalvia, d-f) Gastropoda.

OTHER ORGANISMS AMONG THE ZOOPLANKTON

EGGS

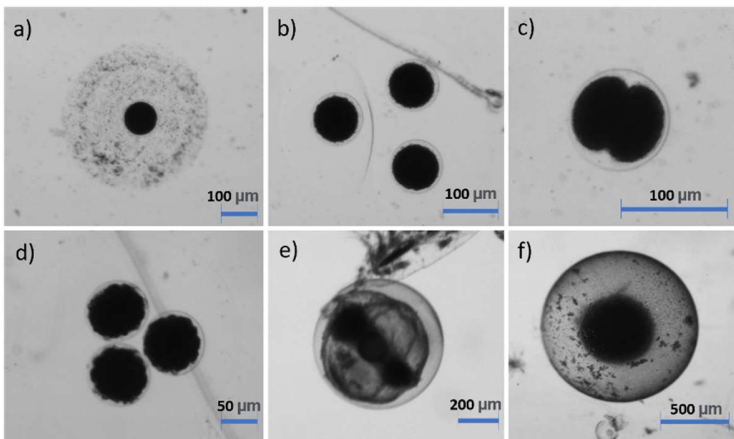


Figure 26: a-d) Gastropod *Littorina littorea* (different developmental stages), e) Fish egg, f) egg (unknown).

PHYTOPLANKTON

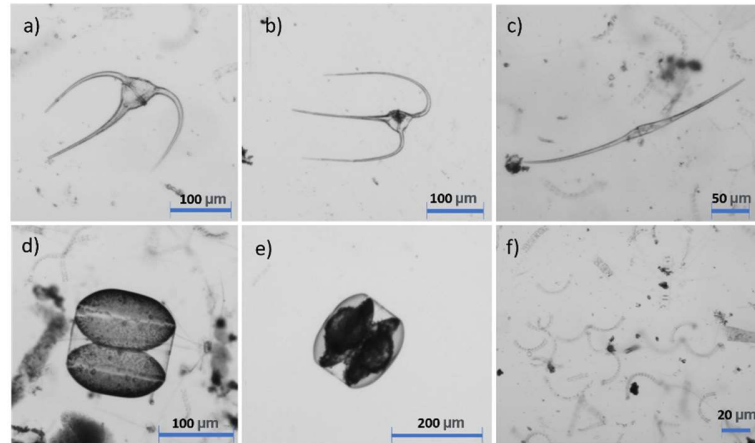


Figure 27: a-c) Dinoflagellata (Dinophyceae), *Tripos longipes* (a), *Tripos macroceros* (b), *Tripos fusus* (c), d-f) Diatoms (Bacillariophyceae), *Coscinodiscus* sp. (d, e), and *Chaetoceros* sp. (f).

3.4.2 Zooplankton community composition in net samples

An overview of the zooplankton groups present in the net samples (Tab. 7) was created to show the actual zooplankton groups present in the water during sampling and investigate qualitative differences in the zooplankton community composition. Only the zooplankton groups that were most abundant and that could be identified to a certain taxonomic level were included. As also associated groups (eggs, certain phytoplankton groups, and faecal pellets) were detected in most samples, an overview of their presence or absence is shown in Table 6. A high abundance of a given group relative to other groups or samples is noted with "xx" but note that this was not a proper quantitative analysis. See Thu (2022) for phytoplankton groups present in phytoplankton net samples gathered during the same fieldwork.

On day M1, two net samples were taken: sample M1A (from station 3) and sample M1B (from station 6) (Tab. 3, Fig. 2). In sample M1A a relatively high abundance of copepods of different sizes was observed. Among the zooplankton groups, the copepods dominated, but there were also a lot of copepod nauplii and Cirripedia (Fig. 19). Some Decapoda, Bryozoa larvae, and Gastropoda were also found in the net sample (Tab. 7). In M1B, a few Echinodermata larvae were also detected. More eggs and diatom chains (more specifically *Coscinodiscus* sp.) were detected in both samples, but no dinoflagellates (Tab. 8). Some faecal pellets were present. Overall, compared to the net samples from later samplings, samples M1A and M1B contained a lot of material, had a high dominance of copepods, but had a somewhat lower biodiversity.

On day M3, net samples M3A and M3B were collected from 30 m depth at stations 3 and 6, respectively (Tab. 3, Fig. 2). In sample M3A, it was still a high abundance of copepods, but not as high as on the first visit to Mausund. Sample M3A also contained a lot of Cirripedia and Echinodermata larva, including some copepod nauplii, a few Decapoda, and Bryozoa (Tab. 7). Sample M3B had significantly fewer copepods, Cirripedia and Echinodermata larva, but more Bryozoa larva. It also had one Bivalvia and one Polychaeta larvae. Considering non-zooplankton groups, both net samples consisted of eggs, faecal pellets, phytoplankton (very little), and detritus (Tab. 8). More faecal pellets were present in this sampling compared to the first.

In Hopavågen, the net samples (H1A to H2F) consisted of significantly less material than at Mausund. The samples contained more detritus and some of it stuck to gelatinous secretions creating aggregates together with plankton. There were relatively few copepods and copepod nauplii present at all depths, and Decapoda was only observed in net samples from day H1 (Tab. 7). Some Cirripedia, Bryozoa larvae, and Polychaeta larva were present, and more Mollusca was present than at Mausund. Also, net samples from Hopavågen included Cnidaria and Radiolaria, which were not present at Mausund. Various gastropod eggs from *Littorina littorea* and fish eggs (Fig. 26) were present on all days, including faecal pellets and phytoplankton (Tab. 8). The faecal pellets had a lower optical density than those at Mausund and were less abundant. There were also significantly more diatom chains and dinoflagellates in Hopavågen, especially on day H2.

Table 7: Presence (x) or absence (-) of selected groups of holo- and meroplankton in the net samples from Mausund (M1A to M3B) and Hopavågen (H1A to H2F, Tab. 3) detected and photographed in the stereomicroscope. A high abundance relative to other groups or samples is marked with xx. The subphylum Crustacea is divided into subclass Copepoda, Copepoda nauplii, infraclass Cirripedia, and the order Decapoda. The phyla Bryozoa, Echinodermata, and Cnidaria are presented. The organisms from phylum Annelida are all Polychaeta larvae and the phylum Mollusca is divided into class Bivalvia and class Gastropoda (snails). The subphylum Radiolaria are protozoans. Images of each group are presented in Figures 18 to 25.

	CRUSTACEA				BRYOZOA LARVAE	ECHINODERMATA LARVAE	CNIDARIA	ANNELIDA Polychaeta larvae	MOLLUSCA		RADIOLARIA
	Copepoda	Copepoda nauplii	Cirripedia	Decapoda					Bivalvia	Gastropoda	
M1A	xx	xx	xx	x	x	-	-	-	-	x	-
M1B	xx	xx	xx	x	x	x	-	-	-	x	-
M3A	xx	x	xx	x	x	xx	-	-	-	x	-
M3B	xx	x	x	x	x	x	-	x	x	-	-
H1A	x	x	x	-	x	x	-	-	x	x	x
H1B	x	x	x	-	x	x	x	x	x	x	-
H1C	x	x	x	x	x	x	x	xx	x	xx	x
H1D	x	x	x	-	x	xx	-	x	x	x	x
H1E	x	x	x	x	x	x	x	x	x	x	-
H1F	x	x	x	-	x	x	x	x	-	x	x
H2A	x	x	x	-	x	x	-	x	x	x	x
H2B	x	x	x	-	x	x	x	x	x	x	-
H2C	x	x	x	-	x	x	x	x	-	x	x
H2D	x	x	x	-	x	x	-	x	-	x	x
H2E	x	x	x	-	x	x	xx	x	x	x	x
H2F	x	x	x	-	x	x	x	x	-	x	x

Table 8: Presence (x) or absence (-) of eggs, phytoplankton, and faecal pellets in the net samples from Mausund (M1A to M3B) and Hopavågen (H1A to H2F, Tab. 3). A high abundance relative to other samples or other groups or samples is marked with xx. Phytoplankton is divided into the phylum Dinoflagellata (Dinophyceae) and the class/phylum Diatom. The diatoms are divided into chain-forming ones and the diatom genus *Coscinodiscus*. Images of the groups are presented in Figures 26 and 27.

	EGGS	PHYTOPLANKTON			MISCELLANEOUS Faecal pellets
		Dinoflagellata	Diatom chains	<i>Coscinodiscus</i> sp.	
M1A	xx	-	x	xx	x
M1B	xx	-	x	xx	x
M3A	x	-	x	x	xx
M3B	x	x	x	x	xx
H1A	x	xx	xx	x	x
H1B	x	x	xx	x	x
H1C	x	x	xx	x	x
H1D	xx	xx	x	x	x
H1E	x	x	x	x	x
H1F	x	x	xx	x	x
H2A	x	x	x	x	x
H2B	x	x	x	x	x
H2C	x	x	xx	x	x
H2D	x	x	xx	x	x
H2E	x	x	xx	x	x
H2F	x	x	x	x	x

3.5 Key Environmental Variables (KEV) data from the LAUV

In this section, the data gathered from the environmental sensors onboard the LAUV is presented for each sampling day and for the depth range pre-programmed in the mission plan.

3.5.1 Seawater temperature

For days M1 and M2, on the first visit to Mausund, the seawater temperature was relatively homogenous throughout the water column down to 40 m depth. Figure 28 shows how the temperature was approximately 6 °C on both days. On the second visit to Mausund (days M3 and M4), the temperature was slightly higher overall and increased towards the surface. A weak stratification could be observed at approximately 20 m on day M3 and M4, with warmer water in the upper layer, although a more scattered distribution of measurements was observed for day M3. In Hopavågen (days H1 and H2), an increase in temperature was observed from 20 m towards the surface (Fig. 28). On day H1, the increase was relatively constant, but with a weak stratification layer at about 5 and 15 m. On day H2, three stratification layers were observed. In the upper 7 meters, the temperature was relatively constant at around 7 °C, but below 7 m it decreased to 6 °C at 15 m, before further decreasing to approximately 5 °C at 20 m.

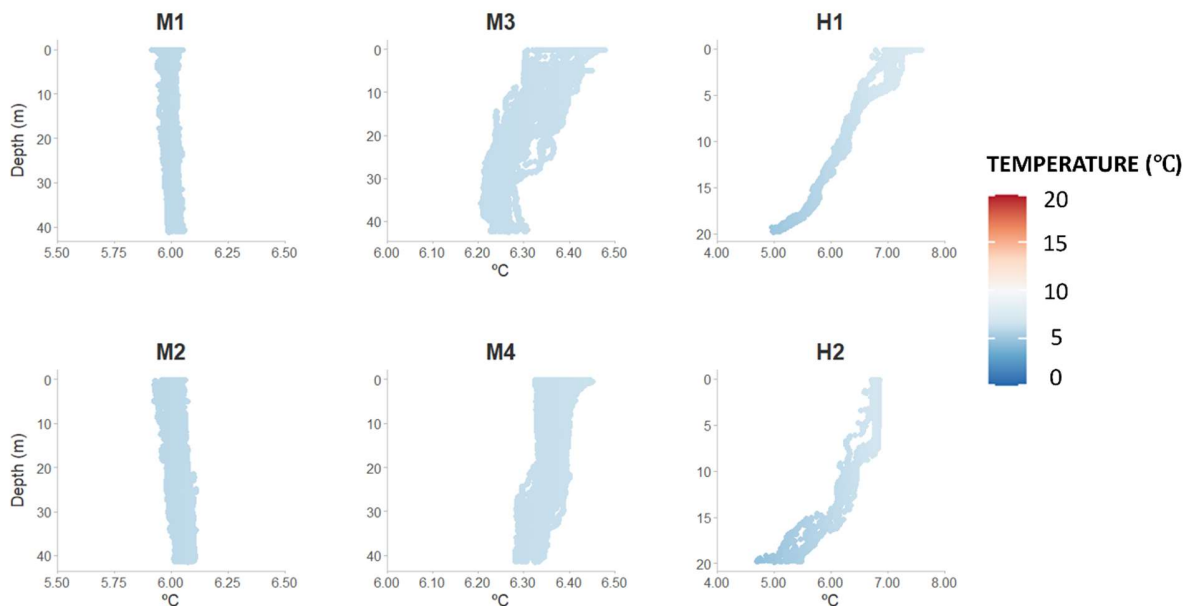


Figure 28: Temperature (°C) measured by the CTD sensor onboard the LAUV. Measurements were taken from 0 to 40 m at Mausund (days M1 to M4) and from 0 to 20 m in Hopavågen (days H1 and H2).

3.5.2 Salinity

As for temperature, the salinity was relatively homogenous on the first visit to Mausund (days M1 and M2, Fig. 29). Except for scattering measurements in the surface layer, the salinity had a constant value at around 33.5 on day M1, with a slight overall increase on day M2. On day M3, the measurements were more scattered and a slight increase in salinity was detected below 20 m. The salinity varied little on day M4. In Hopavågen, the salinity was overall lower. On day H1, it was relatively homogenous around 32.5, but with scattered measurements of lower values. On day H2 the salinity was homogenous down to approximately 7 m before it increased towards 15 m depth. From 15 to 20 m depth the salinity varied from 32.5 to 32.8.

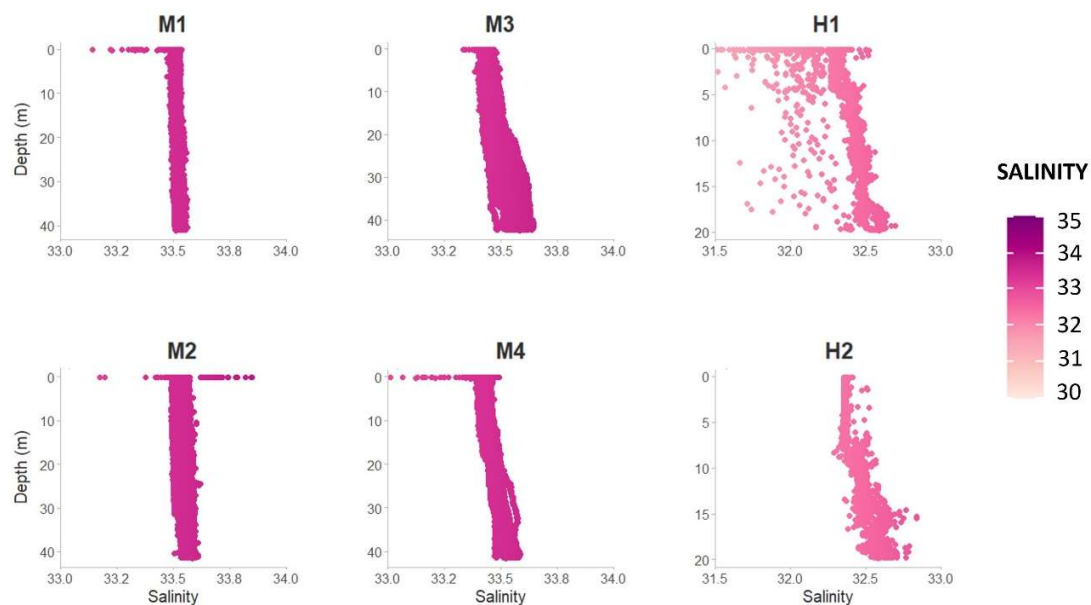


Figure 29: Salinity measured by the CTD sensor onboard the LAUV. Measurements were taken from 0 to 40 m at Mausund (days M1 to M4) and from 0 to 20 m in Hopavågen (days H1 and H2).

3.5.3 Dissolved Oxygen

The concentration of dissolved oxygen, $[O_2]$, was also relatively homogenous throughout the water column on days M1 and M2 (Fig. 30). A concentration between 285 and 288 μM was observed for day M1, while it for day M2 was between 284 and 289 μM . An increase in $[O_2]$ towards the surface was observed for days M3 and M4, from approximately 285 to 300 μM and 289 to 350 μM , respectively. A stratification layer may have been present at 20 m on day M3. On day H1, in Hopavågen, the measurements showed a very different pattern, with a very low $[O_2]$ in the surface layer and then highly increased and scattered measurements from 5 m and down. It also has a pronounced outlier at around 400 μM . Day H2, on the other hand, showed a homogenous value at about 325 μM down to 10 m, then a relatively sharp decrease down towards 250 μM at 20 m depth. A stratification layer was, therefore, present at 10 m depth.

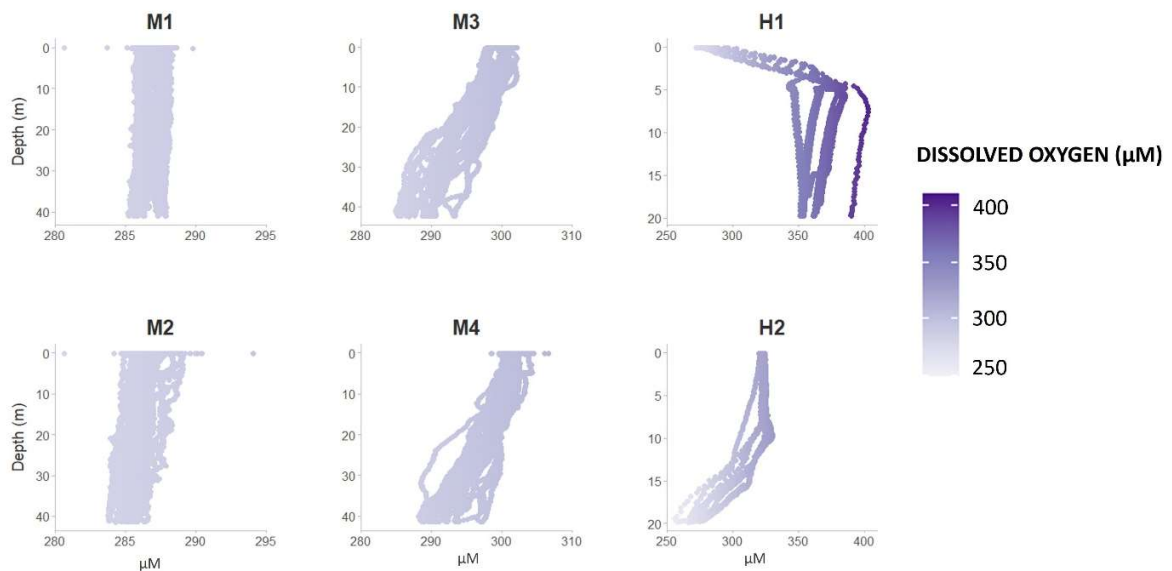


Figure 30: Concentration of dissolved oxygen (μM) measured by the oxygen optode onboard the LAUV. Measurements were taken from 0 to 40 m at Mausund (days M1 to M4) and from 0 to 20 m in Hopavågen (days H1 and H2).

3.5.4 Chlorophyll *a* concentration

The concentration of chlorophyll *a*, [Chl *a*], was measured as a proxy for phytoplankton biomass. Noise in the surface, due to scattering from bubbles influencing the fluorometer, was removed. On days M1 and M2, the concentration kept a constant value of 0.75 $\mu\text{g/L}$ (Fig. 31) from approximately 15 m and down. On days M3 and M4, the [Chl *a*] were overall higher (mostly >1.00), showing an increased concentration from the surface down to 5 and 10 m, respectively, before decreasing towards 40 m depth. In Hopavågen, the [Chl *a*] varied greatly between day H1 and day H2, so mark that the scales in Figure 31, therefore, are different. A distinct layer was present at around 15 m depth on both days. On day H1 the [Chl *a*] increased from almost 0 $\mu\text{g/L}$ in the surface layers, to 18 $\mu\text{g/L}$ at 15 m, and then decreased to 2.5 $\mu\text{g/L}$ at 20 m depth. On day H2, the [Chl *a*] was also close to 0 $\mu\text{g/L}$ in the surface layer, and it increased towards 7 $\mu\text{g/L}$ at 15 m before it decreased again.

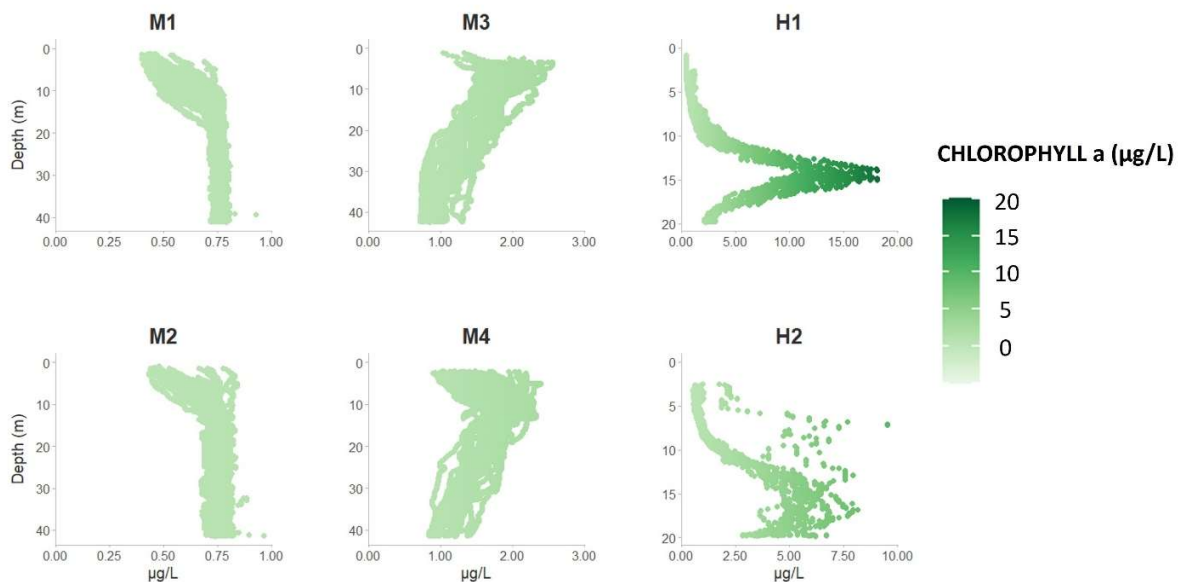


Figure 31: Phytoplankton biomass, measured as chlorophyll *a* concentration ($\mu\text{g Chl } a/\text{L}$) by the fluorometer onboard the LAUV. Measurements were taken from 0 to 40 m at Mausund (days M1 to M4) and from 0 to 20 m in Hopavågen (days H1 and H2). Mark that the scale is different in H1 and H2 due to high values in H1. See Thu (2022) for ground-truthing values from filtrated seawater samples.

3.6 Nutrient availability

The concentration of nitrate, $[\text{NO}_3^-]$, and phosphate, $[\text{PO}_4^{3-}]$, in the seawater was analysed from the seawater samples (Appendix A) collected from the 11 sampling stations (Fig. 2). Due to the highly dynamic exchange of water masses at Mausund, the separate stations were not accounted for, but rather the whole 1 km^2 area of interest. Here, the concentration of nitrate (Fig. 32) and phosphate (Fig. 34) is presented, including boxplots for visualization of the distribution of the data, the outliers, and the median (Fig. 33 and 35).

3.6.1 Nitrate

During the first visit to Mausund (days M1 and M2), the $[\text{NO}_3^-]$ were between 75 and 90 $\mu\text{g/L}$, with a higher nutrient availability at 15 m depth than at the surface on day M1 (Fig. 32). On day M2 the $[\text{NO}_3^-]$ at the surface had increased to the same value as that on 15 m depth on day M1 (Fig. 33). The results from days M3 and M4 showed a reduced nitrate availability on the second visit to Mausund. There was no distinct difference between the $[\text{NO}_3^-]$ at the surface and 15 m depth on day M3, but a reduced concentration was observed in the surface layer on day M4 compared to day M3. In Hopavågen, measurements from four different depths were taken and all of them had a much lower $[\text{NO}_3^-]$ than at Mausund. Measurements from day H1 were around 5 $\mu\text{g/L}$. No distinct difference in $[\text{NO}_3^-]$ was observed between the different depths on day H1, but on day H2, a higher concentration was observed at 20 m depth (Fig. 33).

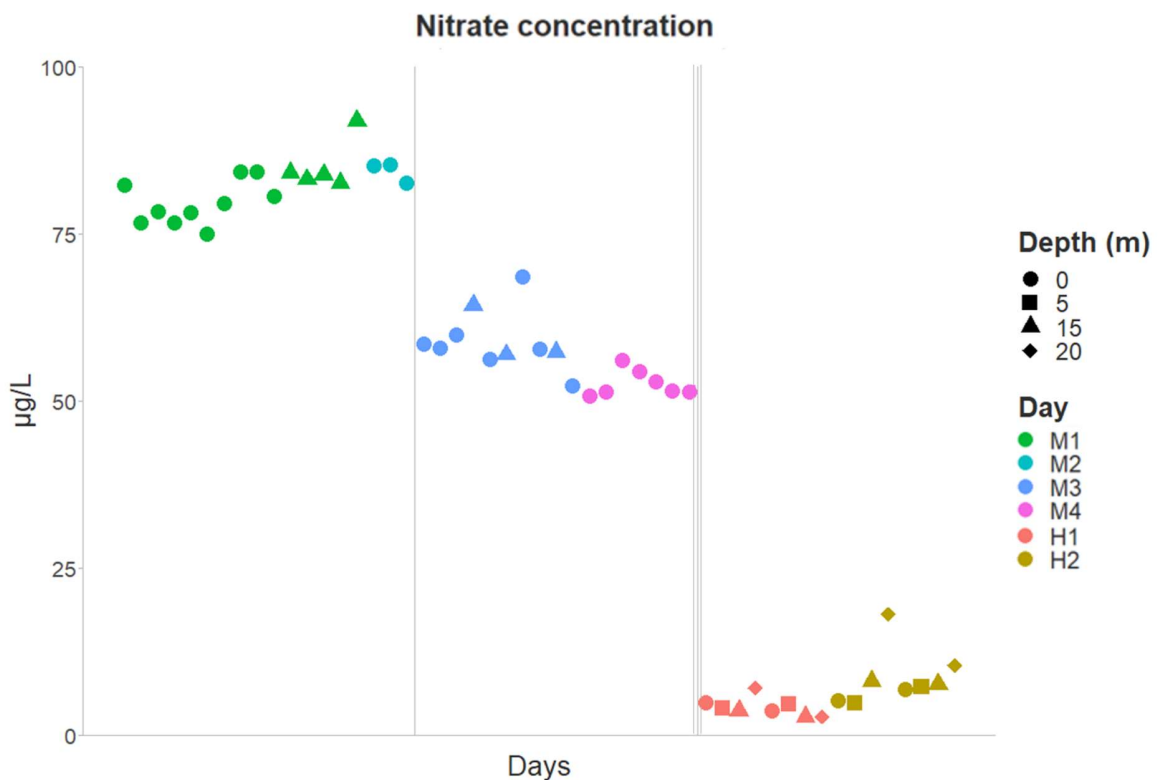


Figure 32: Concentration of nitrate (NO_3^-) ($\mu\text{g/L}$) measured from seawater samples collected at 0-, 5-, 15- and 20-meters depth on days M1 to M4, H1 and H2.

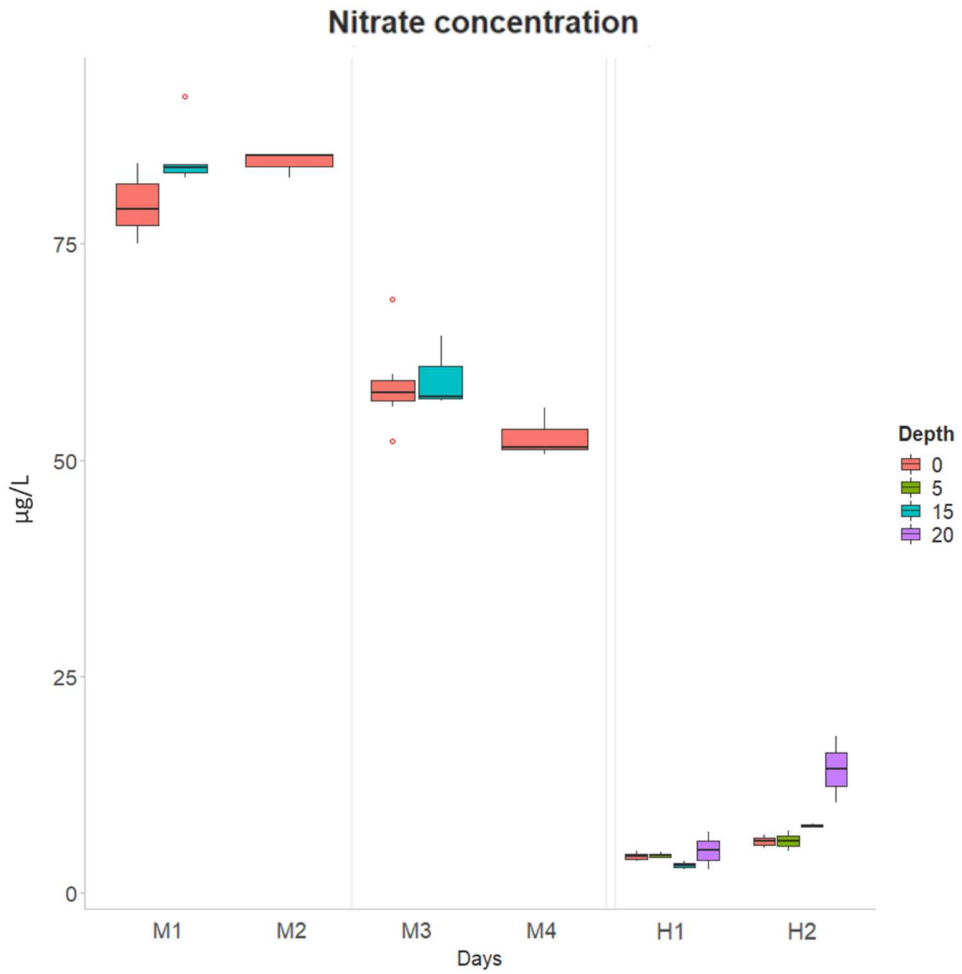


Figure 33: Boxplot of the concentration of nitrate (NO_3^-) ($\mu\text{g/L}$) measured from seawater samples collected at 0-, 5-, 15- and 20-meters depth on days M1 to M4, H1 and H2. The boxplot shows the median (horizontal line) the lower and upper quartile (box) and the maximum and minimum values (whiskers). Outliers are visualized as a red circle.

3.6.2 Phosphate

As for nitrate, the concentration of phosphate, $[\text{PO}_4^{3-}]$, was highest on the first visit to Mausund (over 15 $\mu\text{g/L}$) and then reduced on the second visit (around 12 $\mu\text{g/L}$, Fig. 34 and 35). The $[\text{PO}_4^{3-}]$ was higher at 15 m than at the surface on day M1, but on day M2, the $[\text{PO}_4^{3-}]$ in the surface had increased to that of 15 m the previous day. No distinct difference was observed for the $[\text{PO}_4^{3-}]$ of different depths on day M3. A reduction in $[\text{PO}_4^{3-}]$ was observed in the surface layer on day M4 compared to day M3. Hopavågen had a much lower $[\text{PO}_4^{3-}]$ on both days, but with a higher $[\text{PO}_4^{3-}]$ at 20 m on day H1. On day H2 the surface concentration was similar to that on day H1, but the $[\text{PO}_4^{3-}]$ at 5, 15 and 20 m on H2 was as high as that on 20 m on day H1. The $[\text{PO}_4^{3-}]$ on these depths were also more distributed.

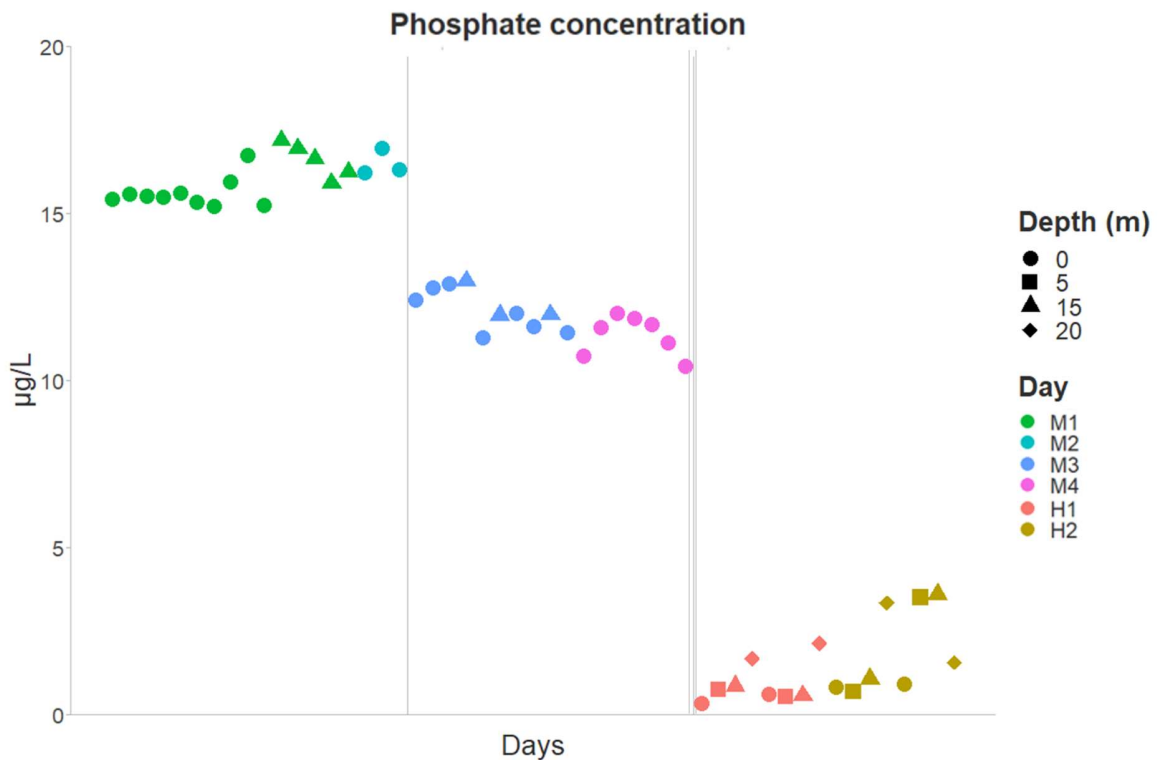


Figure 34: Concentration of phosphate (PO_4^{3-}) ($\mu\text{g/L}$) measured from seawater samples collected at 0-, 5-, 15- and 20-meters depth on days M1 to M4, H1 and H2.

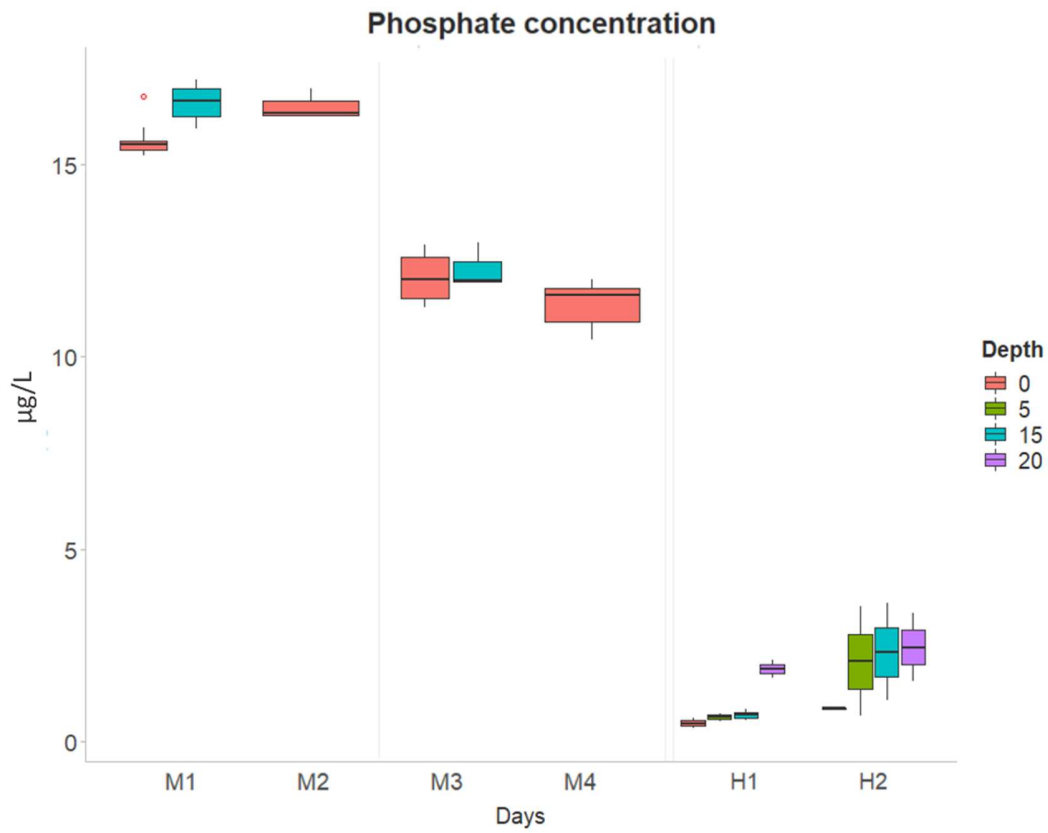


Figure 35: Boxplot of the concentration of phosphate (PO_4^{3-}) ($\mu\text{g/L}$) measured from seawater samples collected at 0-, 5-, 15- and 20-meters depth on days M1 to M4, H1 and H2. The boxplot shows the median (horizontal line) the lower and upper quartile (box) and the maximum and minimum values (whiskers). Outliers are visualized as a red circle.

4 Discussion

This study aimed to assess how an AUV with a fitted sensor suite and a SilCam can be used to analyse KEVs and zooplankton community composition data. Although being a part of projects focusing on several layers in the observational pyramid, this study presents the combined use of an LAUV and a SilCam system, as well as seawater and net samples, to meet the aims of this specific study. See Thu (2022) for ground-truthing of phytoplankton combined with the LAUV data. Only major findings will be discussed, including challenges and future perspectives.

4.1 The SilCam System as a method for plankton studies

The SilCam system has shown to have great potential for plankton studies (Davies et al., 2017; Fragoso et al., 2019a; Fragoso et al., 2021), also in the framework of this study. Its ability to image objects distributed in the water column is valuable for the identification, mapping, and monitoring of the plankton community (Ludvigsen & Sørensen, 2016; Saad et al., 2020). It enables in situ imaging and unlimited storage of visual information that can be revised at a later date (Conradt et al., 2022), which was done in this project. Mounted on an AUV, the SilCam can capture images from large spatiotemporal scales (Berge et al., 2020; Saad et al., 2020), such as the 1 km² survey area at Mausund, providing information about the plankton community, distribution, and abundance (Saad et al., 2020). During this master project, some challenges and constraints related to the method were experienced. These are reviewed to shed light on the areas of improvement.

4.1.1 Optical resolution

The spatial resolution of the SilCam sensor (27.5 µm per image pixel) is hereby referred to as optical resolution to distinguish it from the spatial coverage of the LAUV (Fig. 9.2 in Sørensen et al. 2020). It enabled the identification of copepods, cnidarians, and faecal pellets, but objects smaller than this were rarely identifiable. By increasing the optical resolution, the imaging area would be reduced, and a higher imaging frequency would be needed to cover the same volume of water (Kalmbach et al., 2017). The smaller imaging area could also have led to the loss of identification of bigger organisms, like cnidarians. In the labelling process in Roboflow, several objects with low optical resolution were detected, but could not be identified. They were labelled as "Other". With a higher optical resolution, these objects could maybe be identified as objects with differences in morphology – thus making identification at a higher taxonomic level possible. The low optical resolution also made it hard to differentiate between sharp and diffuse morphological features, which is elucidated by comparison of the SilCam and net sample images of copepods (Fig. 16 and 18, respectively). Overall, the optical resolution used in this study was best suited for the detection of adult copepods (medium size is typically 1-2 mm, (Tseng et al., 2009) and possibly cnidarians small enough to fit the imaging area. A higher optical resolution is advised for the detection of smaller mesozooplankton and morphological traits needed for taxonomic identification, and a

significantly higher resolution is advised for the identification of phytoplankton. The optimal optical resolution is dependent on the group of interest, but ZooSCAN, which has an optical resolution of 10.6 μm has proved to capture mesozooplankton well (Gorsky et al., 2010).

The imaging flow-cytobot (IFCB) presented in Kalmbach et al. (2017) had a considerably higher optical resolution ($\sim 1 \mu\text{m}$) than the SilCam, allowing for the detection of phytoplankton, but losing information about larger organisms. The high optical resolution only allowed for capturing of 5 mL of seawater, much less than the SilCam did (75.6 mL). Additionally, the higher sampling rate (4 fps) of the SilCam enables a more detailed plankton distribution data, compared to the IFCB, only sampling every 20 min (Kalmbach et al., 2017). Davies & Nepstad (2017) compared the SilCam to the LISST-100x (Laser In Situ Scattering and Transmissometer), concluding that LISST-100x was better at discriminating between small objects, but that the SilCam was better at capturing the larger objects and at higher concentrations. Despite the lower optical resolution, Davies & Nepstad (2017) detected diatom chains in the SilCam images, which Saad et al. (2020) also did, together with fish eggs. Before this, Davies et al. (2017) showed that in situ imaging can reveal details of the body and the internals of large copepods, although this was less visible in the images presented in this thesis. Eisenhauer et al. (2020) showed how the SilCam can be used in photography of salmon lice egg strings to assess how far released egg strings disperse from their release point, which is especially valuable in aquaculture. Lombard et al. (2019) present an overview of the size range of plankton captured by different optical and imaging methods available, showing that e.g. the In Situ Ichthyoplankton Imaging System (ISIIS) and VPR can be used for capturing mesozooplankton (Lombard et al., 2019). The ISIIS has an optical resolution of $\sim 68 \mu\text{m}$, capturing objects in the size range of 700 μm (small copepods and larvaceans) and bigger, while still detecting objects as small as 100 μm (e.g. diatoms, Cowen et al., 2013).

4.1.2 Detection and identification of taxonomic groups

Taxonomic groups smaller than copepods were rarely detectable in the SilCam images (Tab. 6). The optical resolution was high enough to detect the longer antennae of some of the copepods (Fig. 17), possibly allowing for separation of the genera calanoid or harpacticoid copepods (Fig. 12), or even species within the genera. The SilCam method is a good method to detect cnidarians, considering that the shape and size of the organisms are preserved, unlike in net samples (Long et al., 2020, Luo et al. 2018, Lombard et al., 2019). Still, as observed in the labelling process, identification of them can be difficult due to their irregular shape in the images and their transparent bodies (Fig. 23), which is also supported by Salvesen (2021). Organisms with a higher optical density, creating a darker colour in the images is most likely easier to detect, including organisms with a defined edge. Mollusca fit this description (Fig. 25, Larink & Westheide, 2011), but no molluscs were detected in the SilCam images, probably due to their small size, as they were present in the net samples on all visits. Echinodermata larvae have long, but thin, arms (Fig. 12 and 24), and were therefore not detectable in the images, except one juvenile (Fig. 13). Bryozoa are small and they appeared almost transparent in the stereomicroscope, so as expected, they were also not detectable in the SilCam images. Faecal pellets with a high optical density were detectable, but those with a lower optical density, which were observed in the net samples, might have

been lost. Phytoplankton were rarely detectable, except from large diatoms, such as *Coscinodiscus* sp. A higher optical resolution is needed to achieve an identification on a higher taxonomic level. Thu (2022) stated that the SilCam method did not successfully detect or classify phytoplankton, but Salvesen (2021) stated that although single phytoplankton usually is too small for image sampling methods, chains, filaments, or colonies of phytoplankton can be detectable. Diatom chains might also be mistaken for faecal pellets, as they have similar features (Salvesen, 2021). The detection of bubbles in the surface layer (Appendix C, Tab. 11 and 12, from 0-10 m) is most likely due to the production of bubbles when the AUV turns at the surface during the yoyo transect.

4.1.3 Overlapping and incomplete organisms

Various reasons could result in objects not being detected, or misread by the classifier, despite being large and having a high optical density. One reason could be overlapping objects, which could prevent the algorithm from detecting separate organisms. This was discovered with the YOLO-based model and in the labelling process (Fig. 13). Additionally, if a relatively large cnidarian overlapped with a copepod, the copepod, or features needed to identify it, might have been undetectable. When using the SilCam for oil and gas studies, objects with a solidity less than 0.95 are removed (Davies et al. 2018). This is to avoid miss-calculation of overlapping objects, but for plankton studies, the goal, and also the challenge, is to capture all the organisms having very different morphological traits (Fig. 12, Lombard et al., 2019). Overlapping may be a bigger problem with a higher density of plankton in the water, especially cnidarians or copepods. Another probable challenge for the algorithm was that some objects were not completely located inside the imaging area, which could have resulted in images of incomplete objects and loss of characteristic traits. An example is how several larger cnidarians, and some copepods, were only partly inside the image frame. Still, copepods with half their body outside the imaging frame were detected with the YOLO-based model, which is promising. In Hopavågen, aggregates of plankton were visible in the net samples, which also might have reduced the ability of the algorithm to detect the individual objects. Additionally, as experienced in this study, a scratch on the lens might be incorrectly detected as a diatom chain.

4.1.4 AI algorithms in copepod classification

Classification of the SilCam images was first done using PySilCam, and after a brief analysis of the results, it was concluded that the identification accuracy was not satisfactory. For example, montages classified as copepods were almost empty, while montages of diatom chains from the same area and time contained a lot of misclassified copepods. Also, as the yellow circles in Figure 14 elucidate, some objects were classified although they were unidentifiable. Nevertheless, the results indicated which plankton groups were detectable by the SilCam.

The new YOLO-based model was created to enhance the identification accuracy and enable classification of the objects in the SilCam images into more groups. The montages of the

objects identified as copepods (Tab. 4 and 5) showed that the algorithm classified several copepods correctly, but that it also misclassified other objects as copepods. The misclassification of faecal pellets as copepods is most likely due to their similar shape, and this can also apply to detritus. Bubbles, on the other hand, have a very different shape, and the misclassification of bubbles as copepods is worth looking further into. A lot of the images also have a very poor optical resolution, resulting in a lot of unidentifiable objects classified as copepods, that most likely are detritus. None of the misclassified objects were from other taxonomic groups of zooplankton, not even in the montages of the group "Other", although some copepods were placed into this group. The absence of other zooplankton in the montages is probably due to the low detectability of these groups in the SilCam, including their less similar shape to copepods.

The light settings in the SilCam raw images showed two vertical lines of LED lights on each side of the image (Fig. 13). The middle part of the image was much darker than the sides, and manual detection and labelling of objects in this area were much harder than on the sides. Figure 15 also shows how the sub-images from this area were very dark. All the images were corrected to get a similar background in the post-processing with the YOLO-based model, but it appeared that the darker sub-images obtained a more grainy background in the post-processing. The sub-images from the more illuminated areas of the SilCam images, on the other hand, appeared overexposed. In some images (Tab. 4 and 5), the images were so overexposed that the contour of the copepod body was completely lost, and only round or elongated parts of the internal body were visible, possibly being astaxanthin (Van Nieuwerburgh et al., 2005) oil droplets or ingested algae (Hansen et al., 2012). This made it hard to evaluate the accuracy of the classification based on these montages, making the montage that was not post-processed (Fig. 15) more reliable when looking at the well-lit areas. Still, some of these sub-images were too dark to view anything at all. The montages showing the objects in their original size can also be valuable for assessing the size distribution of objects in a given group, and for determination of what size is best captured by the SilCam method.

For future analysis using these models, it is advised to train the algorithm on a larger data set with a higher taxonomic resolution to allow separation into distinct taxonomic groups. For species with a distinct morphology detectable by the SilCam, species-level would be beneficial. A higher taxonomic resolution would increase the possibility to use the SilCam method as an ideal tool e.g. for analyses of ecological status in marine ecosystems or biodiversity assessments (Saad et al., 2020). Saad et al. (2020) showed that a quantitative analysis of the zooplankton groups at different depths also can be done, a method that has a high potential to be used for biological monitoring and time-series analyses in the future. This could provide further insights into how marine ecosystems are affected by anthropogenic stressors e.g. global warming and pollution.

With the rise of in situ plankton imaging systems, there is a need for fast and accurate image processing and classification tools (Luo et al., 2018). Previous automated classification methods have shown moderate results (Luo et al., 2018), but recent advances in ML have enabled robust and effective classification of plankton data at a low cost, making automated classification a popular tool in marine ecological science (Conradt et al., 2022; Luo et al., 2018; Pastore et al., 2020; Salvesen, 2021). Some ML algorithms have obtained

an accuracy of >95% (e.g. Al-Barazanchi et al., 2018), but these high values are often a result of running the algorithm on the same dataset as it was trained on (Conradt et al., 2022). Because of irregularities in the number of images of different organisms in the labelling data set, models often classify dominating classes well and less abundant classes poorly (Conradt et al., 2022; Kerr et al., 2020). In this study, copepods were dominating, and the labelled dataset, therefore, contained mostly copepods. Luo et al. (2018) found that excluding the rarest taxa in the imaging processing, the classification accuracy increased from 84% to >90% for the remaining groups. Conradt et al. (2022) proposed a tool for adapting the model to different plankton communities, while Kerr et al. (2020) showed that collaborative DL models can significantly enhance the prediction quality in more rare classes.

Considering the commonly high intra-class morphological variability (e.g. between sub-taxa or life stages) and inter-class similarity (e.g. many bivalve larvae are hard to separate), including small morphological differences separating species of the same class (e.g. differences in the fifth leg of a copepod, Ferrari & Ueda, 2005), ML still performs poorly on species level identification (Conradt et al., 2022; Salvesen, 2021). There is a continuously increasing amount of data captured, creating larger data sets of images with plankton largely differing in morphology. The manual labelling process needed for the supervised classification can then be a potential bottleneck for the use of ML algorithms in situ (Pastore et al., 2020). Unsupervised ML, on the other hand, does not require a labelled dataset, as it instead uses feature extraction and clustering of these features (Salvesen, 2021). Pastore et al. (2020) presented a novel set of algorithms requiring minimal supervision. He found that they approach the level of today's existing supervised algorithms, but when Salvesen (2021) tested three unsupervised ML algorithms, he found that there is still a significant gap between the two approaches. Still, this field of research is relatively unexplored (Salvesen, 2021) and has the potential to become very valuable in future ocean observation, surveillance and monitoring applications.

4.1.5 Effectiveness of the SilCam method

Considering the amount of data captured in time and space, the SilCam method was an effective way to obtain plankton data. Mounted on a LAUV, the SilCam covered a large area in the x, y, and z plane, compared to e.g. net samples, or mounted on a profiling frame (Davies & Nepstad, 2017) or ROV (Brandvik et al., 2021). Much less planning and packaging of materials were needed for the SilCam method compared to net sampling. Once programmed, the LAUV with the SilCam only had to be launched and retrieved once per transect, and the data could be transferred to a computer and processed right after sampling (Sousa, 2012). Net samples, on the other hand, required deployment and retrieval for each station, and onboard handling of the material, including manual identification in a stereomicroscope.

Having the model detect, classify, post-process, and create montages of the findings at different depths, was done in only a few days using the PySilCam software, e.g. creating a background image and correcting the raw image (Davies et al., 2017). Creating the YOLO-based model, on the other hand, turned out to be time-consuming. It took approximately three months to retrieve only a subset of the results created by the PySilCam software, and these results were not optimal. This emphasizes the time saved using a pre-made and trained

model compared to creating a new algorithm for classification. Still, both algorithms could benefit from better automatization of the classification process once the image recognition and the classification are aligned in a better way. For now, proper classification is a time-consuming task, and improvements are needed to make it less labour-intensive and more effective.

The labelling process for ML of the YOLO-based model was also time-consuming. Based on the experience, the time spent labelling is dependent on the number of objects present in each image, the taxonomic level of identification, the detectability of the objects, and the desired size of the data set. Still, training the algorithm only had to be done once, and could then be used to classify several SilCam images captured at any time during multiple future deployments (given that the setup is the same). Considering this, and that manual identification is time-consuming (here; 4 weeks for only 16 point samples identified to a low taxonomic level) and resource-intensive (Fragoso et al., 2021), the SilCam method was more effective in plankton classification, given that a pre-made algorithm is used. Still, a major shortcoming is the reduced taxonomic resolution obtained compared to when identifying net samples in a stereomicroscope, making biodiversity assessments almost impossible at this stage.

To make the SilCam system more effective on a large scale, an establishment of an extensive global training data set is suggested, containing high-resolution taxonomic information about plankton communities in different regions. Collaborative work in maintaining and updating the data set could reduce the overall time spent on manual identification, and the training set could contribute to more accurate image classification and monitoring of plankton communities on a global scale. This is also supported by Luo et al. (2018).

4.1.6 Challenges experienced with the SilCam method

The results presented in this thesis were enough to visualize the benefits and constraints related to the SilCam system, and valuable findings were discovered. Still, there were some challenges related to the data. Because of an unforeseen challenge that cannot be addressed any further due to confidentiality reasons, most of the SilCam montages generated from the first algorithm, the PySilCam, became unavailable. The classification results were thereby lost. This emphasizes that the data is not necessarily stored permanently, as stated by Conradt et al. (2022). Learning from this, saving important material on at least two disks is advised, no matter how large the data set is. Nevertheless, the PySilCam montages with a mix of objects were rescued and used to give an understanding of which objects the SilCam detected and classified.

One of the original ideas for this study was to compare the biodiversity in the net samples with that in the SilCam images. When examining the low taxonomic resolution obtained from the PySilCam, it was decided that a high taxonomic resolution was not needed for the net samples to enable comparison of the findings. Because of this, a low taxonomic level was used, which only considers the difference in zooplankton community rather than biodiversity. It was also intended that the net sample images were to be used as a labelled data set for ML of the PySilCam. Due to the different quality and optical magnification of the net sample

images compared to those the PySilCam was trained on, this was not possible. In the training of the YOLO-based model, labelled raw SilCam images were used instead. For future models, training on stereomicroscope images is advised, if possible, as these images have a higher optical resolution where characteristic features are more pronounced and more taxonomic groups are identifiable. Imaging in a stereomicroscope also allowed for imaging of the objects lying in different angles and directions, which is needed to enable the AI algorithm to account for the 3D nature of the imaged objects. Imaging using holography, allowing for a 3D reconstruction (see Sun et al., 2008) of the imaged plankton has emerged in recent years (Lombard et al., 2019), which might solve this problem in the future.

The process of creating a new algorithm and training it on the labelled data set took longer than the team expected. For that reason, only a subset of the data is presented in this thesis, and the SilCam images from Hopavågen could not be included in the present thesis. As only the classification of copepods was obtained, a comparison of the plankton community was not possible with this model either. By using the plankton groups found in the labelling process, an assessment of the detectability of the groups was done instead. A comparison of the community present in the labelled SilCam images and the net samples was not performed, as the labelled data set contained images from a transect in Hopavågen in September, having a different community than in the spring.

At the beginning of the manual labelling process in Roboflow, there was a lot of uncertainty related to which groups to include and to which taxonomic level. For future labelling, the groups should be at the highest possible taxonomic level, as it is easier to combine groups at a later stage, while achieving a finer taxonomic resolution in retrospect is not possible. Still, there is a payoff when it comes to time spent labelling, as labelling to a higher taxonomic level is more time-consuming and requires advanced taxonomic skills, but then the data can be used repeatedly. Saad et al. (2020) stated that a challenge with this method is obtaining and manually labelling a large imaging data set at a similar magnification, and because of this, a limited number of classes are available. Still, when the AUV performs more missions, Saad et al. (2020) stated that the number of classification groups can be increased and that advances in the optical resolution will allow for a higher taxonomic classification.

More generally, the information content of plankton increases with increasing optical resolution, volume, and imaging frequency. Having the objects in focus and colours, and with enhanced contrast, is also desirable. There is a trade-off between volume captured and the optical resolution, which often results in capturing either small objects with a high resolution in a smaller sample, or bigger objects with a lower resolution in a larger sample (Lombard et al., 2019).

4.2 State of the spring bloom 2021

The KEV data collected by the sensors on the AUV, the zooplankton detected by the SilCam and captured in the net samples, as well as the nutrient availability analysed from the seawater samples were combined to explain the state and succession patterns of the phytoplankton spring bloom 2021 and the zooplankton dynamics at Mausund and in Hopavågen, respectively.

4.2.1 First visit to Mausund (Day M1 and M2)

Before the first visit to Mausund on days M1 and M2, the 13th and 14th of April 2021, there had been a storm that resulted in a mixing of the water column. This was evident in the graphs showing the temperature, salinity, and [O₂], which had little variation from the surface down to 40 m depth (Fig. 28, 29, and 30). A relative homogenous [Chl *a*] was observed below 15 m (Fig. 31), but the [Chl *a*] was too low (0.50 to 0.75 µg/L) for it to be considered a full phytoplankton bloom (Sakshaug et al., 2009; Schalles, 2006), which often exceeds a [Chl *a*] of 5 µg/L (Jonsson et al., 2009). The [NO₃⁻] and [PO₄³⁻] were relatively consistent with the winter values measured in Trondheimsleja from 2018 to 2020, presented by NIVA (The Norwegian Institute for Water Research, winter values: [NO₃⁻]= 79.44 µg/L and [PO₄³⁻]= 16.33 µg/L), which are high relative to the summer values (Fagerli et al., 2021). The high nutrient availability indicated low assimilation of nutrients by phytoplankton. Combined with the low [Chl *a*] detected, it is assumed that there were pre-spring-bloom conditions during the visit (Dale et al., 1999). The higher nutrient concentration observed at 15 m on day M1 (Fig. 33 and 35) could also indicate higher nutrient assimilation by phytoplankton above 15 m. Still, Thu (2022) found that the *in vitro* [Chl *a*] was lower in the surface layers than below 15 m.

The net samples (M1A and M1B) had a high abundance of copepods, where the red colour from the astaxanthin in the copepods (Van Nieuwerburgh et al., 2005) was visible in the nets during sampling. *Calanus finmarchicus* is known for dominating the mesozooplankton biomass in the North Atlantic region (Barange et al., 2010), but the high abundance might also be due to the oblique angle and extended filtration period of the zooplankton net in the water column, as a result of strong winds and drifting. There is a delay in the seasonal peak of zooplankton abundance compared to the phytoplankton bloom, as the population growth rate of the zooplankton depends on the concentration of available food (phytoplankton) (Thackeray, 2012). The presence of faecal pellets indicated zooplankton grazing on phytoplankton, a top-down control (Butler & Dam, 1994; Verity & Smetacek, 1996; Kaiser et al., 2011) and considering the high abundance of copepods and the presence of faecal pellets, there might have been a phytoplankton bloom before the visit. This bloom may have been induced by the favourable light conditions in the previous months, as light is an essential resource for phytoplankton growth (Johnsen et al., 2020). Still, the high abundance of both copepod adults and copepod nauplii could indicate a period of copepod reproduction after winter hibernation (Kaiser et al., 2011), or they could have been transported to the surface layers during the mixing of the water masses. There was no distinct difference in the type of copepods or size from the different depth intervals in the montages from the YOLO-based model, suggesting a

relatively homogenous distribution, and the PySilCam also showed the presence of adult copepods on all depths.

4.2.2 Second visit to Mausund (Day M3 and M4)

The second visit to Mausund was on the 20th and 21st of April 2021, on days M3 and M4, respectively. After a period of storm conditions mixing the water column, and possibly a resupply of nutrients through coastal upwelling in the area (Assmy & Smetacek, 2009; Fragoso et al., 2019a), more calm and sunny conditions between the first and the second visit allowed for stratification of the water column and primary production (Kaiser et al., 2011; Sakshaug et al., 2009; Sundby et al., 2016). The graphs of temperature, salinity, and [O₂] all had an incipient stratification at 20 m, with a higher temperature, lower salinity, and higher [O₂] in the upper layer (Fig. 28, 29, and 30), which is consistent with bloom conditions (Assmy & Smetacek, 2009; Gökçe, 2021; Kaiser et al., 2011). The [Chl *a*] had also increased to 1-2.5 µg/L and the stratification layer had moved from 15 to 10 m depth, which may indicate a migration towards more favourable light conditions and adequate nutrient supply (Paerl, 1988; Reynolds, 1984). The nutrient availability was reduced compared to the first visit (Fig. 33 and 35), which indicated assimilation by phytoplankton (Sauterey & Ward, 2022).

Less material was captured in the net samples compared to the first visit. A possible reason for this could be the more accurate sampling of the water column, due to the calmer conditions, as well as less mixing of material to the surface layers. It might also be that the zooplankton was located below the incipient stratification layer at 20 m, due to DVM (Hays, 2003; Tarling, 2003), and that sampling at 30 m was not deep enough to capture the highest abundance. Although there were fewer copepods in the samples, an increased abundance of faecal pellets was observed, which may be due to a passing of the zooplankton peak biomass with a high grazing pressure (Kaiser et al., 2011). Butler & Dam (1994) found that more faecal pellets are produced early in the phytoplankton bloom, which also indicates a higher contribution to the vertical carbon flux (Steinberg, Goldthwait, & Hansell, 2002), as almost half of the carbon content may be lost as DOM during sinking (Urban-Rich, 1999).

Considering the SilCam montages, no distinct difference was detected between the first and second visit or the different depths on day M3, still suggesting an even distribution. Overall, continued disturbance of mixing and grazing throughout the season has most likely led to the absence of a larger phytoplankton bloom in the spring of 2021 at Mausund, and rather several small ones (Fragoso et al., 2021). Considering the higher [Chl *a*] found in the water surface in May, found by remote sensing data presented in Thu (2022), it might also be that the bloom was delayed due to the storm.

4.2.3 Hopavågen (Day H1 and H2)

The sampling in Hopavågen was done on the 4th and 5th of May, referred to as day H1 and H2, respectively. Due to a traveling delay, the sampling on H1 was conducted slightly earlier than that on H2. This might have resulted in larger differences in the data retrieved than expected, due to different tide levels and directions of the tide.

A pycnocline detected at 5 to 7 m depth (Fig. 28 and 29) trapped the cold and dense water at depth while allowing the warm, less dense water to stay in the upper water column (Johnsen et al., 2018; Kaiser et al., 2011). A relative sudden change was also detected at 15 m for temperature and 10 m for [O₂], but considering the long response time (8 seconds) of the oxygen optode, the position of the change in oxygen levels might have been closer to 15 m. The higher [O₂] in the upper layer indicated a net production of dissolved oxygen following primary production (Kaiser et al., 2011).

The less dynamic nature of the water masses in Hopavågen than at Mausund facilitated a higher [Chl *a*] (Kaiser et al., 2011), with a peak value of 5 to 8 µg/L at 15 m on day H2. The relatively deep position of the Chl *a* layer indicated post-spring-bloom conditions, as the nutrients in the surface layer become depleted during the bloom and the phytoplankton has to descend to a more nutrient-rich depth, while remaining in the euphotic zone (Dale et al., 1999; Kaiser et al., 2011). This coincides with the observation of overall low nutrient availability in the water column, but a higher concentration at 20 m (Fig. 33 and 35).

The net samples contained significantly less plankton in Hopavågen compared to Mausund. A contributing factor to this could be that the zooplankton net used in Hopavågen had a smaller opening (Fig. 9), volume and a lower sampling depth (Tab. 3) compared to that used in Mausund. Less dynamic mixing and input of new water masses in Hopavågen also support the observation of less material (van Marion, 1996). The biodiversity detected in the net samples was higher in Hopavågen than at Mausund, as both Cnidaria and Radiolaria were identified (Tab. 7). A more detailed list of organisms present in Hopavågen is presented in van Marion (1996), but in that study, Radiolaria was not observed. The difference in the zooplankton community might be because Hopavågen receives water from the NCC, while Mausund additionally receives water from NAC. The less exposed nature of the bay also results in a lower supply of new water masses (van Marion, 1996). More meroplankton such as Echinodermata and Mollusca were detected in Hopavågen than at Mausund, which can be due to the proximity to shore. This coincides with the high abundance of Echinodermata in the benthic fauna in Hopavågen (van Marion, 1996). It could also be due to different stages of the seasonal succession patterns, although Skjaeveland (1973) found that in a similar fjord located in the same region, there were no seasonal differences in Echinodermata biomass. Free-dwelling gastropods can also adjust their position to the shore, thereby being less affected by the changing tide levels (van Marion, 1996). Diatom chains dominated the samples on day H2, which was consistent with the high [Chl *a*] and [O₂] but contradicts Volent et al. (2011), stating that a decline in the number of diatoms characterizes a post-bloom.

4.3 Assessment of the combination of LAUV and SilCam

The combination of a LAUV and a SilCam system in this project resulted in valuable information about the plankton community and the KEVs affecting the ocean dynamics. The SilCam system contributed with a vast set of in situ plankton data, and by mounting it on a sensor fitted LAUV that simultaneously sampled KEVs, a high spatiotemporal resolution was obtained, compared to e.g. net sampling. The method thereby gave a more holistic understanding of the ecosystem dynamics.

Using a well-trained plankton classification algorithm can contribute to significantly faster identification than by using a human expert, but improvements to the SilCam system and the evaluated methods are needed to get to this level. The SilCam system captured plankton data at a given depth, which is valuable information for studies of plankton dynamics and DVM, as compared to plankton nets, losing information about the specific vertical distribution, unless using a net with a closing mechanism (Wiebe & Benfield, 2003). Still, physical net samples are necessary for the analysis of e.g. community structures and genetics, and for a higher taxonomic resolution (e.g. for biodiversity assessments), although large-scale imaging is important to investigate gelatinous organisms, predator-prey dynamics, and patchiness (Luo et al., 2018).

The LAUV was prepared, operated, and the data was extracted by the AUV pilots, emphasizing their important role in the study. Sousa et al. (2012) stated that the LAUV is one-man portable and that it can be controlled by a single operator. It is also affordable, robust, reliable, effective and require low logistics (Sousa, 2012). In the field, the LAUV proved to be relatively easy to handle, but considering its weight, price, and high value, it is recommended that two people are carrying it (Fig. 1). It required low logistics, and the open system (Sousa, 2012), enabled customization with a fitting sensor suite. It is still important to be aware of how the sensors differ from each other when combining data from several sensors, as e.g. the sampling frequency, response time, or unit of measurement may differ. With proper preparation of the sensors, as well as information about their sampling frequency and response times, the differences in the data can be accounted for. The LAUV also had the necessary computing power needed for the SilCam to operate, as well as a long residence time in the water (Saad et al., 2020). Still, as the LAUV is best suited for surveys over the mesoscale (Berge et al., 2020), the relatively shallow and small area of Hopavågen proposed a risk of collision. It also had a limited power supply and its possibility of being trapped between water layers of different densities posed a risk of losing the vehicle and the data (Sørensen et al., 2020).

Due to the highly dynamic nature of the zooplankton community and their patchy distribution, rapidly responding to changes in KEVs, measurements with a high temporal resolution are needed to study their fluctuations (Martin-Platero et al., 2018). Combining the SilCam system and the LAUV allows for this. Albeit the potential value of this method in plankton studies and thereby climate change studies, it does not serve as a replacement for net sampling of plankton or seawater sampling for ground-truthing of Chl *a* (Thu, 2022). Hablützel et al. (2021) contradicts with this, stating that physical samples are no longer necessary in the new era of advanced optical techniques. Still, different sampling methods covering different spatial and temporal scales are highly valuable in creating a holistic understanding of the environment (Aguzzi et al., 2020; Sørensen et al., 2020). Data from ground-truthing and the LAUV are just two layers of the observational pyramid, and in combination with data from e.g. USVs, UAVs, small planes, and small satellites valuable insights not detectable in the ground-truthing and AUV data can be obtained (Ludvigsen et al., 2016; Ludvigsen & Sørensen, 2016; Sørensen et al., 2020). Additionally, plankton imaging systems such as the SilCam can provide validation data for ocean ecosystem models (Luo et al., 2018). This elucidates the importance of collaboration in multidisciplinary teams, to enable sharing of knowledge, ideas, competence, and experiences (Sørensen et al., 2020). AMOS is a great example of this, with a vision of providing cutting-edge multidisciplinary research on unmanned vehicles and autonomous marine operations and systems (Ofte Dahl & J. Sørensen). The AILARON project also shows

how each level has a complexity requiring experts in both the technological and biological fields of study, at least (Saad et al., 2020).

4.4 Overall challenges

The major challenge in this study was the loss of the SilCam data from the PySilCam model, and additional data needed to create the new algorithm more effectively. The low optical resolution in the SilCam images was also a challenge, especially in the labelling process, and challenges related to the KEVs were also experienced. The measurements of [O₂] on day H1 show a reversed pattern relative to that detected on day H2, which is probably due to a method or sensor error, and the high [Chl *a*] on day H1 might be due to over-calibration. Combined with the increased response time in the oxygen optode, resulting in the detection of stratification layers at a lower depth, this emphasizes the importance of evaluating and calibrating the sensors in advance.

Turbidity measurements are relevant for zooplankton analysis as turbidity affects the waters transparency and thereby limit the euphotic zone (Goździejewska & Kruk, 2022). This can significantly affect zooplankton feeding efficiency, abundance, and development, and can also be related to the amount of detritus detected by the SilCam. Turbidity measurements were available from the Cyclops-7 sensor on the LAUV. Still, they were discarded in this thesis, as the sampling frequency, and thereby temporal resolution of the measurements was low compared to the variation in the data, resulting in very discrete values. For future projects, the sensor sampling intervals should be accounted for before sampling, making sure that they have the appropriate temporal resolution. Overall, different response times, calibration, and sampling intervals in the AUV sensors made comparison of the data more challenging. Scattering from bubbles created at the surface during the AUV's yoyo transect (Appendix C) also influenced the Chl *a* measurements (Suggett et al., 2010), and surface values were therefore removed.

One of the benefits with the SilCam system is its ability to create minimal disruption when measuring suspended material (Davies & Nepstad, 2017). Still, when mounted on an AUV, a flow pressure is established due to the speed and the shape of the AUV, resulting in water masses being pushed away. This might result in less material being detected by the SilCam system (Fossum et al., 2019; Sousa, 2012).

A possible challenge during sampling on Mausund was that the boat was drifting away from the coordinates of the sampling stations, thereby not sampling the same point as the LAUV. Still, as the water masses are highly dynamic, sampling of the exact same water mass is not possible. Patchiness is also a key feature of pelagic ecosystems (Kaiser et al., 2011), which can result in substantially differing data. Still, sampling at 10 stations in a 1 km² square hopefully reduced this error to some degree.

During the period working on this project, there was a Covid-19 pandemic, which at times was challenging due to the ever-changing guidelines and the unpredictability. Luckily the fieldwork could be conducted safely following the guidelines given at the time.

5 Conclusion

In this study, the usability of a novel method combining an AUV and a SilCam system for an assessment of the zooplankton community composition and its dynamics related to KEVs has been evaluated. Based on findings, the method has the potential to be a very useful tool in plankton studies in the future, if the challenges elucidated in the current study are improved. The SilCam system captured valuable in situ images of zooplankton, but due to a low optical resolution, the subsequent taxonomic resolution obtained was limited, and a higher optical resolution is advised to enable an assessment of biodiversity. As for now, net samples are needed for this. Although the PySilCam had a low identification accuracy, this thesis emphasizes the benefit of having a pre-made algorithm for classification, as the creation of a new algorithm and manually creating a labelled data set is time-consuming and resource-intensive. The YOLO-based model created during this study is the very first version of the model, and the results showed misclassification of copepods in the SilCam images and challenges related to the post-processing. Areas of improvement were elucidated, and future adjustments are expected to increase the identification accuracy.

The LAUV proved to be a valuable sensor-carrying platform for plankton studies as it captured KEV data from a large spatiotemporal scale, and even more valuable data can be obtained when aligning the temporal resolution and response time in the sensors. A holistic assessment of the state of the phytoplankton spring bloom in Mausund and Hopavågen 2021 was enabled through measurements of KEVs obtained by the LAUV sensors, combined with SilCam findings, zooplankton net samples, and nutrient analysis of seawater samples. It was concluded that there were pre-spring-bloom conditions during the first visit to Mausund, an ongoing bloom during the second visit, and a post-bloom during the visit to Hopavågen. Overall, the challenges related to this novel AUV and SilCam method have been elucidated, but even more so its potential value as an important tool for plankton studies on a larger spatiotemporal scale compared to net sampling, thereby enabling monitoring of climate change in the ocean.

Future perspectives

Due to the novel nature of the method assessed in this study, future improvements are expected to increase its value in plankton studies and contribute to even better data gathering. Considering the goal of the AILARON project (1.5), training the algorithm on a larger and more diverse data set is advised if the classification is to be trusted and so that the LAUV can revisit the hotspot consisting of the plankton groups at interest in the adaptive sampling process. The adaptive sampling process is also expected to streamline the classification process and enable data gathering of targeted zooplankton groups (Saad et al., 2020).

As also stated in Saad et al. (2020), improvements in the optical resolution in the SilCam will enable the separation of different plankton groups, thereby potentially improving the identification accuracy and enabling more detailed plankton diversity analyses. A more comprehensive study of the YOLO-based model will be presented in a paper released later in 2022, covering more of the technical aspects of the method. Presented here is just the very first version of the entire pipeline, and more work is planned to improve the training of the

model and improving the post-processing. For future development, Lou et al. (2018) suggests a master, global-level training data set that has filters for different regions, allowing for a faster image classification process of over 100 classes with high precision and little dependence on manual identification. That would enable quick and accurate classification of up to billions of in situ images (Luo et al., 2018).

A coupling of the data gathered by the ground-truthing, LAUV, and SilCam system with data from platforms with a different spatiotemporal resolution will in future projects enable an even more holistic understanding of the ecosystem processes. The Interdisciplinary Algal Bloom Observation Field Experiment at Mausund Field Station again visited Mausund in the spring of 2022, and collected more data from several platforms, utilizing the knowledge obtained from last year's experiences. Findings from this visit will be valuable for comparison with data gathered in 2021.

In future projects, it is advised to have close communication in the interdisciplinary team, as there is a lot to learn from each other's field of study and a common language needs to be established for proper understanding of each other's needs. As it is hard to know how much time is needed for the creation of a new algorithm or labelling, close communication is crucial.

Hopefully, this thesis can bring important insights into how the LAUV and SilCam method performs in biological studies, elucidating areas of improvement for an added value in future plankton studies.

References

- Aguzzi, J., Chatzievangelou, D., Francescangeli, M., Marini, S., Bonofiglio, F., del Rio, J., & Danovaro, R. (2020). The Hierarchic Treatment of Marine Ecological Information from Spatial Networks of Benthic Platforms. *Sensors*, 20(6), 1751. doi:10.3390/s20061751
- Al-Barazanchi, H., Verma, A., & Wang, S. X. (2018). Intelligent plankton image classification with deep learning. *International Journal of Computational Vision and Robotics*, 8(6), 561-571. doi: 10.1504/IJCVR.2018.095584
- AML Oceanographic. (n.d.). X2change Sensors. Canada.
- Assmy, P., & Smetacek, V. (2009). Algal Blooms. In M. Schaechter (Ed.), *Encyclopedia of Microbiology* (pp. 27-41). Oxford: Elsevier Inc. doi: 10.1016/B978-012373944-5.00001-8
- Attayde, J. L., & Hansson, L.-A. (1999). Effect of Nutrient Recycling by Zooplankton and Fish on Phytoplankton Communities. *Oecologia*, 121, 47-54. doi:10.1007/s004420050906
- AUR-lab. (n.d.). LAUV Roald. Retrieved from <https://www.ntnu.edu/aur-lab/lauv-roald> [Accessed April 25 2022].
- Bar-On, Y. M., & Milo, R. (2019). The Biomass Composition of the Oceans: A Blueprint of Our Blue Planet. *Cell*, 179(7), 1451-1454. doi: <https://doi.org/10.1016/j.cell.2019.11.018>
- Barange, M., Field, J. G., Harris, R. P., Hofmann, E. E., Perry, R. I., & Werner, F. E. (2010). *Marine Ecosystems and Global Change USA*, New York: Oxford University Press Inc. doi: 10.1093/acprof:oso/9780199558025.001.0001
- Beaugrand, G. (2014). *Marine Biodiversity, Climatic Variability and Global Change* (1st ed.). London: Routledge. doi: <https://doi.org/10.4324/9780203127483>
- Bellingham, J. G., & Rajan, K. (2007). Robotics in Remote and Hostile Environments. *Science*, 318(5853), 1098-1102. doi:10.1126/science.1146230
- Berge, J., Johnsen, G., & Cohen, J. H. (2020). *Polar Night: Marine Ecology Life and Light in the Dead of Night* (Vol. 4, pp. 1-365). doi:<https://doi.org/10.1007/978-3-030-33208-2>
- Borgersen, J. N., Saad, A., & Stahl, A. (2022). *MOG: a background extraction approach for data augmentation of time-series images in deep learning segmentation*. Paper presented at the Fourteenth International Conference on Machine Vision (ICMV 2021), Rome, Italy. doi: <https://doi.org/10.1117/12.2622899>
- Brander, K. M., Ottersen, G., Bakker, J. P., Beaugrand, G., Herr, H., Garthe, S., Gilles, A., Kenny, A., Siebert, U., & Skjoldal, H. R. (2016). Environmental impacts - marine ecosystems. In M. Quante & F. Colijn (Eds.), *North Sea region climate change assessment* (pp. 241-274): Springer, Cham. doi: https://doi.org/10.1007/978-3-319-39745-0_8
- Brandvik, P. J., Davies, E., Nepstad, R., & Nordmark, L.-O. (2021). Controlling and Documenting Dispersant Effectiveness During Subsea Dispersant Injection (SSDI) - A Novel System for Dispersant Dosage and In-Situ Monitoring of Oil Droplet and Gas Bubble Sizes. *International Oil Spill Conference Proceedings, 2021*(1). doi:10.7901/2169-3358-2021.1.689511
- Brun, P., Stamieszkin, K., Visser, A. W., Licandro, P., Payne, M. R., & Kiørboe, T. (2019). Climate change has altered zooplankton-fuelled carbon export in the North Atlantic. *Nature Ecology & Evolution*, 3(3), 416-423. doi:10.1038/s41559-018-0780-3
- Butler, M., & Dam, H. (1994). Production rates and characteristics of fecal pellets of the copepod *Acartia tonsa* under simulated phytoplankton bloom conditions: Implications for vertical fluxes. *Marine Ecology Progress Series*, 114, 81-91. doi:10.3354/meps114081

- Conradt, J., Börner, G., López-Urrutia, Á., Möllmann, C., & Moyano, M. (2022). Automated Plankton Classification With a Dynamic Optimization and Adaptation Cycle. *Frontiers in Marine Science*, 9. doi:10.3389/fmars.2022.868420
- Conway, D. V. P. (2012). *Marine zooplankton of southern Britain. Part 2: Arachnida, Pycnogonida, Cladocera, Facetotecta, Cirripedia and Copepoda*. Plymouth, United Kingdom: Occasional Publications.
- Cowen, R., Greer, A., Guigand, C., Hare, J., Richardson, D., & Walsh, H. (2013). Evaluation of the In Situ Ichthyoplankton Imaging System (ISIIS): Comparison with the traditional (bongo net) sampler. *Fishery Bulletin*, 111, 1-12. doi:10.7755/FB.111.1.1
- Dale, T., Rey, F., & Heimdal, B. R. (1999). Seasonal development of phytoplankton at a high latitude oceanic site. *Sarsia*, 84(5-6), 419-435. doi:10.1080/00364827.1999.10807347
- Davies, E., Ahnell, A., Leirvik, F., & Brandvik, P. (2018). *Optical monitoring of subsea blowout droplets and subsea dispersant efficacy*. Paper presented at the Forty-First AMOP Technical Seminar, Environment and Climate Change, Ottawa, Canada. Retrieved from <https://www.bsee.gov/sites/bsee.gov/files/research-reports//1084aa.pdf>
- Davies, E. J., Brandvik, P. J., Leirvik, F., & Nepstad, R. (2017). The use of wide-band transmittance imaging to size and classify suspended particulate matter in seawater. *Marine Pollution Bulletin*, 115(1), 105-114. doi:<https://doi.org/10.1016/j.marpolbul.2016.11.063>
- Davies, E. J., & Nepstad, R. (2017). In situ characterisation of complex suspended particulates surrounding an active submarine tailings placement site in a Norwegian fjord. *Regional Studies in Marine Science*, 16, 198-207. doi:<https://doi.org/10.1016/j.rsma.2017.09.008>
- Druon, J.-N., Hélaouët, P., Beaugrand, G., Fromentin, J.-M., Palialexis, A., & Hoepffner, N. (2019). Satellite-based indicator of zooplankton distribution for global monitoring. *Scientific Reports*, 9(1), 4732. doi:10.1038/s41598-019-41212-2
- Dwyer, B., & Nelson, J. (2019). Roboflow. Retrieved from <https://roboflow.com/> [Accessed February 21 2022]
- Eisenhauer, L., Solvang, T., Alver, M., Franklin Krause, D., & Hagemann, A. (2020). Dispersal of salmon lice (*Lepeophtheirus salmonis* Krøyer, 1837) egg strings from open-cage salmon farming: A neglected source for infestation dynamics. *Aquaculture Research*, 51(11), 4595-4601. doi:<https://doi.org/10.1111/are.14805>
- Estes Jr., M., Muller-Karger, F., Forsberg, K., Leinen, M., Kholeif, S., Turner, W., Cripe, D., Gevorgyan, Y., Fietzek, P., Canonico, G., Werner, F. & Bax, N. (2022). Integrating Biology into Ocean Observing Infrastructure: Society Depends on It. *Oceanography*, 34(No. 4), 36 - 43. doi:<https://doi.org/10.5670/oceanog.2021.supplement.02-16>
- Estes, M., Anderson, C., Appeltans, W., Bax, N., Bednaršek, N., Canonico, G., Djavidnia, S., Escobar, E., Fietzek, P., Greogoire M., Hazen, E., Kavanaugh, M., Lejzerowicz, F., Lombard, F., Miloslavich, P., Möller, K. O., Monk, J., Montes. E., Moustahfid, H & Weatherdon, L. V. (2021). Enhanced monitoring of life in the sea is a critical component of conservation management and sustainable economic growth. *Marine Policy*, 132, 104699. doi:<https://doi.org/10.1016/j.marpol.2021.104699>
- Fagerli, C. W., Trannum, H. C., Golmen, L. G., Eikrem, W., & Mengeot, C. (2021). *Økokyst – DP Norskehavet Sør (II). 2020 report*. Retrieved from <https://hdl.handle.net/11250/2780231>
- Ferrari, F. D., & Ueda, H. (2005). Development of Leg 5 of Copepods Belonging to the Calanoid Superfamily Centropagoidea (Crustacea). *Journal of Crustacean Biology*, 25(3), 333-352. doi:10.1651/c2554
- Fossum, T. O., Eidsvik, J., Ellingsen, I., Alver, M. O., Fragoso, G. M., Johnsen, G., Mendes, R., Ludvigsen M., & Rajan, K. (2018). Information-driven robotic sampling in the coastal ocean. *Journal of Field Robotics*, 35(4), 1101-1121. doi:10.1002/rob.21805

- Fossum, T. O., Fragoso, G. M., Davies, E. J., Ullgren, J. E., Mendes, R., Johnsen, G., Ellingsen, I., Eidsvik, J., Ludvigsen, M., & Rajan, K. (2019). Toward adaptive robotic sampling of phytoplankton in the coastal ocean. *Science Robotics*, 4(27), eaav3041. doi:10.1126/scirobotics.aav3041
- Fragoso, G. M., Davies, E. J., Ellingsen, I., Chauton, M. S., Fossum, T., Ludvigsen, M., Steinhovden K. B., Rajan, K., & Johnsen, G. (2019a). Physical controls on phytoplankton size structure, photophysiology and suspended particles in a Norwegian biological hotspot. *Progress in Oceanography*, 175, 284-299. doi:https://doi.org/10.1016/j.pocean.2019.05.001
- Fragoso, G. M., Johnsen, G., Chauton, M. S., Cottier, F., & Ellingsen, I. (2021). Phytoplankton community succession and dynamics using optical approaches. *Continental Shelf Research*, 213. doi:https://doi.org/10.1016/j.csr.2020.104322
- Fragoso, G. M., Poulton, A. J., Pratt, N. J., Johnsen, G., & Purdie, D. A. (2019b). Trait-based analysis of subpolar North Atlantic phytoplankton and plastidic ciliate communities using automated flow cytometer. *Limnology and Oceanography*, 64(4), 1763-1778. doi:10.1002/lno.11189
- Gliwicz, M. Z. (1986). Predation and the evolution of vertical migration in zooplankton. *Nature*, 320(6064), 746-748. doi:10.1038/320746a0
- Gorsky, G., Ohman, M. D., Picheral, M., Gasparini, S., Stemmann, L., Romagnan, J.-B., Cawood, A., Pesant, S., García-Comas, C., & Prejger, F. (2010). Digital zooplankton image analysis using the ZooScan integrated system. *Journal of Plankton Research*, 32(3), 285-303. doi:10.1093/plankt/fbp124
- Goździewska, A. M., & Kruk, M. (2022). Zooplankton network conditioned by turbidity gradient in small anthropogenic reservoirs. *Scientific Reports*, 12(1). doi:10.1038/s41598-022-08045-y
- Gökçe, A. (2021). A mathematical study for chaotic dynamics of dissolved oxygen-phytoplankton interactions under environmental driving factors and time lag. *Chaos, Solitons & Fractals*, 151. doi:https://doi.org/10.1016/j.chaos.2021.111268
- Hablützel, P. I., Rombouts, I., Dillen, N., Lagaisse, R., Mortelmans, J., Ollevier, A., Perneel, M., & Deneudt, K. (2021). Exploring New Technologies for Plankton Observations and Monitoring of Ocean Health. In *Frontiers in Ocean Observing* (Vol. 34, pp. 20-25). doi:https://doi.org/10.5670/oceanog.2021.supplement.02-09
- Hansen, B. H., Altin, D., Olsen, A. J., & Nordtug, T. (2012). Acute toxicity of naturally and chemically dispersed oil on the filter-feeding copepod *Calanus finmarchicus*. *Ecotoxicology and Environmental Safety*, 86, 38-46. doi:https://doi.org/10.1016/j.ecoenv.2012.09.009
- Haug, M. L., Saad, A., & Stahl, A. (2021a). CIRAL: a hybrid active learning framework for plankton taxa labeling. *IFAC-PapersOnLine*, 54(16), 450-457. doi:https://doi.org/10.1016/j.ifacol.2021.10.130
- Haug, M. L., Saad, A., & Stahl, A. (2021b). *A combined informative and representative active learning approach for plankton taxa labeling*. Paper presented at the Thirteenth International Conference on Digital Image Processing. https://doi.org/10.1117/12.2601096
- Hays, G. (2003). A review of the adaptive significance and ecosystem consequences of zooplankton diel vertical migration. *Hydrobiologia*, 503, 163-170. doi:10.1023/B:HYDR.0000008476.23617.b0
- Hays, G. C., Richardson, A. J., & Robinson, C. (2005). Climate change and marine plankton. *Trends in Ecology & Evolution*, 20(6), 337-344. doi:https://doi.org/10.1016/j.tree.2005.03.004
- HELCOM. (2009). *Eutrophication in the Baltic Sea. An integrated thematic assessment of eutrophication in the Baltic Sea region*. Retrieved from <http://www.helcom.fi/Lists/Publications/BSEP115B.pdf>.

- HELCOM. (2010). *Ecosystem Health of the Baltic Sea*. Retrieved from Helsinki, Finland: <http://www.helcom.fi/Lists/Publications/BSEP122.pdf>.
- HELCOM. (2014). *Eutrophication status of the Baltic Sea 2007–2011. - A concise thematic assessment*. Retrieved from Helsinki, Finland: <http://www.helcom.fi/Lists/Publications/BSEP143.pdf>
- Horton, T., Kroh, A., Ahyong, S., Bailly, N., Bieler, R., Boyko, C. B., Brandão, S. N., Gofas, S., Hooper J. N. A., Hernandez, F., Mees, J., Molodtsova, T. N., Paulay, G., Bourig, K., Decock, W., Dekeyzer, S., Vandepitte, L., Vanhoorne, B., Adlard, R., . . . & Zullini, A. (2022). World Register of Marine Species (WoRMS). Retrieved from <https://www.marinespecies.org>. [Accessed April 25 2022]
- Xylem Inc. (n.d.). Bergen, Norway. Aanderaa Data Instruments AS
- Jenssen, B. M., Åsmul, J. I., Ekker, M., & Vongraven, D. (2010). To go for a swim or not? Consequences of neonatal aquatic dispersal behaviour for growth in grey seal pups. *Animal Behaviour*, *80*(4), 667-673. doi:<https://doi.org/10.1016/j.anbehav.2010.06.028>
- Johnsen, G., Leu, E., & Gradinger, R. (2020). Marine Micro- and Macroalgae in the Polar Night. In J. Berge, G. Johnsen, & J. H. Cohen (Eds.), *Polar Night Marine Ecology: Life and Light in the Dead of Night* (pp. 67-112). Cham: Springer International Publishing. doi: 10.1007/978-3-030-33208-2_4
- Johnsen, G., Norli, M., Moline, M., Robbins, I., von Quillfeldt, C., Sørensen, K., Cottier, F., & Berge, J. (2018). The advective origin of an under-ice spring bloom in the Arctic Ocean using multiple observational platforms. *Polar Biology*, *41*(6), 1197-1216. doi:10.1007/s00300-018-2278-5
- Jonsson, P. R., Pavia, H., & Toth, G. (2009). Formation of harmful algal blooms cannot be explained by allelopathic interactions. *Proceedings of the National Academy of Sciences*, *106*(27), 11177-11182. doi:10.1073/pnas.0900964106
- Kaiser, M. J., Attrill, M. J., Jennings, S., Thomas, D. N., Barnes, D. K. A., Brierley, A. S., Hiddink J. G., Kaartokallio, H., Polunin, N. V. C., & Raffaelli, D. G. (2011). *Marine ecology: processes, systems, and impacts* (2nd ed.). UK: Oxford University Press.
- Kalmbach, A., Girdhar, Y., Sosik, H. M., & Dudek, G. (2017, 29 May-3 June 2017). *Phytoplankton hotspot prediction with an unsupervised spatial community model*. Paper presented at the 2017 IEEE International Conference on Robotics and Automation (ICRA). doi: 10.1109/ICRA.2017.7989568
- Kerr, T., Clark, J. R., Fileman, E. S., Widdicombe, C. E., & Pugeault, N. (2020). Collaborative Deep Learning Models to Handle Class Imbalance in FlowCam Plankton Imagery. *IEEE Access*, *8*, 170013-170032. doi:10.1109/ACCESS.2020.3022242
- Kjørboe, T. (2010). What makes pelagic copepods so successful? *Journal of Plankton Research*, *33*, 677-685. doi:10.1093/plankt/fbq159
- Larink, O., & Westheide, W. (2011). *Coastal plankton: Photo Guide for European Seas*. (2nd ed.): Verlag Dr. Friedrich Pfeil.
- Ljungström, G., Claireaux, M., Fiksen, Ø., & Jørgensen, C. (2020). Body size adaptations under climate change: zooplankton community more important than temperature or food abundance in model of a zooplanktivorous fish. *Marine Ecology Progress Series*, *636*, 1-18. doi:10.3354/meps13241
- Lombard, F., Boss, E., Waite, A. M., Vogt, M., Uitz, J., Stemmann, L., Sosik, H. M., Schulz, J., Romagnan, J.-B., Picheral, M., Pearlman, J., Ohman, M. D., Niehoff, B., Möller, K. O., Miloslavich, P., Lara-Lpez, A., Kudel, R., Lopes, R. M., Kiko, R. & Appeltans, W. (2019). Globally Consistent Quantitative Observations of Planktonic Ecosystems. *Frontiers in Marine Science*, *6*. doi:10.3389/fmars.2019.00196
- Long, A. P., O'Donnell, C., Haberlin, D., Lawton, C., & Doyle, T. K. (2020). A novel platform for monitoring gelatinous mesozooplankton: The high-speed Gulf VII sampler quantifies gelatinous mesozooplankton similar to a ring net. *Limnology and Oceanography: Methods*, *18*(11), 696-706. doi:<https://doi.org/10.1002/lom3.10395>

- Lorentsen, S.-H., Sjøtun, K., & Grémillet, D. (2010). Multi-trophic consequences of kelp harvest. *Biological Conservation*, 143(9), 2054-2062. doi:<https://doi.org/10.1016/j.biocon.2010.05.013>
- Ludvigsen, M., Albrektsen, S. M., Cisek, K., Johansen, T. A., Norgren, P., Skjetne, R., Zolich, A., Sousa Dias, P., Ferreira, S., de Sousa, J. B., Fossum, T. O., Sture, Ø., Røbekk Krogstad, T., Midtgaard, Ø., Hovstein, V., & Vågsholm, E. (2016a). *Network of heterogeneous autonomous vehicles for marine research and management*. Paper presented at the OCEANS 2016 MTS/IEEE Monterey, Monterey, CA, USA. doi: 10.1109/OCEANS.2016.7761494
- Ludvigsen, M., & Sørensen, A. J. (2016b). Towards integrated autonomous underwater operations for ocean mapping and monitoring. *Annual Reviews in Control*, 42, 145-157. doi:<https://doi.org/10.1016/j.arcontrol.2016.09.013>
- Luo, J., Irisson, J.-O., Graham, B., Guigand, C., Sarafraz, A., Mader, C., & Cowen, R. (2018). Automated plankton image analysis using convolutional neural networks. *Limnology and oceanography, methods*, 16, 814-827. doi: 10.1002/lom3.10285
- Martin-Platero, A. M., Cleary, B., Kauffman, K., Preheim, S. P., McGillicuddy, D. J., Alm, E. J., & Polz, M. F. (2018). High resolution time series reveals cohesive but short-lived communities in coastal plankton. *Nature Communications*, 9(1), 1-11. doi: 10.1038/s41467-017-02571-4
- Masson-Delmotte, V., Zhai, P., Pirani, A., Connors, S. L., Péan, C., Berger, S., Caud, N., Chen, Y., Goldfarb, L., Gomis, M.I, Huang, M., Leitzell, K., Lonnoy, E., Matthews, J. B. R., Maycock, T. K., Waterfield, T., Yelekçi, O., Yu, R., & Zhou, B. (2021). *Climate Change 2021: The Physical Science Basis. Contribution of Working Group I to the Sixth Assessment Report of the Intergovernmental Panel on Climate Change*. Cambridge University Press. Retrieved from <https://www.ipcc.ch/report/ar6/wg1/> [Accessed January 18 2022].
- Moline, M., Blackwell, S., Alt, C., Allen, B., Austin, T., Case, J., Forrester, N., Goldsborough, R., Purcell, M., & Stokey, R. (2005). Remote Environmental Monitoring Units: An Autonomous Vehicle for Characterizing Coastal Environments*. *Journal of Atmospheric and Oceanic Technology*, 22. doi:10.1175/JTECH1809.1
- Morel, F. M. M., Milligan, A. J., & Saito, M. A. (2014). Marine Bioinorganic Chemistry: The Role of Trace Metals in the Oceanic Cycles of Major Nutrients. In H. D. Holland & K. Turekian (Eds.), *Treatise on Geochemistry* (2nd ed., pp. 123-150). Oxford: Elsevier. doi: <https://doi.org/10.1016/B978-0-08-095975-7.00605-7>
- Moriceau, B., Iversen, M. H., Gallinari, M., Everts, A.-J. O., Le Goff, M., Beker, B., Boutorh, J., Corvaisier, R., Coffineau, N., Donval, A., Giering, S. L. C., Koski, M., Lambert, C., Lampitt, R. S., Le Mercier, A., Masson, A., Stibor, H., Stockenreiter, M., & De La Rocha, C. L. (2018). Copepods Boost the Production but Reduce the Carbon Export Efficiency by Diatoms. *Frontiers in Marine Science*. doi:<https://doi.org/10.3389/fmars.2018.00082>
- Nortek. (n.d.). Doppler Velocity Log: DVL1000 - 300 m. Retrieved from <https://www.nortekgroup.com/products/dvl-1000-300m> [Accessed May 25 2022]
- Norway, S. (1991). Water analysis - Determination of the sum of nitrite nitrogen and nitrate nitrogen (NS 4745:1991). Standards Norway.
- Norway, S. (2004). Water quality - Determination of phosphorus - Ammonium molybdate spectrometric method (ISO 6878:2004). Standards Norway.
- Oftedahl, L., & J. Sørensen, A. (2022). *NTNU AMOS Centre for Autonomous Marine Operations and Systems: Annual Report 2021*. Retrieved from https://www.ntnu.edu/documents/20587845/621664524/NTNU_AMOS_2021_Scr.pdf/a925fcbd-c90f-9e4d-5a5b-27dd41003e57?t=1648810597413

- OSPAR. (2003). *The OSPAR Integrated Report 2003 on the Eutrophication Status of the OSPAR Maritime Area based upon the first application of the Comprehensive Procedure*. Retrieved from <https://www.ospar.org/documents?v=6962>
- OSPAR. (2008). *Second integrated report on the eutrophication status of the OSPAR maritime area*. Retrieved from <https://www.ospar.org/documents?v=7107>
- Overland, J. E., Alheit, J., Bakun, A., Hurrell, J. W., Mackas, D. L., & Miller, A. J. (2010). Climate controls on marine ecosystems and fish populations. *Journal of Marine Systems*, 79(3-4), 305-315. doi:<https://doi.org/10.1016/j.jmarsys.2008.12.009>
- Paerl, H. W. (1988). Nuisance phytoplankton blooms in coastal, estuarine, and inland waters. *Limnology and Oceanography*, 33(4), 823-843. Retrieved from <https://aslopubs.onlinelibrary.wiley.com/doi/pdfdirect/10.4319/lo.1988.33.4part2.0823>
- Pastore, V. P., Zimmerman, T. G., Biswas, S. K., & Bianco, S. (2020). Annotation-free learning of plankton for classification and anomaly detection. *Scientific Reports*, 10(1). doi:[10.1038/s41598-020-68662-3](https://doi.org/10.1038/s41598-020-68662-3)
- Philippart, C. J. M., Anadón, R., Danovaro, R., Dippner, J. W., Drinkwater, K. F., Hawkins, S. J., Oguz, T., O'Sullivan, G., & Reid, P. C. (2011). Impacts of climate change on European marine ecosystems: Observations, expectations and indicators. *Journal of Experimental Marine Biology and Ecology*, 400(1), 52-69. doi:<https://doi.org/10.1016/j.jembe.2011.02.023>
- Pinto, J., Calado, P., Braga, J., Dias, P., Martins, R., Marques, E., & Sousa, J. B. (2012). Implementation of a Control Architecture for Networked Vehicle Systems. *IFAC Proceedings Volumes*, 45(5), 100-105. doi:<https://doi.org/10.3182/20120410-3-PT-4028.00018>
- Ramírez-Pérez, M., Goncalves-Araujo, R., Wiegmann, S., Torrecilla, E., Bardaji, R., Röttgers, R., Bracher, A., & Piera, J. (2017). Towards cost-effective operational monitoring systems for complex waters: Analyzing small-scale coastal processes with optical transmissometry. *PLoS One*, 12(1). doi:<https://doi.org/10.1371/journal.pone.0170706>
- Redmon, J., Divvala, S., Girshick, R., & Farhadi, A. (2016). *You only look once: Unified, real-time object detection*. Paper presented at the Proceedings of the IEEE conference on computer vision and pattern recognition, Las Vegas, NV, USA. doi: 10.1109/CVPR.2016.91
- Reynolds, C. S. (1984). *The ecology of freshwater phytoplankton*: Cambridge university press.
- Richardson, A. J. (2008). In hot water: zooplankton and climate change. *ICES Journal of Marine Science*, 65(3), 279-295. doi:[10.1093/icesjms/fns028](https://doi.org/10.1093/icesjms/fns028)
- Richon, C., & Tagliabue, A. (2021). Biogeochemical feedbacks associated with the response of micronutrient recycling by zooplankton to climate change. *Global Change Biology*, 27(19), 4758-4770. doi:<https://doi.org/10.1111/gcb.15789>
- Saetre, R. (2007). *The Norwegian coastal current; oceanography and climate*. Norway: Tapir akademisk forlag.
- Sakshaug, E., Johnsen, G., Kristiansen, S., Quillfeldt, C. v., Rey, F., Slagstad, D., & Thingstad, F. (2009). Phytoplankton and primary production. In E. Sakshaug, G. Johnsen, & K. Kovacs (Eds.), *Ecosystem Barents Sea* (pp. 167-208). Trondheim: Tapir Academic Press.
- Salvesen, E. (2021). *Unsupervised methods for in-situ classification of plankton taxa*. (Master's degree). NTNU, Retrieved from <https://hdl.handle.net/11250/2781016>
- Salvesen, E., Saad, A., & Stahl, A. (2022). *Robust deep unsupervised learning framework to discover unseen plankton species*. Paper presented at the Fourteenth International Conference on Machine Vision (ICMV 2021), Rome, Italy. <https://doi.org/10.1117/12.2622489>

- Sauterey, B., & Ward, B. A. (2022). Environmental control of marine phytoplankton stoichiometry in the North Atlantic Ocean. *Proceedings of the National Academy of Sciences*, 119 (1), e2114602118. doi:10.1073/pnas.2114602118
- Schalles, J. (2006). Optical remote sensing techniques to estimate phytoplankton chlorophyll a concentrations in coastal waters with varying suspended matter and CDOM concentrations. In L. L. Richardson & E. F. LeDrew (Eds.), *Remote Sensing of Aquatic Coastal Ecosystem Processes: Science and Management Applications* (pp. 27-79). Netherlands: Springer. doi: 10.1007/1-4020-3968-9_3
- Skagseth, Ø., Drinkwater, K. F., & Terrile, E. (2011). Wind-and buoyancy-induced transport of the Norwegian Coastal Current in the Barents Sea. *Journal of Geophysical Research: Oceans*, 116(C8). doi:https://doi.org/10.1029/2011JC006996
- Skjæveland, S. H. (1973). *Ecology of echinoderms in Borgenfjorden, North-Trøndelag, Norway*. Trondheim, Norway. Retrieved from <http://hdl.handle.net/11250/228158>
- Sommer, U., Hansen, T., Stibor, H., & Vadstein, O. (2004). Persistence of phytoplankton responses to different Si:N ratios under mesozooplankton grazing pressure: A mesocosm study with NE Atlantic plankton. *Marine Ecology Progress Series*, 278, 67-75. doi:10.3354/meps278067
- Sosik, H. M., & Olson, R. J. (2007). Automated taxonomic classification of phytoplankton sampled with imaging-in-flow cytometry. *Limnology and Oceanography: Methods*, 5(6), 204-216. doi:https://doi.org/10.4319/lom.2007.5.204
- Sousa, A. (2012). *LAUV: The Man-Portable Autonomous Underwater Vehicle*. Paper presented at the Navigation, Guidance and Control of Underwater Vehicles. doi: <https://doi.org/10.3182/20120410-3-PT-4028.00045>
- Steinberg, D., Goldthwait, S., & Hansell, D. (2002). Zooplankton vertical migration and the active transport of dissolved organic and inorganic carbon in the Sargasso Sea. *Deep Sea Research Part I: Oceanographic Research Papers*, 49, 1445-1461. doi:10.1016/S0967-0637(02)00037-7
- Suggett, D. J., Prášil, O., & Borowitzka, M. A. (2010). *Chlorophyll a Fluorescence in Aquatic Sciences: Methods and Applications* (1 ed. Vol. 4): Springer Dordrecht. doi: <https://doi.org/10.1007/978-90-481-9268-7>
- Sun, H., Benzie, P. W., Burns, N., Hendry, D. C., Player, M. A., & Watson, J. (2008). Underwater digital holography for studies of marine plankton. *Philosophical Transactions of the Royal Society A: Mathematical, Physical and Engineering Sciences*, 366(1871), 1789-1806. doi:10.1098/rsta.2007.2187
- Sundby, S., Drinkwater, K. F., & Kjesbu, O. S. (2016). The North Atlantic Spring-Bloom System - Where the Changing Climate Meets the Winter Dark. *Frontiers in Marine Science*, 3. doi:10.3389/fmars.2016.00028
- Sørensen, A. J., Ludvigsen, M., Norgren, P., Ødegård, Ø., & Cottier, F. (2020). Sensor-Carrying Platforms. In J. Berge, G. Johnsen, & J. H. Cohen (Eds.), *Polar Night Marine Ecology: Life and Light in the Dead of Night* (pp. 241-275). Cham: Springer International Publishing. doi: 10.1007/978-3-030-33208-2_9
- Saad, A., Stahl, A., Våge, A., Davies, E., Nordam, T., Aberle, N., Ludvigsen, M., Johnsen, G., Sousa, J., & Rajan, K. (2020). Advancing Ocean Observation with an AI-Driven Mobile Robotic Explorer. *Oceanography*, 33, 50-59. doi:10.5670/oceanog.2020.307
- Tarling, G. (2003). Sex dependent diel vertical migration in Northern krill and its consequences to population dynamics. *Marine Ecology-Progress Series*, 260, 173-188. doi:10.3354/meps260173
- Taylor, A. H., Allen, J., & Clark, P. A. (2002). Extraction of a weak climatic signal by an ecosystem. *Nature*, 416(6881), 629-632. doi:10.1038/416629a
- Teigen, A. L., Saad, A., Stahl, A., & Mester, R. (2021). Few-Shot Open World Learner. *IFAC-PapersOnLine*, 54(16), 444-449. doi:https://doi.org/10.1016/j.ifacol.2021.10.129

- Thackeray, S. J. (2012). Mismatch revisited: what is trophic mismatching from the perspective of the plankton? *Journal of Plankton Research*, 34(12), 1001-1010. doi:10.1093/plankt/fbs066
- Thu, M. (2022). *Phytoplankton spring bloom mapping in coastal areas using Autonomous Underwater Vehicle (AUV) and optical approaches*. (Master's thesis). NTNU, Trondheim, Norway.
- Tseng, L.-C., Dahms, H.-U., Chen, Q.-C., & Hwang, J.-S. (2009). Copepod feeding study in the upper layer of the tropical South China Sea. *Helgoland Marine Research*, 63(4), 327-337. doi:10.1007/s10152-009-0162-y
- Turner Designs. (2007). USA Patent No. Turner Designs. Retrieved from <http://docs.turnerdesigns.com/t2/doc/brochures/S-0060.pdf>
- Urban-Rich, J. (1999). Release of dissolved organic carbon from copepod fecal pellets in the Greenland Sea. *Journal of Experimental Marine Biology and Ecology*, 232(1), 107-124. doi:[https://doi.org/10.1016/S0022-0981\(98\)00104-X](https://doi.org/10.1016/S0022-0981(98)00104-X)
- van Marion, P. (1996). *Ecological studies in Hopavågen, A Landlocked Bay at Agdenes*. Trondheim, Norway. Retrieved from <http://hdl.handle.net/11250/228116>
- Van Nieuwerburgh, L., Wänstrand, I., Liu, J., & Snoeijs, P. (2005). Astaxanthin production in marine pelagic copepods grazing on two different phytoplankton diets. *Journal of Sea Research*, 53(3), 147-160. doi:<https://doi.org/10.1016/j.seares.2004.07.003>
- Verity, P. G., & Smetacek, V. (1996). Organism life cycles, predation, and the structure of marine pelagic ecosystems. *Marine Ecology Progress Series*, 130, 277-293. doi:10.3354/meps130277
- Villarino, E., Chust, G., Licandro, P., Butenschön, M., Ibaibarriaga, L., Larrañaga, A., & Irigoien, X. (2015). Modelling the future biogeography of North Atlantic zooplankton communities in response to climate change. *Marine Ecology Progress Series*, 531, 121-142. doi:10.3354/meps11299
- Visbeck, M. (2018). Ocean science research is key for a sustainable future. *Nature Communications*, 9(1), 690. doi:10.1038/s41467-018-03158-3
- Wiebe, P. H., & Benfield, M. C. (2003). From the Hensen net toward four-dimensional biological oceanography. *Progress in Oceanography*, 56(1), 7-136. doi:[https://doi.org/10.1016/S0079-6611\(02\)00140-4](https://doi.org/10.1016/S0079-6611(02)00140-4)
- ZEISS. (n.d.). Germany Patent No. Microscope World. Retrieved from <https://www.zeiss.com/microscopy/us/products/microscope-cameras/axiocam-erc-5s.html> [Accessed May 7 2022].
- Zsolt, V., Geir, J., Erlend, K. H., Are, F., Lasse, M. O., Karl, T., & Kai, S. (2011). Improved monitoring of phytoplankton bloom dynamics in a Norwegian fjord by integrating satellite data, pigment analysis, and Ferrybox data with a coastal observation network. *Journal of Applied Remote Sensing*, 5(1), 1-22. doi:10.1117/1.3658032

APPENDIX A: Seawater samples for nutrient analysis

Table 9: Seawater sample depth (m) from the 10 stations (Fig. 2) at Mausund (day M1 to M4). The samples were obtained by a bucket (0 m) and a NTNU-made seawater sampler (Fig. 9, a and d).

Water sample depth (m) from Mausund				
Station	Day M1	Day M2	Day M3	Day M4
1	0	0	0	0
	15	-	-	-
2	0	-	0	0
	15	-	-	-
3	0	0	0	0
4	0		15	0
5	0	-	0	0
	15	-	-	-
6	0	15	15	0
7	0	-	0*	0
	15	-	-	-
8	0	-	0	-
9	0	-	15	-
	15	-	-	-
10	0	-	0	-

Table 10: Seawater sample depth (m) from station 11 (Fig. 2) in Hopavågen (day H1 and H2). The samples were obtained by a bucket (0 m) and a NTNU-made seawater sampler (Fig. 9, a and d).

Water sample depth (m) from Hopavågen

Station	Day H1	Day H2
11	0	0
	5	5
	15	15
	20	20

APPENDIX B: Taxonomic groups of zooplankton

PICTORIAL KEY TO ZOOPLANKTON

(Not to scale; numbers in brackets are part numbers of the guide)

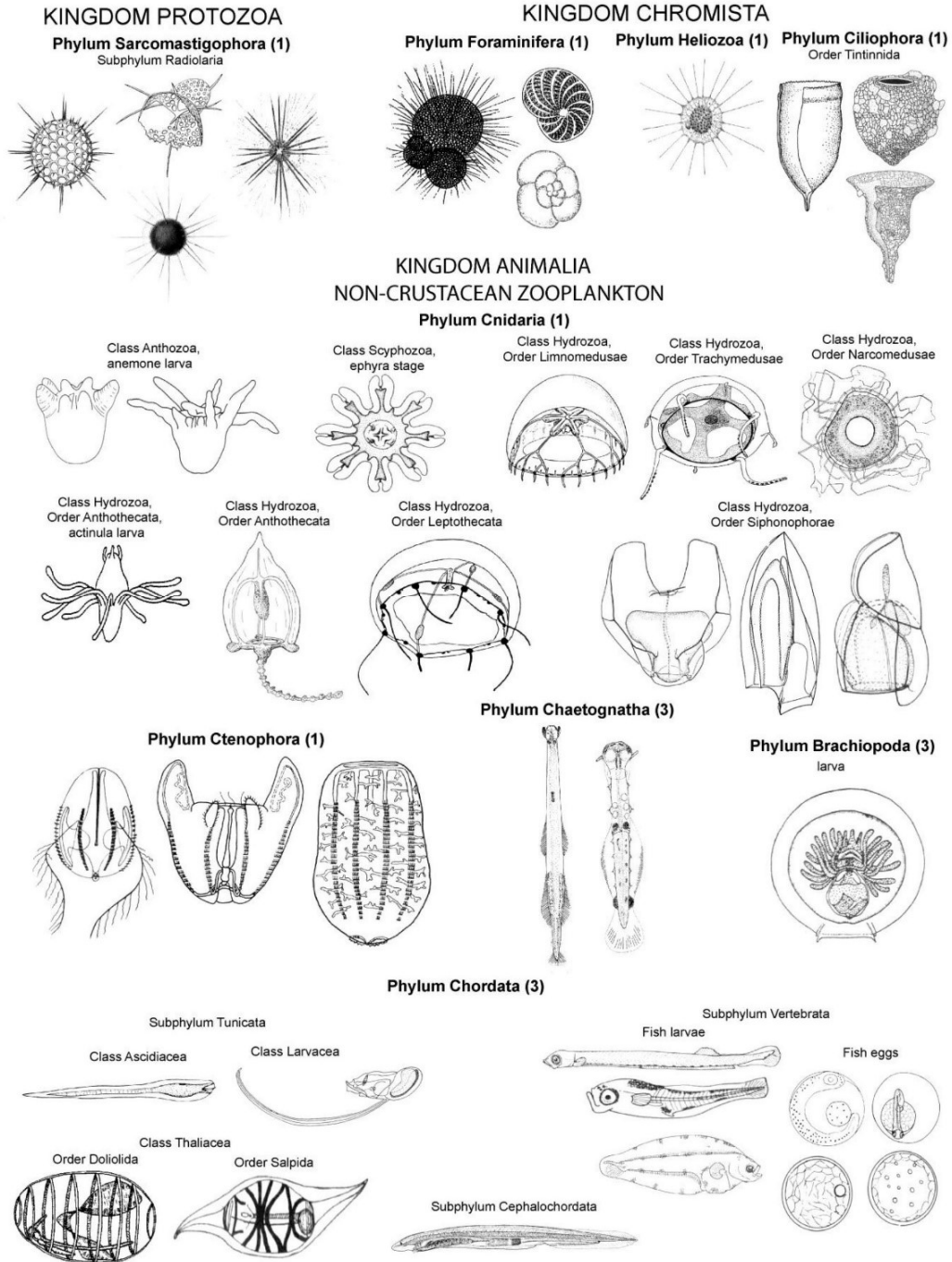


Figure 36: Pictorial key to taxonomic groups of zooplankton, obtained from Conway (2012).

NON-CRUSTACEAN ZOOPLANKTON AND LARVAE

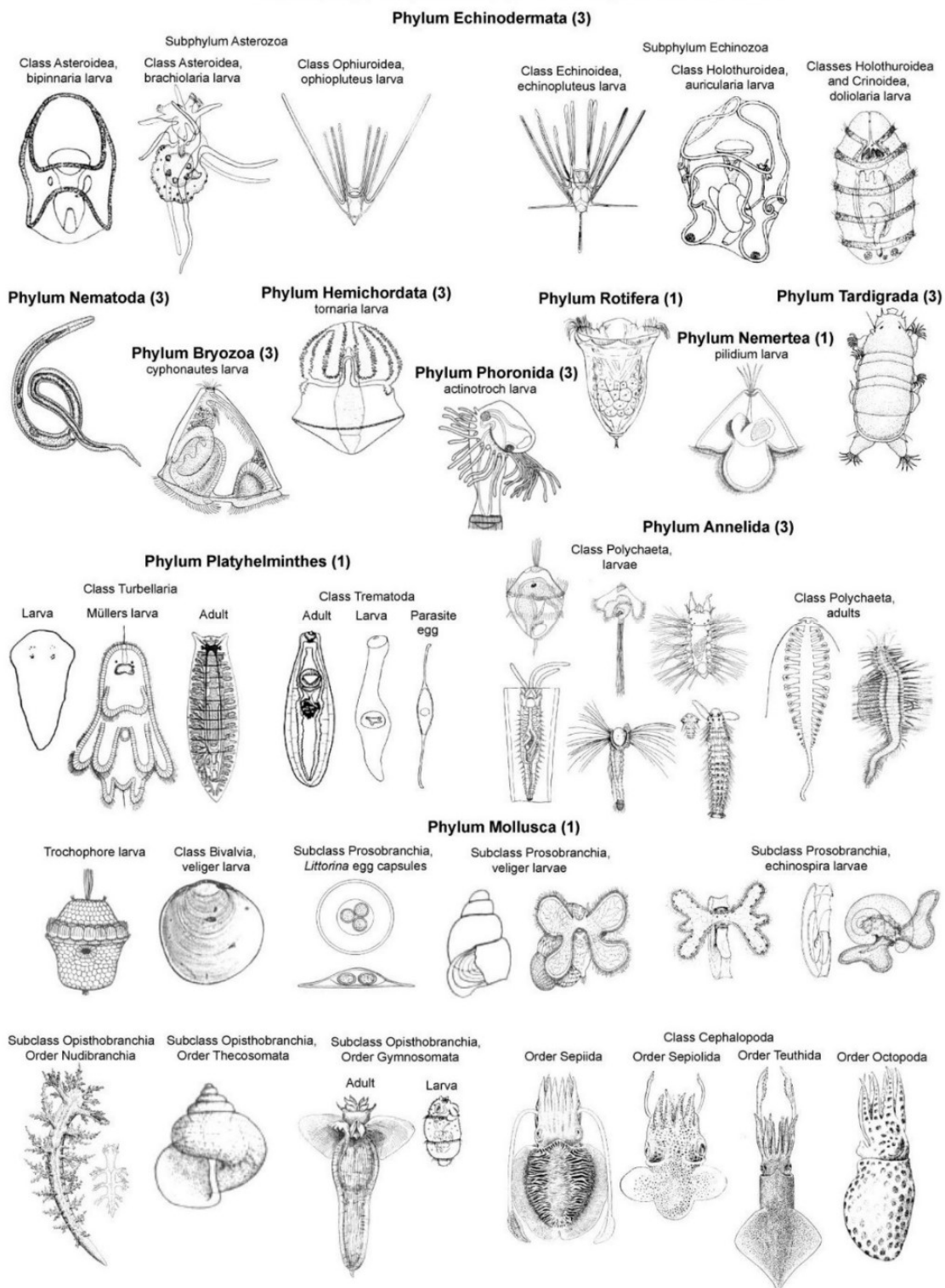


Figure 37: Pictorial key to non-crustacean zooplankton and larvae, obtained from Conway (2012).

CRUSTACEAN ZOOPLANKTON

Phylum Arthropoda - Subphylum Crustacea Subclass Copepoda (2)

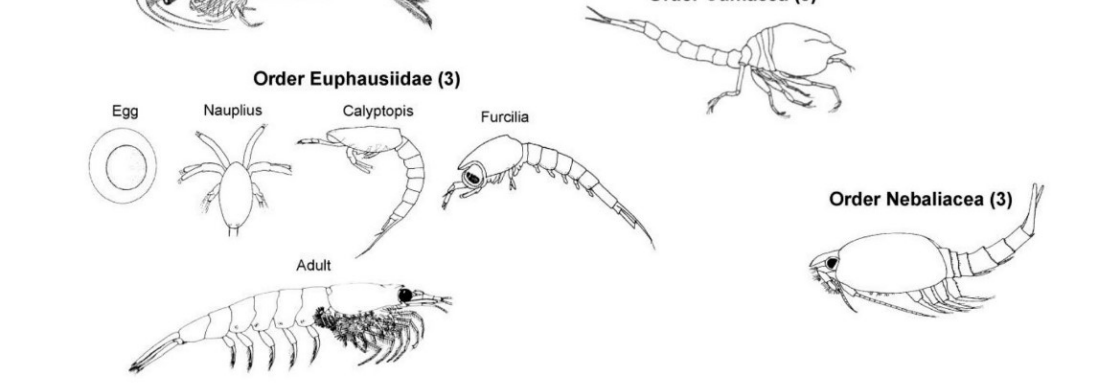
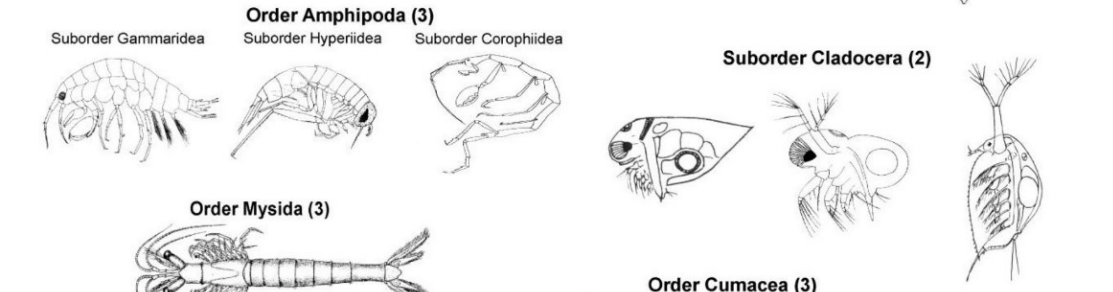
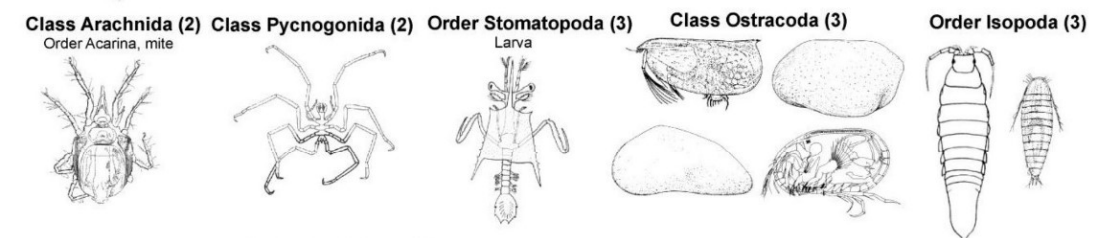
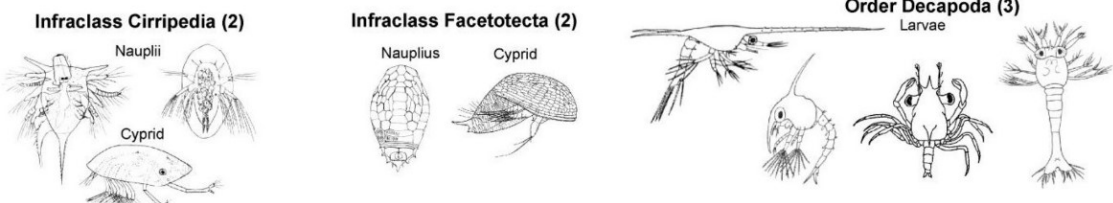
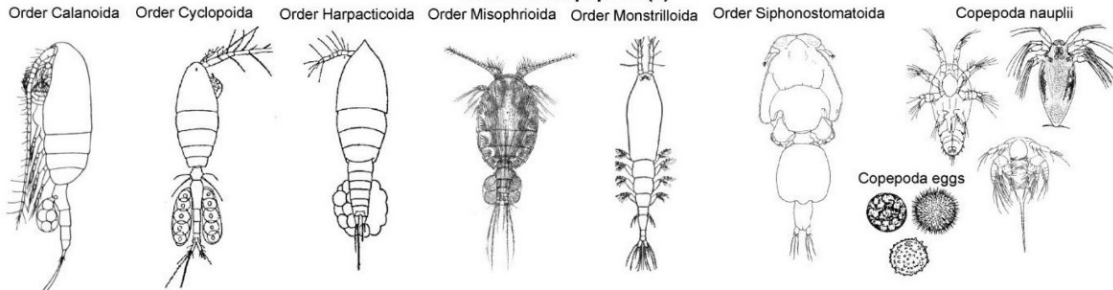


Figure 38: Pictorial key to crustacean zooplankton, obtained from Conway (2012).


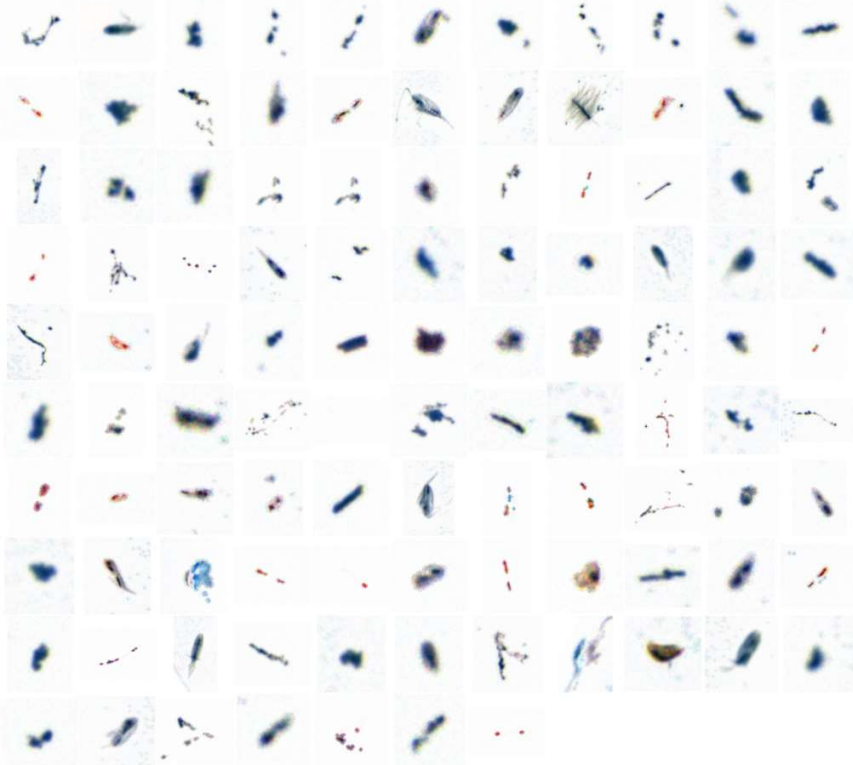
APPENDIX C: Additional classified SilCam images from the YOLO-based model

Presented here are the montages of the objects in the SilCam images classified as belonging to the group "Other", from different depths at day M1 and M3. The objects are normalized, and the images are scaled. The montages from the upper 10 m contain mostly bubbles, while copepods, detritus and fecal pellets are observed at lower depths.

Table 11: Montages of objects in the SilCam images from day M1 classified by the YOLO-based model as "Other", presented for the depth intervals 0-10, 10-20, 20-30, and 30-40 m. The objects are normalized and scaled.

	OTHER Normalized objects – scaled images												
Depth (m)	DAY M1												
0-10													

(Table 11 proceeds on the next page)

<p>10-20</p>	
<p>20-30</p>	

(Table 11 proceeds on the next page)

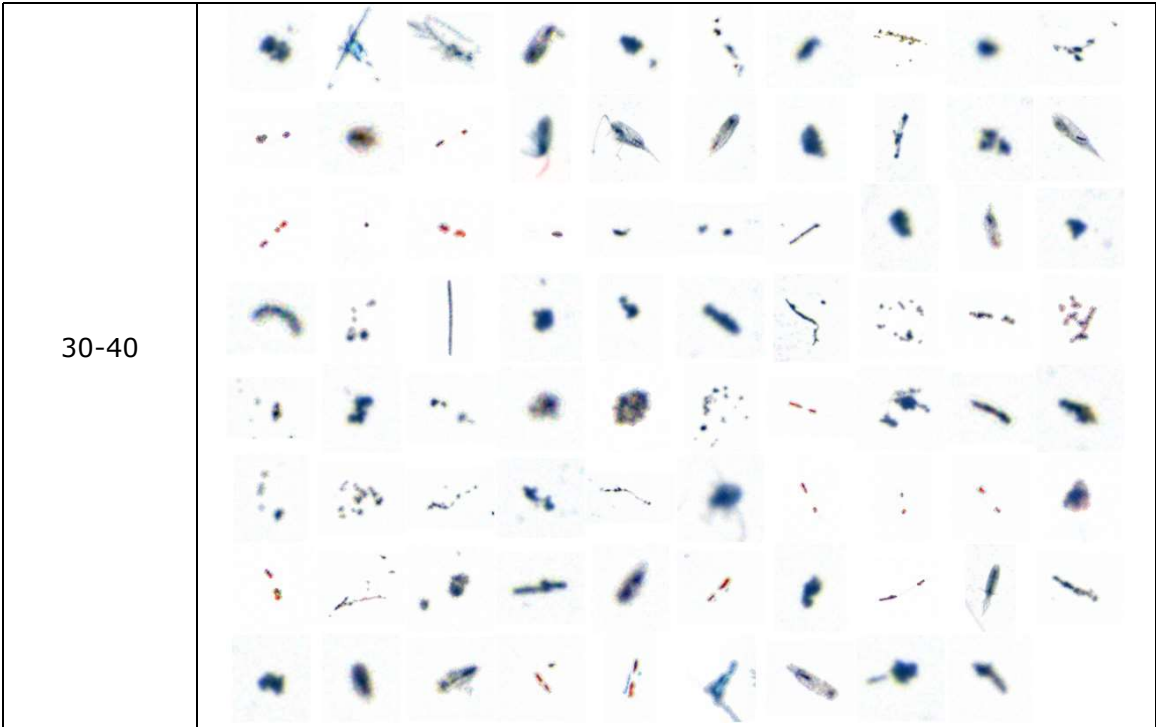

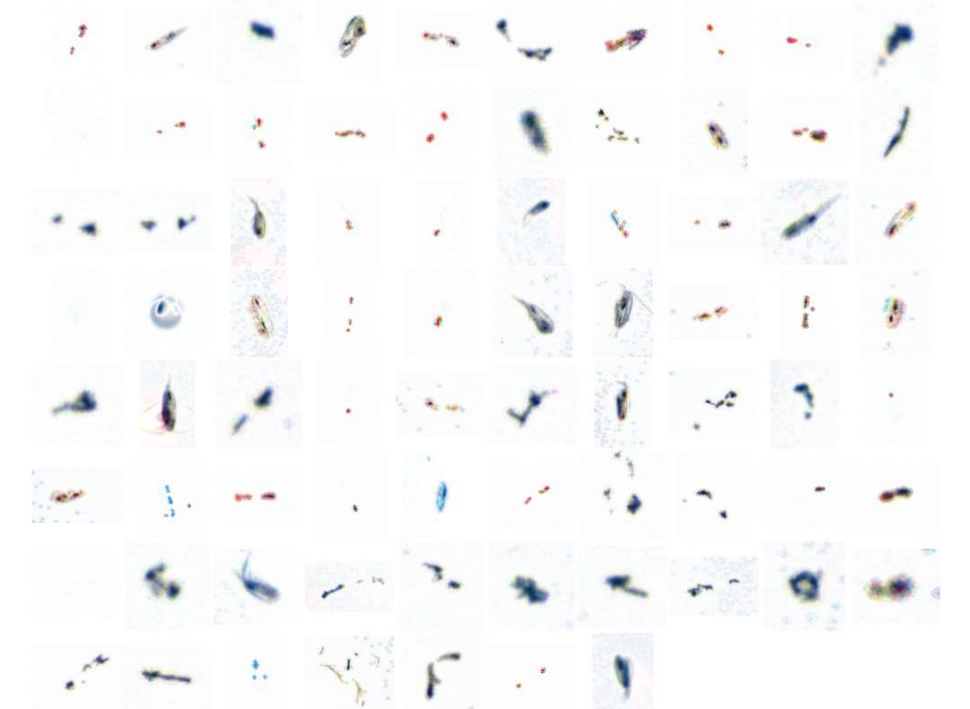


Table 12: Montages of objects in the SilCam images from day M3 classified by the YOLO-based as "Other", presented for the depth intervals 0-10, 10-20, 20-30, and 30-40 m. The objects are normalized and scaled.

	OTHER: Montage B: Normalized objects – scaled
Depth (m)	DAY M3
0-10	

(Table 12 proceeds on the next page)

10-20	
20-30	

(Table 12 proceeds on the next page)

